2-15-2019

Experimental Study on Transient Behavior of Water and Nanofluid in Multiport Slab Minichannel Heat Exchangers

Shahram Fotowat
University of Windsor

Experimental Study on Transient Behavior of Water and Nanofluid in Multiport Slab Minichannel Heat Exchangers

By

Shahram Fotowat

A Dissertation

Submitted to the Faculty of Graduate Studies

through the Department of Mechanical, Automotive and Materials Engineering

in Partial Fulfillment of the Requirements for

the Degree of **Doctor of Philosophy**

at the University of Windsor

Windsor, Ontario, Canada

2019

Experimental Study on Transient Behavior of Water and Nanofluid in Multiport Slab Minichannel Heat Exchangers

by

Shahram Fotowat

APPROVED BY:

_____

K. Siddiqui, External Examiner

Western University

_____

G. Rankin

Department of Mechanical, Automotive and Materials Engineering

_____

R. Riahi

Department of Mechanical, Automotive and Materials Engineering

_____

N. Zamani

Department of Mechanical, Automotive and Materials Engineering

_____

A. Fartaj, Advisor

Department of Mechanical, Automotive and Materials Engineering

January 16, 2019

DECLARATION OF CO-AUTHORSHIP/PREVIOUS PUBLICATION

I. Co-Authorship

I hereby declare that this thesis incorporates material that is result of joint research, as follows: Chapters 2-7 of the thesis were co-authored with Ms. S. Askar and Mr. M. Ismail under the supervision of Professor A. Fartaj, University of Windsor. In all cases, the key ideas, primary contributions, experimental designs, data analysis, interpretation, and writing were performed by the author, and contribution of Professor Amir Fartaj was primarily through the provision of supervision. The contribution of Serena Askar and Mohammed Ismail was primarily through the provision of data, feedback on refinement of ideas and editing of the manuscript.

I am aware of the University of Windsor Senate Policy on Authorship and I certify that I have properly acknowledged the contribution of other researchers to my thesis, and have obtained written permission from each of the co-author(s) to include the above material(s) in my thesis.

I certify that, with the above qualification, this thesis, and the research to which it refers, is the product of my own work.

II. Previous Publication

This thesis includes 3 original papers that have been previously published/submitted for publication in peer reviewed journals, as follows:

Thesis Chapter	Publication title/full citation	Publication status
Chapter 2	S. Fotowat, S. Askar, and A. Fartaj "Experimental transient response of a minichannel heat exchanger with step flow variation" Experimental thermal and fluid science, 89 (2017) 128–139	Published

Chapter 3	S. Fotowat, S. Askar, and A. Fartaj "Transient response of a compact heat exchanger with temperature step variation" International Journal of heat and mass transfer, 122 (2018) 1172–1181	Published
Chapter 4	S. Fotowat, S. Askar, and A. Fartaj "Comparison on the transient response of a conventional heat exchanger with a minichannel heat exchanger with mass flow and temperature step variations" Experimental thermal and fluid science	In press
Chapter 5	S. Fotowat, S. Askar, M. Ismail, and A. Fartaj "A study on corrosion effects of a water based nanofluid for enhanced thermal energy applications" Journal of Sustainable Energy Technologies and Assessments, 24 (2017) 39–44	Published
Chapter 6	S. Fotowat, S. Askar, and A. Fartaj "An experimental transient response of a heat exchanger with the Al_2O_3/water nanofluid mass flow and temperature step variations" Journal of fluid flow, heat and mass transfer	Under review

I certify that I have obtained a written permission from the copyright owner(s) to include the above-published material(s) in my thesis. I certify that the above material describes work completed during my registration as a graduate student at the University of Windsor.

General

I declare that, to the best of my knowledge, my thesis does not infringe upon anyone's copyright nor violate any proprietary rights and that any ideas, techniques, quotations, or any other material from the work of other people included in my thesis, published or otherwise, are fully acknowledged in accordance with the standard referencing practices. Furthermore, to the extent that I have included copyrighted material that surpasses the bounds of fair dealing within the meaning of the Canada Copyright Act, I certify that I have

obtained a written permission from the copyright owner(s) to include such material(s) in my thesis.

I declare that this is a true copy of my thesis, including any final revisions, as approved by my thesis committee and the Graduate Studies office, and that this thesis has not been submitted for a higher degree to any other University or Institution.

ABSTRACT

Heat exchangers are essential components of many systems and their use is extended to include various industrial, chemical, and automotive applications. A dynamic response study of a heat exchanger is essential for better representation of its design, selection, and analysis as it operates in conjunction with other process equipment. This study aims to experimentally investigate the transient performance of compact heat exchangers. A wide-range well prepared experimental setup is designed and assembled to examine the transient behavior of various types of cross-flow liquid to air heat exchangers. This set up is capable of stepping up or down the temperatures and flow rates for both hot and cold fluids covering a broad range of perturbations that occur in transient scenarios. A step function is a close approximation of a transient variation in heat exchangers, therefore, this work examines the transient response of both fluids under hot liquid side step changes in mass flow from 0.5 to 2.5, and inlet temperature from 1.5 to 3.5 while air inlet conditions are kept constant. Results are presented in terms of transient dimensional and non-dimensional outlet responses of fluids temperatures, heat transfer rates, heat balance, normalized outlet temperatures, and effectiveness. The current experimental findings provide an overview of the characteristic behavior of specific parameters such as response time, initial delay and time constant of both fluids. A comparison of the results obtained is made with the limited experimental work found in the literature. It is observed that the response time is faster for both fluids with the increase of the mass and temperature perturbations and it is higher for the hot liquid than the cold air side. An adverse trend is found between the hot and cold fluids' effectiveness in temperature step changes, while the same trend is found in mass

flow steps. Mass flow step changes for positive and negative steps exhibit an asymmetric trend of both fluids.

This work also examines the transient effect of using an engineered fluid, such as Al2O3/water nanofluid, in heat exchangers due to their improved thermophysical properties. The nanofluid is analyzed in terms of its particle size distribution, chemical characterization, and agglomeration of suspensions using the Transmission electron microscopy (TEM), Energy- Dispersive Spectrometry (EDS) and Dynamic light scattering (DLS). Experimental results show that the response time of the nanofluid for the temperature and mass flow steps are faster compared to water. An increase of up to 19% in heat transfer rate is observed when using nanofluid.

A comparison of the dynamic performance of a minichannel heat exchanger and a conventional radiator using step variations in inlet liquid temperature and mass flow rate is investigated. Results show longer response time for the conventional radiator compared to the minichannel heat exchanger. In addition, the analytical model for transient heat exchanger response is assessed with the non-dimensional outlet temperature response of a traditional tube and fin heat exchanger subjected to mass flow step changes. A more than 20% overestimate prediction is found for the transient temperature responses using the analytical model. The Empirical correlations developed for temperature and mass flow rate steps are found in a good agreement with the experimental data. The conclusion reached in this study provides an insight on the transient behavior of conventional and minichannel heat exchangers under liquid mass flow and temperatures steps. This experimental work is used to further establish and enrich a database for future advances on the dynamic response of heat exchangers subjected to step changes in liquid inlet conditions.

DEDICATION

To my family

ACKNOWLEDGEMENTS

TABLE OF CONTENTS

xiii

LIST OF TABLES

LIST OF FIGURES

LIST OF APPENDICES

CHAPTER 1

INTRODUCTION

1.1 Motivation and Background

The motivation of performing this work comes from the lack of availability of experimental

data on dynamic performance of heat exchangers due to the challenges of performing and

controlling such experiments. It is obvious from the amount of literature provided that

transient analysis of heat exchangers is still a growing subject and needs more attention

due to the vital use of heat exchangers in many industries. A heat exchanger usually does

not operate at the design point. It is important to predict heat exchanger execution at off-

design conditions. Moreover, a heat exchanger usually operates in concert with other

process equipment, so, its performance under transient conditions is important [1].

Heat transfer is an essential process in many industrial systems. This includes adding or

removing heat energy from the process fluids and yield energy recovery. The improvement

in heat transfer rate decreases the operation time leads to energy saving, enhances the

working life of the equipment, and increases the quality of a process. Therefore, the

enhancement of the heat transfer performance is now more demanding.

Thermal performance can be influenced by several aspects such as heat exchanger types,

tube/ channel size, operating conditions, and working fluid. Heat exchanger geometry has

a vital role in the selection of proper types of heat exchangers. Heat exchangers are

designed to work under particular steady state conditions. However, dynamic variation

occurs under real life scenario, such as start-up, shut down and any changes result from

other process. Numerous references are available in the literature pertaining to steady state

heat exchanger performance. Nonetheless, there are rare experimental work could be found

in open literature. The transient performance for a particular heat transfer process

differentiate their applicability, improved principal investment, returns on capital investments and guarantee reliable operations with longer life cycles, Master and Chunangad [1]. Compact heat exchangers, which exhibit higher heat duties attained by smaller size and higher heat transfer coefficients due to low flow pass hydraulic diameter, can be considered. This compactness is reachable through higher surface densities ß$\geq$1000 m^2/m^3: heat transfer surface area per unit volume of heat exchanger. The minichannel heat exchanger (MICHX) of current study possesses high area density of ß=4000 m^2/m^3.

The advancement in technology systems and processes requires an understanding of each component of the system taking into consideration the change in the operating conditions that may occur. For better representation of heat exchanger designs, a response study of this equipment is essential as a step to enhance its performance. When the inlet and outlet flow conditions do not change over time, the heat exchangers operate in a steady state. However, while one of the fluid flows comprises a change, the heat exchanger goes through a transient situation. Owing to the fact that heat exchangers play a crucial role in the response of heating-cooling systems, analyzing the transient performance of heat exchangers is essential for their precise controlling. In addition, recurrent temperature and fluid flow changes in heat exchangers desire a precise anticipation of the dynamic response of heat exchangers in the transition period. The dynamic perturbation that occurs in different types of heat exchangers in real life scenarios is approximated nearly by a step function according to Bunce and Kandlikar [2].

Numerical studies of the transient performance of heat exchangers are reported next due to the limited availability of the experimental work. Demand in the dynamic response of heat exchangers is growing due to the growth in the process control. Moreover, the transient

behaviour of all component should be known for the full automation of the process plant. For these reasons, Kabelac et al. [3] presented an analytical and numerical model to calculate the transient response of a liquid and gas outlet temperature of a finned cross flow heat exchanger for inlet temperature and mass flow variation. A general mathematical model for predicting the temperature responses of one-dimensional flow heat exchangers which can be used for the transient response of multistream/ multipass shell-and-tube heat exchangers, plate heat exchangers, plate-fin heat exchangers and their networks was presented by Roetzel et al. [4]. Based on the analytical and numerical analyses the dynamic parameters of heat exchangers used for automatic control of systems were assessed. Xuan et al. [5] presented two algorithms of numerical inversion of the Laplace transform to find the final temperature distribution in the real-time domain of parallel and counterflow heat exchangers. They found that the Fourier series technique is better than the Gaver-Stehfest algorithm to compute the response to disturbances with oscillatory components. Bunce [6] numerically studied the transient performance of a counterflow heat exchanger under a wide range of temperature changes using a commercial software, Thermonet. He verified that the solution agrees well with other solutions found in literature for the counterflow heat exchangers which are frequently used in industry due to their thermal advantage.

Lachi et al. [7] studied numerically and experimentally the dynamic behavior of a double pipe and one pass shell and tube heat exchanger subjected to a sudden change in flow rate of one of the inlet fluids. An analytical expression was established to determine the time constant of a double pipe heat exchanger. They observed that the time constant drop by a rise in the mass flow step change causes a quicker response of the heat exchanger and 10% inconsistency between analytical and experimental results. An analytical model created by

Yin and Jensen [8] for the temperature dynamic response of a heat exchanger for a single-phase fluid with a constant temperature fluid. The heat exchanger was subjected either to a temperature step variation in the change phase fluid or a mass flow step in the single-phase fluid. The transient behaviour of the heat exchanger was estimated by an integral method with the assumption that the single-phase fluid temperature distribution is expressed by a combination of the initial and final temperature distribution and a determined time function. The results were validated against numerical simulation. Mishra et al. [9], numerically investigated the transient temperature response of both fluids in unmixed crossflow heat exchangers considering finite wall capacitance for the temperature and mass flow changes. Step and ramp changes in the mass flow of the both hot and cold fluids, and exponential and sinusoidal changes in the hot fluid inlet temperature were applied. They found a rise in the mean exit temperatures with larger change in the hot fluid, whereas a drop was found when the larger change was in the cold fluid.

Naterer and Lam [10] studied the transient change of fluid and wall temperatures in a two-phase heat exchanger. Their model based on the varying convection coefficient is related to vapour fraction between the inlet and outlet of the heat exchanger. The wall and fluid temperature stabilized sooner at lower thermal inertia of the wall. It was found that the fluid outlet temperature increases faster to the outlet value when involving higher inlet vapor fraction. The results were compared with a numerical simulation. Master et al. [11] studied the transient performance of heat exchangers and concluded that appropriate predicted transients in heat exchanger design guidelines, would significantly increase heat exchanger performance and mechanical integrity. A dynamic response of the thermal environment in air cooled data centers was studied by Erden [12]. A CFD model was

created under particular conditions of cooling disruption, server shutdown and cooling air flow variations to appraise the thermal response of data centers and validated by experimental results for specific condition of cooling. They validated experimentally their model to predict data center transient thermal response after typical disturbances within an RMS error usually less than 1°C. Gao et al. [13] numerically investigated the characteristics of the dynamic performance behavior of heat exchangers for the thermal management to improve the design of control strategies and energy efficiency. They developed mathematical models using the transient effectiveness concept. These models were used to solve and analyze the transient problems of cross flow heat exchangers.

Convective heat transfer of the fluid could be increased by passively changing boundary conditions, flow geometry, or increasing thermal conductivity of the fluid Wang et al. [14]. Working fluids like water and ethylene glycol have low thermal conductivity compared to solids. Hence, one way to increase the thermal conductivity of fluids is by means of adding solid particles to the fluids. Several theoretical and experimental investigations of suspensions solid particles into a base fluid to improve the heat transfer characteristics have been presented since Maxwell explored this idea more than a century ago [15]. He was a pioneer who presented a theoretical basis for computing the effective thermal conductivity of suspending solid particles into the base fluid. Nanofluids are the new generation of nanotechnology fluids produced by dispersing nanoparticles into the base fluid. The term "nanofluids" was coined by researchers at Argonne National Laboratory and referred to a two-phase mixture composed of a continuous liquid phase and dispersed nanoparticles. The investigation was continued theoretically and experimentally by many researchers such as Hamilton and Crosser [16], and Wasp [17]. Their model accurately predicted the

thermal conductivity of slurries. However, the size of the particle was restricted on micro to macro-size with some reported disadvantages. The thermal conductivities of three different nanofluids that have diamond, silver, and silica nanoparticles was measured using transient hot-wire method by Kang et al. [18]. The experimental results were compared with a theoretical model and indicated that the heat transfer mechanism should be taken into account while assessing the exact nanofluid thermal conductivity. Convective heat transfer performance of nanofluid and base fluid in laminar and transition flow regime was experimentally investigated by Yang et al. [19]. The results showed that the rise in thermal conductivity as a function of concentration could be anticipated by the effective medium theory. It was also found that the pressure drop penalty for dilute nanofluids in laminar flow is negligible. Fotowat et al. [20] experimentally presented safety and chemical interactions of the Al2O3/water nanofluid flow with common metallic surfaces used in various industrial applications by means of Scanning Electron Microscopy/ Energy Dispersion X-ray Spectroscopy (SEM/EDS) and Raman Spectroscopy. Among the three common materials used in several industries, Cu showed the highest corrosion while SS revealed the lowest corrosion at environmental condition. This was explained by a considerable increase of oxygen on all the metal surfaces due to the increase in the pH value of the nanofluid. The higher amount of oxygen refers to higher oxygen partial pressure on the metals surface compared to the environmental condition which results in higher pitting and intergranular corrosion.

Knowledge gap in current scientific literature:

- No experimental work is available on transient cross flow MICHX.
- Experimental transient work on crossflow heat exchanger is very limited.

- Majority of transient work on heat exchangers are numerical/ analytical work.

- Almost all the exp. work related to heat exchanger is under steady state conditions.

- Numerical work was verified only with the steady state experimental data (due to the lack of transient experimental work).

- The reason for the lack of transient experimental work in heat exchangers is due to its inherent challenges that exist in conducting the experimental work.

- Work on the transient response of heat exchangers using nanofluid is very limited.

1.2 Objectives and method of approach

The main objectives of the present work are to find the different approaches to enhance the heat energy transfer, characterize the dynamic performance of heat exchangers under different perturbations and provide a precise experimental database. This is due to advance in improving the design of control strategies and full automation in the precise process plant [21]. A precise attention on the transient response of a particular heat exchanger would help in the selection procedure for appropriate type of heat exchanger. Leading heat exchanger technologies, while examining dynamic behavior authentication for processes, can distinguish their applicability and assure reliable with longer life cycles of operation. A well-equipped experimental setup with ultimate precise instrumented devices was used to minimize the uncertainties of the devices. The primary fluids selected are water due to its common use in many applications, low cost, high thermal conductivity, and availability, and Al2O3/water nanofluid owing to the improved thermal conductivity of the base fluid and enhance the heat transfer performance of the system. In order to achieve this goal, the

inlet conditions of both fluids were kept constant. The effect of hot fluid mass flow rate and inlet temperature perturbations on the outlet temperatures and thermal performance of both fluids will be presented and discussed. Uncertainty analysis for the experimental data is performed and accounted for while plotting the results.

The objectives of the current study are appended below;

- Design, development, and instrumentation of a transient experimental test facility to examine cross flow heat exchangers

- Investigate the effect of corrosivity of Al_2O_3/W nanofluid on materials used in the test facility (Cu, Al and SS) and measuring the k_{eff} of the nanofluid

- Determine nanoparticle uniformity, and agglomeration in order to find characteristics of the nanofluid as the working fluid using SEM and Spectroscopy

- Investigate experimentally the transient heat transfer characteristics of MICHX using DI-Water and Al_2O_3/water nanofluid

- Compare transient experimental results of MICHX with a bench mark conventional heat exchanger

- Develop transient empirical correlations on the transient responses of cross flow conventional HX for water and MICHX for Al2O3/W nanofluid

- Generate experimental database on transient characteristics of the cross-flow heat exchanger for process control strategy for future researchers

Chapter 2

The key goal of this chapter is to experimentally study the transient response of a cross flow multi-pass serpentine minichannel heat exchanger with step flow rate variation. The influence of the hot-fluid mass flow step change on the outlet temperature of both fluids is

presented and discussed. For completing this task, the mass flow rate of the hot fluid was varied in a step change while the inlet conditions of the two fluids were kept constant. It is obvious from the literature that the transient analysis of heat exchangers is still an emergent topic and needs more attention owing to the frequent use of heat exchangers in many industries.

Chapter 3

In this chapter, the experimental dynamic analysis of a cross flow meso heat exchanger subjected to a step change in inlet temperature of the hot fluid is presented. The two fluids mass flow rate and the cold fluid inlet temperature were kept constant. Heat was transferred from the hot fluid DI-water to the cold fluid air. The heat transfer of both sides was calculated, and the results were illustrated over time. The dynamic response of the exit temperature of the two fluids and the thermal performance of the heat exchanger are discussed. The uncertainty analysis for the experimental data was calculated and demonstrated in the graphs. The heat balance error to display the variance in heat transfer of the two fluid sides was found.

Chapter 4

The lack of the experimental work and the need to analyze the behaviour of different types of heat exchangers, such as compact ones, triggered the current investigation. This study aims to examine the dynamic response of a multiport slab finned mini-channel and a traditional tube and fin heat exchangers with both subjected to variations in liquid temperature and flow rate. Different step changes in a wide range of temperature and flow rate are applied using the well instrumented experimental setup. The outlet temperatures

of the hot and cold fluids, transient heat transfer rates, transient effectiveness and time constant are presented and discussed in the form of dimensional and dimensionless format.

Chapter 5

This chapter presents the pH impact of aluminum oxide/water (Al2O3/W) nanofluid on aluminum (Al), copper (Cu), and stainless steel (SS), which have common applications in the industrial equipment. Experiments were performed on the most common materials to display the highest and lowest corrosive metals to be used in contact with the nanofluid. Two different solutions of the same pH level of (3.7) of the Al2O3/W nanofluid were prepared using H2SO4+NaOH and HCl+NaOH. The effect of the solutions on the materials over a long period of time was examined with Scanning Electron Microscope/Energy Dispersive Spectroscopy (SEM/EDS) and WiTec system with an accelerating voltage of 5.0 kV. The result of adding nanoparticles to a base fluid on the thermal conductivity of the fluid at different temperatures (20, 30, and 40°C) is also presented. The measured thermal conductivity as a function of temperature and fluid concentration is presented. Results from this investigation will offer understanding on the interaction of these nanofluids with the contact materials. Knowledge of the interaction of these fluids with the contact material serves as an important parameter once designing a thermal system with a nanofluid as the working fluid.

Chapter 6

In this study, the utilization of engineered fluids, nanofluids, in heat exchangers to enhance the heat transfer owing to their improved thermophysical properties will be discussed. The dynamic behaviour of a minichannel heat exchanger subjected to nanofluid mass flow and temperature step changes is investigated. The mass flow rate of the Al2O3/Water nanofluid

is subjected to steps of 0.5 to 2.5, while the temperature steps varied from 1.5 to 3.5. The nanofluid is analyzed in terms of its particle size distribution, chemical characterization, and agglomeration of suspensions using the Transmission Electron Microscopy (TEM), Energy- Dispersive Spectrometry (EDS) and Dynamic Light Scattering (DLS). The current experimental findings provide an overview of the characteristic behavior of certain parameters such as response time, initial delay and time constant of both fluids. The initial delay time for steps in inlet liquid temperature and mass flow are found higher on the hot liquid side than the cold air. Moreover, the response time of the nanofluid for the temperature and mass flow steps are shorter compared to water. In addition, the dispersion of aluminum oxide nanoparticles in water showed a 19% enhancement heat transfer rate in the minichannel heat exchanger.

Chapter 7 (Summary and Conclusion)

This chapter summarizes the concluding points for all the presented previous work. It covers the investigation of the transient behaviour in heat exchangers with different working fluids. Additionally, the comparison of a compact and a traditional heat exchanger is also studied and reported. Ways of heat transfer enhancement is conveyed for future consideration of heat exchangers design.

Further information is found in the enclosed appendices with more details description of the work investigated

References

1. B. I. Master, and K. S. Chunangad, "Dynamic performance of heat exchangers" Heat Transfer Eng., 29(3), 217 – 218, 2008.

2. D.J. Bunce, and S.G. Kandlikar, "Transient response of heat exchangers" Proceedings of the 2nd ISHMT-ASME Heat and Mass Transfer conference. Surathkal, India, PP. 729–736, 1995.

3. S., Kabelac "The transient response of finned crossflow heat exchanger" International journal of Heat Mass Transfer 32(6): 1183-4189, 1989.

4. W., Roetzel, M., Li, X., Luo "Dynamic behaviour of heat exchangers" Advanced Computational Methods in Heat Transfer, 451-460, 2002, ISBN 1-85312-906-2.

5. Y., Xuan, and W., Roetzel "Dynamics of shell-and-tube HX to arbitrary temperature and step flow variations" AIChE Journal, vol. 39, no. 3, PP. 413-421, Mar.1993. https://doi.org/10.1002/aic.690390305.

6. D., Bunce, "The Transient response of heat exchangers" Master thesis, Mechanical Engineering, College of engineering, Rochester institute of technology, May 1995.

7. M., Lachi, N.El., wakil, J., Padet "The time constant of double pipe and one pass shell-and-tube heat exchangers in the case of varying fluid flow rates" Int. Journal of Heat and Mass Transfer, vol. 40, no. 9, PP. 2067-2079, 1997. https://doi.org/10.1016/S0017-9310(96)00274-8

8. J., Yin, M.K., Jersen "Analytical model for transient heat exchanger response" International Journal of heat and mass transfer, vol. 46, 3255-3264, 2003. https://doi.org/10.1016/S0017-9310(03)00118-2

9. M., Mishra, P.K., Das, S., Sarangi "Transient behaviour of crossflow heat exchangers due to perturbations in temperature and flow" International Journal of Heat and Mass Transfer 49:1083–1089, 2006.

10. G.F., Naterer, and C.H., Lam "Transient response of two-phase heat exchanger with varying convection coefficients, Journal of Heat Transfer" vol. 128, pp. 953-962, 2006. doi:10.1115/1.2241974

11. B.L., Master, and K.S., Chunangad "Dynamic performance of heat exchangers" Heat Transfer Engineering, vol. 29, no. 3, PP. 217-218, 2008. https://doi.org/10.1080/01457630701755761.

12. H.S., Erden "Experimental and Analytical Investigation of the Transient Thermal Response of Air Cooled Data Centers" Ph.D. dissertation, Mechanical and Aerospace Engineering, Syracuse University, Syracuse, NY, U.S.A, 2013.

13. T., Gao, B., Sammakia, J., Geer, A., Ortega, and R., Schmidt "Transient Effectiveness Characteristics of Cross Flow Heat Exchangers in Data Center Cooling Systems" 14th IEEE ITHERM Conference, 688-697, 2014.

14. X.Q., Wang and A.S., Mujumdar "A review on nanofluids - part i: theoretical and numerical investigations" Brazilian Journal of Chemical Engineering, Vol. 25, No. 04, pp. 613 - 630, 2008, ISSN 0104-6632.

15. J.C., Maxwell "A Treatise on Electricity and Magnetism" vol. 1, 2nd ed., Clarendon Press, Oxford, U.K., 1873.

16. R.L., Hamilton, and O.K., Crosser "Thermal Conductivity of Heterogeneous Two Component Systems" Industrial and Engineering Chemistry Fundamentals, vol1, no. 3, PP. 187–191, Aug1962, DOI: 10.1021/i160003a005.

17. E.J., Wasp, J.P., Kenny, and R.L., Gandhi "Solid-Liquid Flow Slurry Pipeline Transportation, Series on Bulk Materials Handling" Trans. Tech. Publications, vol.1, no. 4, Clausthal, Germany, 1977.

18. H.U., Kang, S.H., Kim, and J.M., Oh "Estimation of thermal conductivity of nanofluid using experimental effective particle volume" Journal of Experimental Heat Transfer, vol. 19, no. 3, PP. 181-191, 2006, https://doi.org/10.1080/08916150600619281.

19. Y., Yang "Characterizations and convective heat transfer performance of nanofluids" PhD dissertation, Mechanical engineering, Lehigh University, Jan 2011

20. S., Fotowat, S., Askar, and A., Fartaj "A study on corrosion effects of a water based nanofluid for enhanced thermal energy applications" journal of Sustainable Energy Technologies and Assessments, vol. 24, PP. 39–44, 2017.

21. C., Guha, and A., Chaudhuri "Transient analysis of heat exchanger network" Journal of the Institution of Engineers, Chemical Engineering Division, v 87, PP. 51-59, March 2007, ISSN: 00203351.

CHAPTER 2

EXPERIMENTAL TRANSIENT RESPONSE OF A MINICHANNEL HEAT

EXCHANGER WITH STEP FLOW VARIATION

2.1 Introduction

Industries worldwide are thriving to save space, energy and cost. Energy savings can be

done either by using renewable energy sources instead of the conventional ones or by

modifying the existing resources and system components to yield higher overall

performance. One of these system components is the heat exchanger which is widely used

to transfer heat in many applications such as: air conditioning, automotive, power

generation, chemical, and oil & gas industries. The recent advances in technology made it

necessary to use compact yet efficient heat exchangers.

High thermal performance can be affected by several factors such as heat exchanger types,

tube/channel size, operating conditions, and working fluid. Studies on any of these

parameters are important for the design of an efficient heat exchanger. Heat exchangers are

usually part of a system and enhancing the efficiency of these exchangers contributes to

the general system efficiency. Classification of heat exchangers can be found in Kandlikar

and Grande [1] where they present the recent advances in channel diameter and define the

range of 10µm – 200µm as microchannels, between 200µm – 3mm as minichannels, and

> 3mm as conventional channels. The research work on mini/microchannels heat

exchangers has shown their outstanding thermal performance in addition to energy and

space savings [2-6].

Steady state solutions of heat exchangers are widely accessible, well demonstrated, and strongly verified. The aforementioned statement cannot be said for the transient analysis. The performance of the heat exchanger varies with time and various interruptions in the operating conditions affect the exchanger behavior. A system performance varies when improper control of a heat exchanger inlet conditions happens. Therefore, the change in the behavior of a heat exchanger affects the other components connected to it. When considering a transient analysis, a car radiator can be set as a good example. The main use of a radiator is to remove the undesired heat from the engine. Through the use of a thermostat, the amount of coolant that needs to be passed through to the radiator is controlled. This change in mass flow leads to the radiator working under transient conditions. For this regard, studying the transient response of a radiator is noteworthy for engine temperature optimization when mass flow perturbations occur.

Most of the analyses are based on the assumption that the heat exchanger works under steady state conditions, however, in practice, maintaining all the conditions fixed is a very challenging process. Several other issues may occur in practice such as at startup, shutdown, malfunction of the system and accidents. These variations affect the heat exchanger performance, therefore, it is essential to study the behavior of the heat exchanger when these issues occur for system improvement and to provide precautionary arrangements for its ultimate thermal performance.

The analyzation methods that tackle the transient response of heat exchangers are numerical, analytical, and experimental which can be used to assess the heat exchanger thermal behavior under transient conditions. Nevertheless, the lack of availability of experimental data leaves it open for present and future investigations. In order to validate

16

the outcomes of analytical models or numerical simulations, some researchers verified their numerical work by analytical models or by experimental data conducted under steady state. Only very little work has been done experimentally and it involved a specific type of heat exchanger, flow arrangement or inlet condition change.

Studies also extended to include analytical investigation of the behavior of a single pass plate heat exchanger subjected to flow maldistribution by Srihari et al. [7]. Laplace transform method and numerical inversion of frequency were utilized to signify the effect of flow rate changes and back mixing on the transient response of the heat exchanger thermal performance. Time delay and time constant are extremely dependent on the flow rate change. Prashant Regulagadda [8] studied analytically the transient behavior of the heat exchanger in a Marnoch heat engine. He investigated this behavior using laminar and turbulent flows. A model created for a parallel flow heat exchanger with a step change in mass flow rate and its effect on the temperature of the working fluid was performed. His model was compared with previous research done by Yin and Jensen [9] and found good agreement.

Numerical analysis of a multi-pass cross flow heat exchanger to examine its transient performance was performed by Silaipillayarputhur and Idem [10]. The minimum capacity rate fluid was subjected to a step change in its inlet temperature and mass flow rate separately. Results of the multi-pass exchanger were compared with multi-pass parallel and counter cross flow heat exchangers. As a step change in mass flow rate is applied, it is noticed that the cross-flow arrangement reduces the thermal performance of the heat exchanger when compared to parallel and counter flow arrangements. However, the main

17

advantage of the cross-flow arrangement is the enhanced thermal response time for three or more heat exchanger passes. Another advantage found was the decreased pressure loss in the tube side.

One of the early studies of the dynamic response of flow in heat exchangers was made by Stermole and Larson [11]. They used a double pipe counter current heat exchanger to conduct their experimental and theoretical analyses to investigate the dynamic response of such an exchanger. They found that as the flow rate varies, the system behaved linearly. Pearson et al. [12] used tube and plate-fin heat exchanger to study the dynamic response of air outlet temperature when a mass flow rate change is applied on the other fluid. They depended on the steady state experimental results to validate the numerical and mathematical models. Air outlet temperature and time constant results were compared to Gartner's model [13]. Their main findings are: the mathematical model satisfactory predicted the air outlet temperature of the heat exchanger for a step change in water mass flow rate and they extended Gartner's model to include a serpentine heat exchanger with fins. Idrissi et al. [14] investigated the transient response of temperature along a counter flow double pipe heat exchanger with a sudden change in the hot fluid mass flow rate. First order response to time constant was used to study the dynamic performance of the heat exchanger. Two responses were found from the cold fluid: the time response along the longitudinal axis to the counter flow and along the heat exchanger. Experimental data were used to verify the theoretical results. A linear decrease in time constant of the hot fluid was obtained as it undergoes a step change.

Transient behavior in a heat exchanger with two fluids, one is a single phase while the other has a constant temperature was performed by Yin and Jensen [9] for step changes in temperature and mass flow rate. Explicit analytical solutions were acquired and verified by the numerical simulation at various operating conditions. They stated that since one of the fluid is subjected to constant temperature, it is independent of flow arrangement and their model can therefore be used for different flow arrangements.

Chopra and Prajapati [15] presented analytically the effect hot fluid mass flow rate changes and its composition percentages in a tube and fin heat exchanger on the outlet temperatures and the overall heat transfer coefficient. Two fluids were used, the water-coolant mixture as hot fluid was subjected to mass flow rate variations of the air as cold fluid. A comparison of the obtained analytical solution was made with the steady state numerical results. It was found that as the hot fluid mass flow rate increased its outlet temperature decreased. When the hot fluid is more than 50% coolant to water mixture, the heat exchanger performance was depreciating.

A cross flow heat exchanger used in data center was numerically modeled by Del Valle et al. [16] using the finite difference method. Experiments were conducted to validate the model by subjecting the tube heat exchanger to a step and ramp changes, as well as, sinusoidal variation in both temperature and mass flow rate inlet conditions. When the step change in mass flow rate is applied, the experiment was running under a constant inlet air temperature of approximately 23°C, inlet water temperature of 50°C and yielded a change in the outlet water temperature to about 2°C. For the aforementioned case, their model was able to predict the temperature response.

While these studies are important in providing an insight on the transient behavior of the heat exchanger, there is no adequate data to cover all the types of heat exchangers or the wide range of operating conditions for future design and analysis. The motivation of performing this work comes from the lack of availability of experimental data on transient response of heat exchangers due to the challenges of performing and controlling such experiments. The main objective is to experimentally investigate the transient response of a cross flow multi-pass serpentine minichannel heat exchanger. The primary fluid chosen is water due to its common use in many applications, low cost, high thermal conductivity, and availability. The effect of hot fluid mass flow perturbation on the outlet temperature of the two fluids will be presented and discussed. In order to accomplish this goal, the inlet conditions of the two fluids will be kept constant while only varying the mass flow rate of the hot fluid step wise. It is evident from the amount of literature provided that transient analysis of heat exchangers is still a growing subject and needs more attention due to the vital use of heat exchanger in many industries.

2.2 Experimental setup

A comprehensive well-equipped experimental setup is designed and assembled to examine the transient behavior of dynamic forced convection in a heat exchanger with a step change in the inlet hot fluid mass flow rate. The full experimental setup is illustrated in Figure 2.1 and a schematic of the basic components of the experimental setup is demonstrated in Figure 2.2. The main components of the system are: an open cycle well equipped wind tunnel, test chamber, multichannel multiport slab minichannel heat exchanger, gear pump, in-line infusion heater, and in-built heat exchanger to control the temperature of air. Other measuring devices and equipment are Resistance Temperature Detectors (RTDs) and

20

pressure transducers (PTDs) for water inlet and outlet temperatures and pressures, different sets of valves, data acquisition system to record the data as well as a Coriolis type mass flow meter is used for accurate real-time water mass flow rate and temperature. For air velocity, a flow kinetics monometer (FKT series) is used to obtain inlet air flow velocity. The manometer connected to a pitot tube which is located at the entrance of the test section. The velocity of air is calculated with measuring the dynamic and static pressure of the air flow using the following equation. The correction factor C' is based on the Pitot tube construction, mostly the spacing of the holes. For the current study it is taken as 1.

$$V = C' \sqrt{\frac{2\Delta P}{\rho}}$$

Figure 2.1 Experimental setup

2.2.1. Air side

The main component of the air side circuit is the wind tunnel. It is made of fiberglass with high thermal resistant and it has no or negligible heat loss to or from the environment. The inside of the wind tunnel is lined with a smooth surface coating to prevent any disturbance in the air flow. The air inlet temperature is measured at the inlet of the wind tunnel via the use of a T-type thermocouple. Airside temperatures before the inlet to the heat exchanger are measured by a grid of 9 thermocouples, while after exiting the heat exchanger a grid of

18 thermocouples is used for measurement. Air enters the tunnel passing through a fine filter to eliminate any dust particles or dirt that can affect the air quality. Air then flows through an in-built blower with an electronic control panel and a precise digital processor to control the desired flow rate. After air gets pushed by the blower, it passes through the inbuilt tube heat exchanger to manage the air inlet temperature to the test section to the desired temperature. The well insulated inbuilt heat exchanger uses cold or hot water, control needle and mixing valves to precisely regulate the inlet temperature.
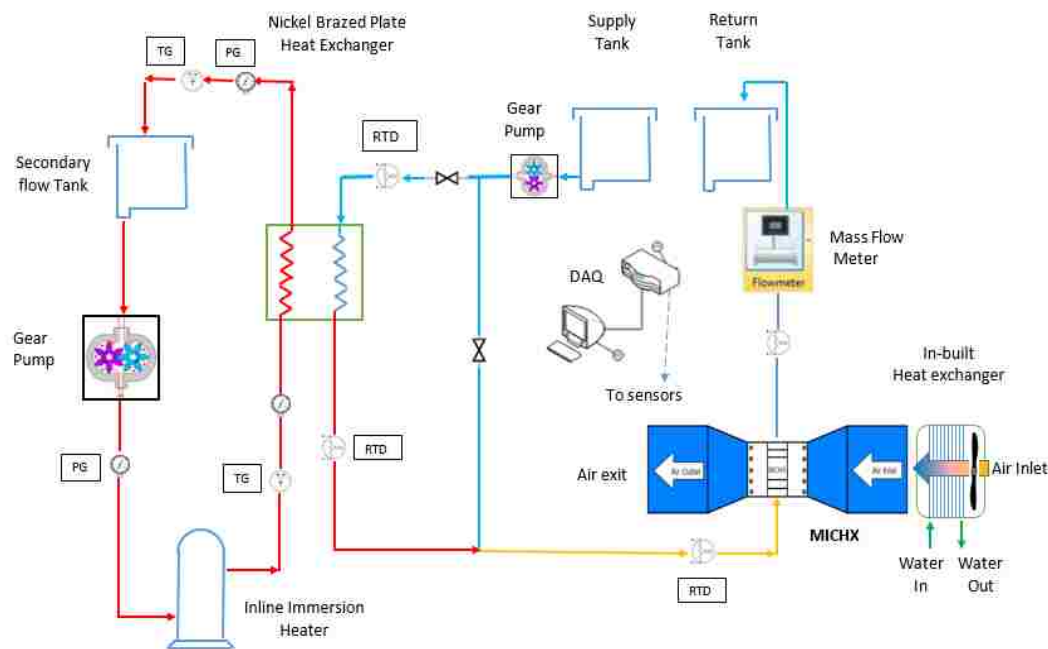
Figure 2.2 Schematic diagram of the equipment

Air, with the desired temperature and flow rate, travels through the wind tunnel. A honeycomb structure with smooth surface and fine wire-mesh are used to straighten and keep the air flow uniform before reaching the test section. The temperature of the air side is measured using a net of 9 thermocouples at the inlet and 18 at the outlet of the test

22

chamber cross section. Thermocouples are T- type with a temperature range of -250℃ to 350℃ and special limits of error 0.5°C or 0.4%. Additionally, a Pitot tube is mounted at the inlet of the test chamber to measure the velocity of the air and reading it using the flow kinetic manometer. The test section is well insulated, to eliminate any heat loss to or from the surrounding and is located in the center of the wind tunnel and contains the heat exchanger. The wind tunnel is an open type where air is supplied at constant temperature and steady operating conditions and then exits outside the facility. A schematic of the air side circuit with the main components is explained in Figure 2.3.
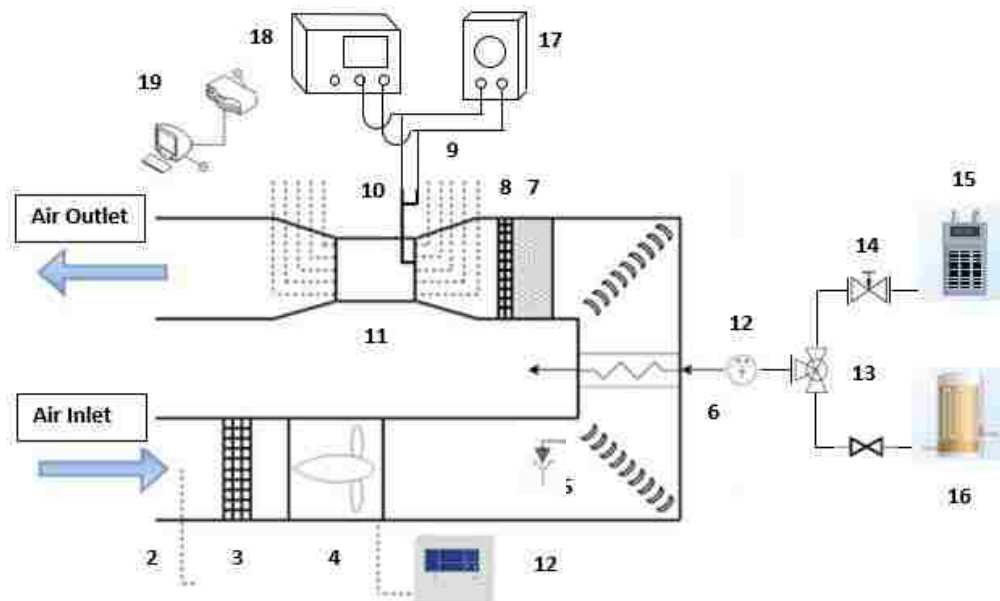
1	Thermal Wind tunnel	11	Test section
2	T-type Thermocouple	12	Temperature Gauge
3	Air filter	13	Mixture Valve
4	Air blower	14	Needle Control Valve
5	Air vanes	15	Chiller
6	Inbuilt heat exchanger	16	Heater
7	Honeycomb Straightener	17	Differential Pressure Transducer
8	Flow net	18	Flow Kinetics FKT
9	T-type thermocouples	19	Data Acquisition System
10	Pitot tube		

Figure 2.3 Diagram of the Airside circuit

2.2.2.   Test chamber and test specimen

The test chamber is made of clear 1/4" polycarbonate sheets due to its light weight, transparency, ease of use, high thermal resistance, and excellent impact resistance. The geometry is a rectangular shape with a cross section of 4"X 12" [0.1016 m X 0.3048 m] and 24" [0.6096 m] in depth. It is placed in the center of the wind tunnel and used to contain the main heat exchanger and to eliminate any heat transfer between the heat exchanger and the environment. At the center the test chamber, a minichannel heat exchanger with an area density β of 4000 m^2/m^3 is positioned. The heat exchanger consists of 68 channels, 5 slabs with 4 serpentines. Aluminum channels with a diameter of 1mm are used in this exchanger. Several thermocouples are mounted on the outer surface of the serpentines to monitor the temperature variation. Thermocouple readings are monitored and recorded using a data acquisition system (LabVIEW). To obtain velocity profiles, the test section has 5 ports on each side at the inlet and outlet to the minichannel heat exchanger. The test specification of the minichannel heat exchanger is shown in the table 2.1. Moreover, the test chamber is made flexible to accommodate other compact heat exchangers. A schematic of the test chamber is illustrated in Figure 2.4.
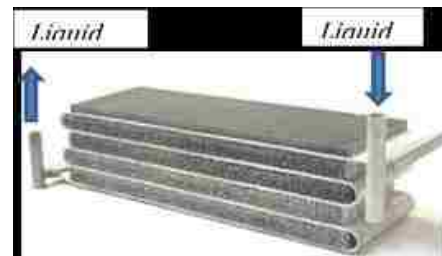
| (a) | (b) |

Figure 2.4 (a) Test chamber, (b) Minichannel heat exchanger

24

Table 2.1 Heat exchanger Specifications

Heat exchanger specifications	Dimensions
No. of slabs	*5*
No. of channels in a slab	*68*
No. of serpentine	*4*
Diameter of channel (m)	*0.001*
Thickness of slab (m)	*0.002*
Slab's material	*Aluminum*
Width of slab (m)	*0.1*
Fin height (m)	*0.018*
Type of fin	*Wavy (4 wave along the slab width)*
Fin density (Number of fins per inch)	*12*
Fins material	*Aluminum*

2.2.3. Liquid side

The main fluid used in the minichannel heat exchanger is DI-water and it is considered the primary fluid. The main primary fluid circuit mainly consists of inlet tank, pump motor, piping network, flow monitoring devices, minichannel heat exchanger, flow measuring instruments, and outlet tank. Water at a certain temperature flows from the inlet tank by means of a gear pump then exchanges heat with the fluid flowing from the secondary plate heat exchangers. These plate type heat exchangers work with liquid to liquid and are used to exchange the heat with the main working fluid to bring its temperature to the desired value of 70°C. The secondary circuit of the plate heat exchangers has hot fluid (water) flowing into it. This water is heated using an inline 20 kW immersion heater. This heater

has two microprocessors to control the temperature of water with a maximum accuracy of $\pm 1\%$ error. Fig. 2.5 shows the diagram of the secondary liquid circuit.

1	Heater and controller
2	Valve
3	Temperature gauge
4	Pressure gauge
5	First plate heat exchanger
6	Second plate heat exchanger
7	Tank
8	Gear pump and controller
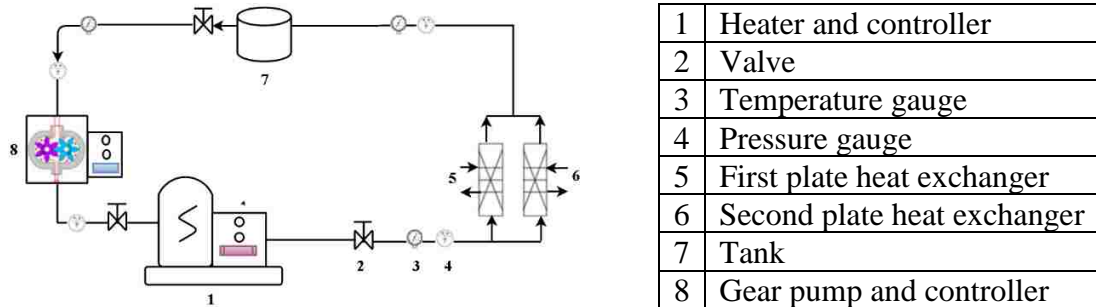
Figure 2.5 Diagram of the Secondary liquid circuit

The exiting primary fluid (water) then passes through the test section and exchanges heat with the air. Finally, cooled water exits the heat exchanger and is collected in an 80 liter stainless steel tank.

To measure the variation of the mass flow rate in the liquid side, an inline Coriolis type mass flow meter is placed as shown in figure 2.6 with an accuracy of 0.1%. It consists of a transmitter and a sensor that use Coriolis measuring principal to accurately measure the mass flow of the liquid. Temperatures at the surface of the 4 serpentines are measured using 48 T-type thermocouples as well as RTDs to measure the inlet and outlet temperatures of the heat exchanger.

Figure 2.6 Mass flow meter (Coriolis technology)

All the readings at different measurement locations from the measuring instruments such as thermocouples, PTDs, and RTDs were recorded using a data acquisition system equipped with LabVIEW software. This Multi-Channel Data Acquisition (DAQ) system is capable of monitoring and recording of 96 separate experimental measurements.

2.2.4. Experimental procedure

There are many operating parameters that need to be considered during the experiments. The parameters are set according to the desired operating conditions and are as follows: inlet water temperature at 70°C, inlet air temperature at 13°C, and inlet air velocity 6 m/s. The experiment included a step change in water mass flow rate, this change was chosen to be from 20 g/s to 30 g/s which correspond to Reynolds number of 420 to 760.

- The secondary circuit of plate heat exchangers initializes first by starting the heater which is pre-set to a desired value. Water warms up and its temperature rises till it reaches the desired pre-set value with a calibration accuracy of 0.1°C of span.

- The air blower is turned on and used to control the air inlet velocity which will provide a constant air mass flow rate. Then hot and cold water flows through the

wind tunnel inbuilt heat exchanger that has flow control and mixing valves to manage the inlet temperature of the air.

- Once the air inlet temperature and secondary circuit reaches steady state of the desired values, the main circuit gear pump is turned on letting primary fluid, water, passes through the system. Mass flow rate of the primary fluid is controlled using the pump frequency. It usually takes about 30 minutes for the whole system to reach steady state.

- While the system is running, the data acquisition system is used to monitor and record temperatures and pressure readings. Once it is steady, a step change in the primary fluid mass flow rate is applied. This is done by changing the frequency of the gear pump to the final mass flow rate.

- This experiment is repeated for the next step change in mass flow rate.

2.3 Data Reduction for the experiments

Assumptions considered for the current analysis are as follows: heat transfer from or to the environment is negligible, axial heat conduction in the heat exchanger is negligible, and there is no phase change in the fluids. For the purpose of generalizing the findings, parameters were made dimensionless and presented in the following equations.

The dimensionless temperature is determined as,

$$T_{h,o}^* = \frac{T_{h,o}\,(t^*) - T_{c,in}}{T_{h,in} - T_{c,in}} \qquad\qquad 2.1$$

The dimensionless time is defined as the time divided by the residence time (t_{res}). The time is calculated from the instance the step change occurs.

28

$$t^* = \frac{t}{t_{res}} \qquad\qquad 2.2$$

While, the residence time represents the time that takes the liquid to enter and leave the heat exchanger,

$$t_{res} = \frac{n A_c L}{\dot{\forall}} = \frac{L}{V} \qquad\qquad 2.3$$

Reynolds number for the primary fluid is simplified as given below,

$$Re_w = \frac{\rho_w v_w D_{h,w}}{\mu_w} = \frac{\dot{m}_w}{17 \pi \mu_w D_{h,w}} \qquad\qquad 2.4$$

2.4 Uncertainty analysis

The uncertainty in the experimental data are due to two components: bias (B) and precision (P). There are two types of parameters that are included in the calculation, dependent parameters that are functions of measured variables such as air/liquid heat transfer and fluid flow parameters, thermophysical properties, and geometric dimensions. Independent parameters, however, can be directly measured, for example the simple geometric dimensions and the measured fluids parameters. Another source of uncertainty can be found in the DAQ system which is accounted for in this work. The overall uncertainty of a single measured data is found using the Root Sum Square (RSS) method [17] as shown in the following equation.

$$U_x = \pm \sqrt{B^2 + P^2} \qquad\qquad 2.5$$

Where, the precision and bias errors are calculated according to the subsequent equations,

$$P = \pm\sqrt{P_1^2 + P_2^2 + P_3^2}$$ 2.6

$$B = \pm\sqrt{B_1^2 + B_2^2 + B_3^2}$$ 2.7

While, total precision and Bias errors are based on the elemental precision and bias errors.

When considering the uncertainty of multiple samples with a confidence level of 95%, the following equation is used.

$$U_{x(0.95)} = \pm\sqrt{B^2 + (t_{v,95\%}P)^2}$$ 2.8

It is very essential to take into consideration the sources of errors that influence the end results of the measured variables. The following is a set of equations to show the uncertainty calculated for the major variables used in the results. The overall uncertainty in the air mass flow rate can be found using the RSS method of finding the uncertainties of velocity, frontal area, and the density as in the following,

$$\dot{m}_a = f(A_{fr},\ v_a,\ \rho_a) = A_{fr} \cdot v_a \cdot \rho_a$$ 2.9

$$U_{\dot{m}_a} = \pm\sqrt{\left(\frac{\partial\dot{m}}{\partial A_{fr}} \cdot U_{A_{fr}}\right)^2 + \left(\frac{\partial\dot{m}}{\partial v_a} \cdot U_{v,a}\right)^2 + \left(\frac{\partial\dot{m}}{\partial\rho} \cdot U_{\rho,a}\right)^2}$$ 2.10

$$U_{\dot{m}_a} = \pm\sqrt{(\rho_a \cdot v_a \cdot U_{A_{fr}})^2 + (A_{fr}\rho_a \cdot U_{v,a})^2 + (A_{fr}v_a \cdot U_{\rho,a})^2}$$ 2.11

The data acquisition system uncertainty is considered using the uncertainties in the DAQ card and the signal conditioner SCXI which is shown in the following equation,

$$U_{DAQ\ system} = \pm\sqrt{B_{DAQ\ card}^2 + B_{SCXI}^2}$$ 2.12

The total uncertainty in the inlet air and water temperature is comprised of the uncertainty in the data acquisition system as well as the uncertainty in the thermocouples or RTDs readings. The RTD or thermocouples uncertainty is found using equation 2.8 and the final air/water temperatures uncertainty is given as,

$$U_{T,a} = \pm \sqrt{U_{DAQ}^2 + U_{Thermocouples}^2} \qquad 2.13$$

$$U_{T,w} = \pm \sqrt{U_{DAQ}^2 + U_{RTD}^2} \qquad 2.14$$

The expression for Re_w is found in equation 2.4 and therefore, the uncertainty in Re_w is determined in the following equation,

$$U_{Re_w} = \pm \sqrt{\left(\frac{\partial Re_w}{\partial \dot{m}_w} U_{\dot{m}_w}\right)^2 + \left(\frac{\partial Re_w}{\partial \mu_w} U_{\mu_w}\right)^2 + \left(\frac{\partial Re_w}{\partial D_{h,w}} U_{D_{h,w}}\right)^2} \qquad 2.15$$

The estimated uncertainties of the main parameters are shown in Table 2.2.

Table 2.2 Estimated Uncertainties

Parameters	Mean value	Uncertainties %
$T_{a,i}$ (°C)	13	± 7.6
$T_{w,i}$(°C)	70	± 1.1
Mass flow rate of air, $\dot{m}_a$, (kg/s)	0.22	± 0.98
Mass flow rate of water, $\dot{m}_w$ (kg/s)	0.01 to 0.04	± 1.5
D_h (m)	0.001	± 3.48
$A_{fr,a}$ (m^2)	0.03097	± 0.16

2.5 Results and discussion

2.5.1. Step change in water mass flow rate

Figure 2.7 shows the repeatability for various step changes of water mass flow rates with respect to time. The experiment is repeated 3 times to check the short and long-term repeatability. Outlet temperatures measurements are found to be within 2% for all the experimental trials. To check the accuracy and repeatability of the data, the experiment was repeated at different periods of time. The system runs at the same conditions for three times, every time the data was recorded. It was found that changes along the runs are found too small to be considered with a repeatability of less than 3%. This emphasizes that the data collected are very accurate. Different positive and negative step changes are implied: 2.0, 1.5, 0.8, and 0.5 by changing the mass flow from 20 to (10, 16, 30 and 40) g/s.
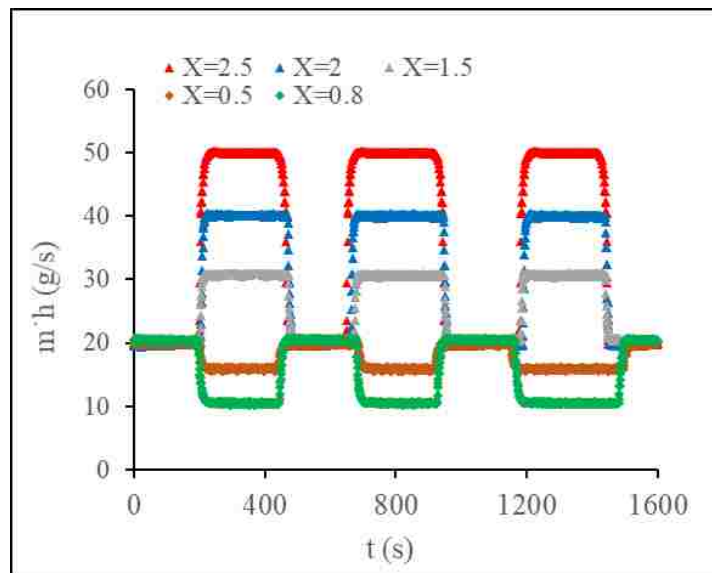
Figure 2.7 Fluid mass flow step change with time

2.5.2. Effect of step change on the outlet water temperature

Figure 2.8 shows the comparison of temperature responses of the outlet hot fluid subjected to inlet flow maldistribution. Two cases of positive and negative step changes are considered: the first case is for a step change of 1.5 and 2.0. It can be noticed that for a

32

higher step change, the response time, the time the heat exchanger takes to reach the steady state, is shorter than that at lower step change. For a step of 2, the response time is 55s compared to a step of 1.5 which gives 60s. The residence time is lower when the step is 2.0 compared to a step of 1.5 because more flow is being forced through the channels. A 15% lower residence time is found for the higher step compared to the lower. As the mass flow rate increases, lower temperature drop between inlet and outlet is obtained since the time it takes to transfer the heat between the fluids is shorter.
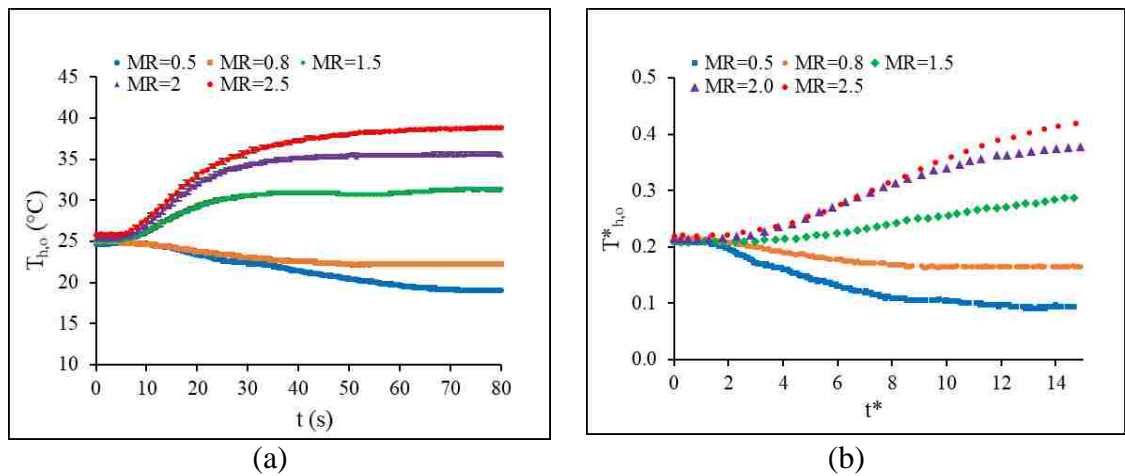
Figure 2.8 Flow maldistribution effect on hot fluid outlet temperature

The second case is varying the mass flow rate in a negative step change of 0.5 and 0.8. When comparing the two cases together, the negative and positive step changes, a symmetrical trend cannot be found but a similar conclusion can be derived for the temperature drop. However, it is the opposite for the response time which is found to be 70s for a step of 0.5 and 65s for step of 0.8. An observation of an initial delay time is noticed for all the step changes and increases as the step change decreases. The uncertainties of the experimental data are calculated and included in the results. The faster response time for the higher mass flow step variation could be explained by the increase in

33

the heat transfer coefficient. The increase of mass flow rate results higher Reynolds number and consequently increase the thermal entrance length as well as heat transfer coefficient.

2.5.3. *Effect of m_w step change on the outlet air temperature*

The cold fluid temperature response as the hot fluid is subjected to a step change in its mass flow rate is shown in Figure 2.9. The airside conditions are kept constant at Reynolds number of 1900 and inlet temperature of 13°C. For a higher step change, the trend of the curve is found steeper. The response time at different steps 2.5, 2, 1.5, 0.8, and 0.5 is approximately 20, 27, 34, 45, and 56 s. The response time for the airside decreases with the increase in the step change. A delay time is also observed for the air outlet temperature, but it is found shorter when compared to the results of water. The effect of mass flow step change on the response time, residence time and their ration are illustrated in figure 2.10.
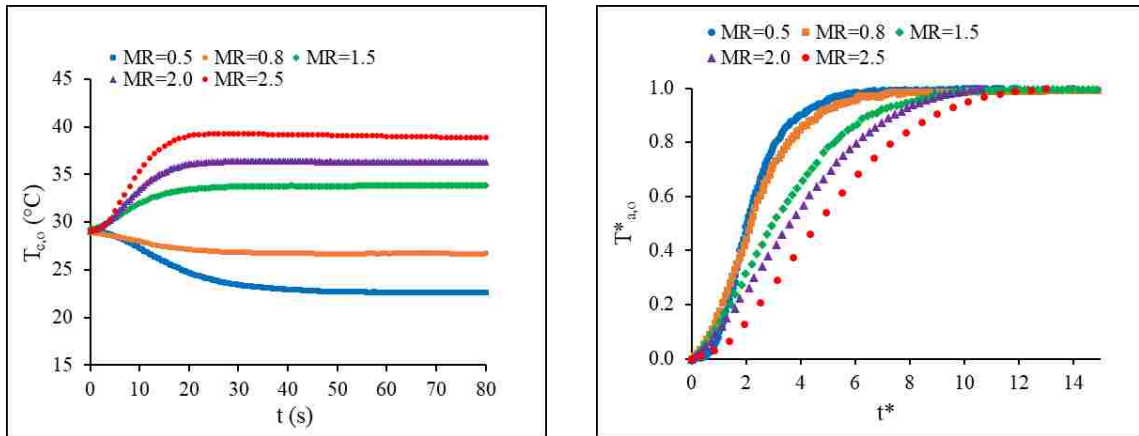
Figure 2.9 Flow maldistribution effect on cold fluid outlet temperature
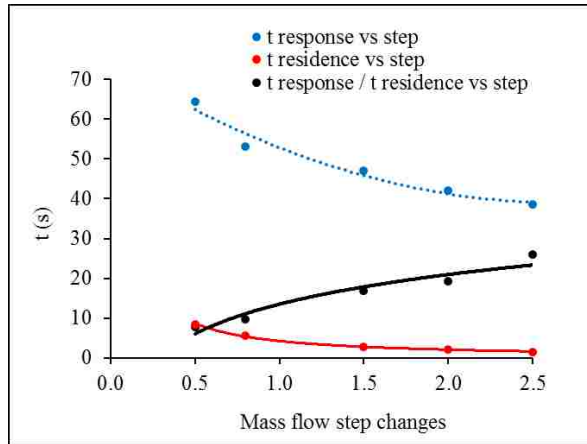
Figure 2.10 Response, residence, and their ratio effect on mass flow changes

2.5.4. Dimensionless temperature variation at different Re_w

The dimensionless temperature response as Re_w changes is shown in Figure 2.11. The step change in the hot fluid mass flow rate increases Reynolds numbers. Two conclusions can be reached; the first one, for a positive step change, the initial delay time increases as Reynolds number increases. The second conclusion for the negative step change case, the delay time decreases as Reynolds number increases. The end of each curve represents the final steady state. Which means longer time to reach the steady state conditions for higher Re numbers. The calculated Reynolds numbers were found to be 420 to (185, 310, 760 and 1040) putting the primary fluid in the laminar regime.
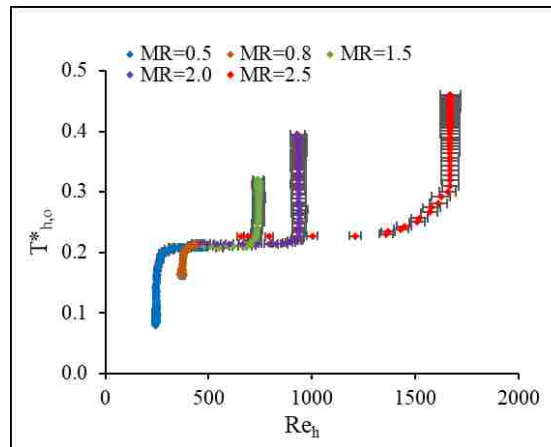
Figure 2.11 Water Reynolds numbers versus dimensionless temperature

2.5.5. *Comparison of results with literature (previous work)*

2.5.5.1 Comparison of results for the airside

Figure 2.12 shows the current experimental results comparison with the results obtained by Pearson et al. [12]. The dimensionless airside outlet temperature, defined in equation 2.16, with respect to time is illustrated in the figure. At the step change of 0.5 for both studies, the current time constant 44s is much higher than that of the compared result 2.3s. They have shorter time constant since their mass flow rate is 5 times higher than the current results as well as bigger tube size compare to the small channel diameter.

$$T_{a,o}^* = \frac{T_{a,o}\,(t^*) - T_{a,i}}{T_{ao,f} - T_{ao,i}} \qquad\qquad 2.16$$

The heat exchanger used in the referenced work was tube and plate-fin liquid to air cross flow arrangement. Both studies seem to follow a similar trend, but their temperature transient response is found steeper. A delay time of 10s is found in this study while no initial delay can be seen with the reference work.
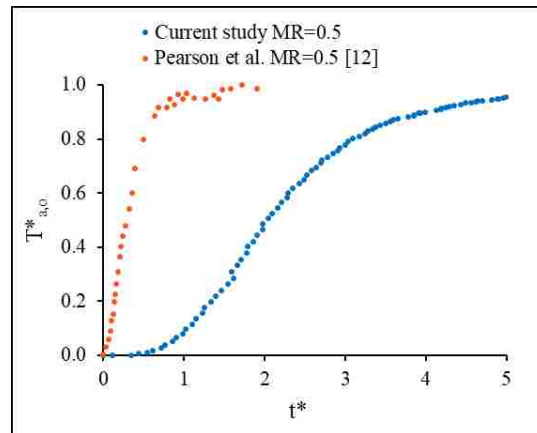
Figure 2.12 Effect of flow rate change on airside temperature compared with Pearson et

al. [12]

2.5.5.2 Comparison of results for the waterside

There are some numerical and analytical analyses done on the transient response of the

heat exchangers due to step change in a fluid mass flow rate. However, it is very difficult

to find experimental work. A recent work of [16] can be considered as good comparison to

current study. The present multi-slab cross flow minichannel heat exchanger is compared

to a liquid to air tube heat exchanger. The comparison is made in terms of dimensionless

parameters for temperature and time. The compared step changes are 2 and 4.8 for the

current and the referenced work respectively as show in Figure 2.13. It is found that the

total response time of 55s is needed for this study to bring the temperature outlet of the hot

fluid from (25-35) °C, while it takes 10s for the hot fluid temperature in the reference to

change approximately from (44-48) °C, Del Valle et al. [16]. Therefore, the difference in

the response time can be interpreted by the difference in the step change which is 2.4 times

and the differences in the outlet temperatures which are 10°C for the current compared to

4 °C for the referred work. The change in T* represents the change in the outlet temperature

37

of the heat exchanger, the lower T* is, the lower outlet temperature keeping all other parameters constant. The graph shows that the presented study provides very low T*.
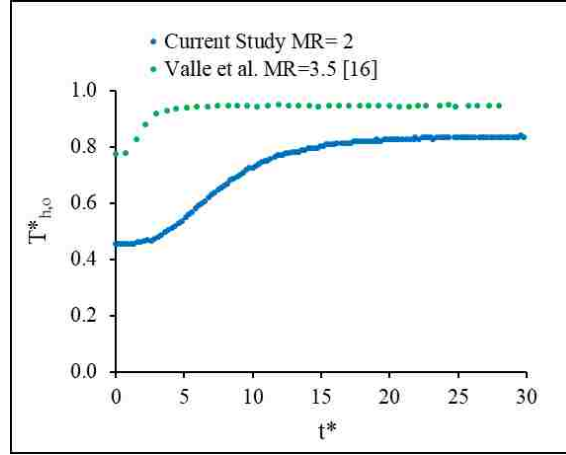
Figure 2.13 Dimensionless temperature vs. dimensionless time with comparison to Del Valle et al. [16]

In the present heat exchanger, the water mass flow rate is distributed into 68 channels equally compared to a single tube as in the referred study. Longer residence time is found from the current results as t* is smaller. Higher residence time can be interpreted as more time for the heat transfer between the two fluids to occur and this is obvious from the rise change in the outlet temperature.

Current experimental results are used for comparison with Idrissi et al. [14] in terms of dimensionless time and temperature, as shown in Figure 2.14. The compared heat exchanger is a double pipe counter flow, liquid to liquid heat exchanger while a liquid to air cross flow minichannel heat exchanger is used in the current study. Longer time is required for this study to reach steady which is represented by the first-order time constant of 27s, when compared to 7s, [14]. A sharp increase of the temperature when the transient

condition is applied can be seen in the referenced results while a gradual evolution is noticed in the current experiment. The difference that is noticed in the graph between the current results and the referenced one is due to several factors: the flow arrangement, the tube diameter, mass flow, and the tube length. These parameters can affect the temperature results to be higher or lower. The residence time of the double pipe was found 252 to 70s for a 4.5m long tube compared to the present heat exchanger that has a 1.6m long channel and a residence time of 4.5 to 2.2s. This corresponds to a step change of 2.0 for the current investigation compared to 3.6.
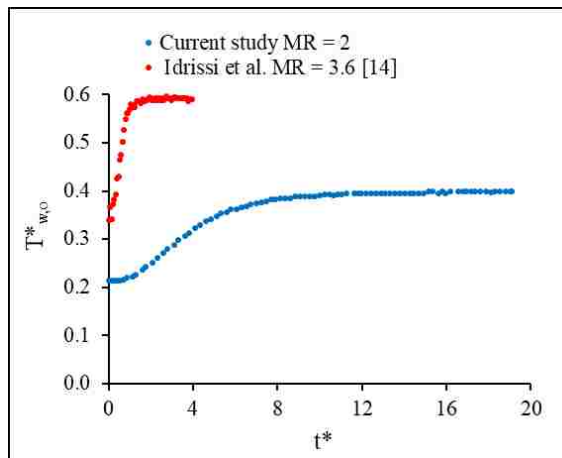
Figure 2.14 Flow maldistribution effect on hot fluid outlet temperature compared to Idrissi et al. [14]

2.6 Conclusion

Experiments were conducted on a serpentine cross flow minichannel heat exchanger subjected to different step changes in hot fluid mass flow rate. The step changes used are 0.5, 0.8, 1.5, 2.0 and 2.5 in the current work, a designed and built test facility that can perform transient experiments on a minichannel cross flow heat exchanger is used. The experimental setup is designed to accommodate accurate control on the fluid inlet

parameters such that varying the primary fluid mass flow rate in a step change while keeping the other parameters fixed. The behavior of the heat exchanger in terms of its outlet fluid temperatures is examined.

The outlet temperatures of the fluids do not respond instantly to the change in the primary fluid mass flow rate which is shown by the delay time. However, the cold fluid showed a faster response time of its outlet temperature to flow rate change than the hot fluid. It is likewise observed that the inlet to outlet temperature drop of the primary hot fluid is higher than the temperature rises of the cold fluid. The $\dot{m}c_p$ of airside is higher compared to water side. A step change in mass flow rate increases Re number which leads to faster response time for the primary fluid to reach the steady state. An initial delay time is found, and it increases with the increase of the mass flow rate step change. An asymmetric trend between the positive and negative step changes was found with respect to response time as the mass flow rate changes.

The experimental results found from this study are compared with the limited experimental findings on transient response of double pipe, and tube and flat fin heat exchangers available in literature. When observing the effect of the step of mass flow rate with respect to dimensionless time for all the compared studies and the current heat exchanger, it is found that the dimensionless time is the highest in the case of the current study heat exchanger. That can be due to the small cross-sectional area and the length of the channels that resulted in a lower residence time. The fluctuation of the outlet fluid temperature is noticed to be less with the use of a minichannel heat exchanger compared to other exchangers when all were subjected to step change in mass flow rate. It is recommended

for heat exchangers manufacturers to include the response time with their product as part of specification.

Nomenclature

A_c Channel cross section area, m^2

D Diameter, m

D_h Channel hydraulic diameter, m

L Channel length along the water fluid, m

$\dot{m}$ Mass flow rate, kg/s

n Number of channels

Re Reynolds Number

T Temperature, °C

t Time, s

t_{res} Resident time, s

v Velocity, m/s

$\dot{\forall}$ Volume flow rate m^3/s

X Mass flow step change

Greek symbols

β Area density, m^2/m^3

μ Dynamic viscosity

ρ *Mass density, kg/m^3*

Subscripts

a   *Air stream*

c   *Cold fluid*

f   *Final*

i   *Initial*

in   *Inlet*

h   *Hot fluid*

o   *Outlet*

w   *Water stream*

Superscripts

*   *Non-dimensional parameters [2]*

References

[1] S. G. Kandlikar and W. J. Grande "Evolution of Microchannel Flow Passages—Thermohydraulic Performance and Fabrication Technology" Heat Transfer Eng., 24: 3–17, 2003.

[2] Engr Sarbadaman Dasgupta, Serena Askar, Mohammed Ismail, Amir Fartaj, Md Abdul Quaiyum "Air cooling by multiport slabs heat exchanger: An experimental approach" Experimental Thermal and Fluid Science, Volume 42, October 2012, Pages 46-54.

[3] M. E. Steinke and S. G. Kandlikar "Single-Phase Liquid. Heat Transfer in Plain and Enhanced Microchannels" Proceedings of ICNMM2006 Fourth International Conference on Nanochannels, Microchannels and Minichannels June 19-21, 2006, Limerick, Ireland. ICNMM2006-96227.

[4] W. Qu and I. Mudawar "Experimental and numerical study of pressure drop and heat transfer in a single-phase micro-channel heat sink" Internat. J. Heat Mass Transfer 45 (2002) 2549–2565.

[5] S. Fotowat, M. Ismail, M. A. Quaiyum, S. Askar, and A. Fartaj "Experimental study on air-heating through a cross-flow minichannel heat exchanger" CSME Biennial International Conference, Winnipeg, Manitoba, Canada, June 2012, (1569554279).

[6] Ismail, S. Fotowat, and A. Fartaj "Effect of Channel Size on Heat Transfer and pressure drop in Thin Slabs" ICMEM International Journal of Mechanical Engineering and Mechatronics, 2(1): 33-42, 2014, DOI: 10.11159/ijmem.2014.004.

[7] N. Srihari, R. B. Prabhakara, S. Bengt, and K. D. Sarit "Transient response of plate heat exchangers considering effect of flow maldistribution" International Journal of Heat and Mass Transfer, 48(15): 3231-3243, 2005.

[8] P. Regulagadda "Transient Heat Transfer Analysis of Heat Exchangers in a Marnoch Heat Engine" Master thesis, University of Ontario Institute of Technology, Oshawa, Ontario, 2009.

[9] J. Yin, M. K. Jensen "Analytic model for transient heat exchanger response" International Journal of Heat and Mass Transfer, 46(17): 3255-3264, 2003.

[10]   K. Silaipillayarputhur and S. A. Idem "Transient Response of a Cross Flow Heat Exchanger Subjected to Temperature and Flow Perturbations" ASME. ASME International Mechanical Engineering Congress and Exposition, Volume 8A: Heat Transfer and Thermal Engineering: V08AT10A019. DOI: 10.1115/IMECE2015-52562.

[11]   F. J. Stermole and M. A. Larson "The dynamics of flow forced distributed parameter heat exchangers" AIChE J., 10: 688–694, 1964, DOI:10.1002/aic.690100522.

[12]   J. T. Pearson, R. G. Leonard, and R. D. McCutchan "Gain and time constant for finned serpentine crossflow heat exchangers" ASHRAE Trans 80(11):255–267, 1974.

[13]   J. R. Gartner "Simplified dynamic response relations Control of Dynamic for finned-coil heat exchangers" ASHRAE Transactions, 78 Part 2: 163-169, 1972.

[14]   M. A. Abdelghani-Idrissi, F. Bagui, and L. Estel "Analytical and experimental response time to flow rate step along a counter flow double pipe heat exchanger" International Journal of Heat and Mass Transfer, 44(19): 3721-3730, 2001.

[15]   M. K. Chopra and R. S. Prajapati "Thermal performance analysis of cross-flow unmixed-unmixed heat exchanger by the variation of inlet condition of hot fluid" International Refereed Journal of Engineering and Science (IRJES), 3(1): 29-31, 2014, ISSN 2319-183X.

[16]   M. del Valle, C. Caceres and A. Ortega "Transient modeling and validation of chilled water based cross flow heat exchangers for local on-demand cooling in data centers" 15th IEEE Intersociety Conference on Thermal and Thermomechanical Phenomena in Electronic Systems (ITherm), Las Vegas, NV, 727-736, 2016. DOI: 10.1109/ITHERM.2016.7517619.

[17]   R. S. Figliola and D. E. Beasley "Theory and design for mechanical measurements" Wiley, New York; Chichester, 4th ed., 2006.

CHAPTER 3

TRANSIENT RESPONSE OF A MESO HEAT EXCHANGER WITH EMPERATURE

STEP VARIATION

3.1. Introduction

Heat exchangers are widely used equipment in many industries. Their significant existence

in industrial systems is due to their need in transferring the heat from one medium to

another. Many industrial systems are required to work with a certain temperature and in

order to protect these systems from overheating and damaging the equipment; a heat

exchanger is used to ensure the function of the system within safe operating conditions.

Another gain from heat exchangers is to make use of the wasted heat released by a process

and use it in another process that leads to energy and cost savings.

A heat exchanger classification by Shah and Seculik [1] arranged heat exchangers into

categories according to many considerations such as: transfer process, surface

compactness, number of fluids, flow arrangement, etc. One important category is the

surface compactness due to the recent urgent needs in many applications to utilize compact

and highly effective exchangers with reduced weight, space and cost. Their classification

set a distinctive line distinguishing a compact from a conventional heat exchanger for gas

to liquid as 700 m^2/m^3 above which any heat exchanger is considered compact. They

considered the hydraulic diameter that can be used to separate compact from non-compact

exchangers to be Dh $\leq$ 6mm. within the compact heat exchangers category, other

classification is considered, when the surface area to volume ratio is more than

3000m2/m3, the heat exchanger is called meso heat exchanger corresponding to a hydraulic

diameter between 1µm $\leq$ Dh $\leq$ 1mm.

The current investigation is concerned with the use of a heat exchanger that has a surface area density (β) of 4000m2/m3 and according to [1], it is called a meso heat exchanger. Extensive studies regarding this type of a heat exchanger have been conducted to provide information regarding its thermal performance under steady state conditions [2-6]. These investigations proved that this type of heat exchangers delivers high heat transfer rate with enhanced thermal efficiency.

The requirements of any thermal system are higher heat transfer rate and efficiency, lower cost, and energy saving. A heat exchanger usually is a single component of a multi component system such as in residential HVAC or automotive industry. Consequently, enhancing the exchanger thermal performance results in improved overall system efficiency. Most heat exchanger analysis is performed assuming steady state operations. Any change that may occur on the steady state conditions of a process may lead to a substantial effect on its behavior and on the safety of operation. It is important to be acquainted with the knowledge on the dynamic performance of the heat exchanger for reasons of designing, controlling and safety handling. In most heat exchanger analyses, theoretical assumptions of steady state operations are made, however, it is very difficult to maintain these steady conditions and a transient behavior will occur. Adding to that, certain cases of starting, shutting down the system and breakdown may occur. This signifies the need for the transient response investigation of the heat exchanger.

Studies on heat exchangers working under steady state operation are widely published and discussed whether numerical, analytical, or experimental analysis or a combination of any two of them. On the other hand, due to the difficulty in running a setup with transient state

operating conditions, very limited investigations on the dynamic response of heat exchangers can be found and the available ones are using either numerical or analytical. Rare experimental work can be found with limited range of operating conditions. The following are some of the published work concerning investigating the transient response in heat exchangers.

An early numerical analysis was done by Romie [7] for a counter flow heat exchanger subjected to a step change in the inlet temperature of either of the working fluids. The exit temperature responses were studied using a finite difference method and shown in simple empirical equations. Gao et al. [8] performed another numerical study on transient response of step, ramp and exponential changes in the inlet temperature of an unmixed-unmixed cross flow heat exchanger. They used transient effectiveness method to build the analytical models that were used to analyze the transient behavior of cross flow heat exchangers. Their results were compared with the experimental transient response of an IBM rear door heat exchanger and were found to be in a good agreement.

Abdallah and Rooke [9] considered a finned-tube cross flow liquid to gas heat exchanger to study its thermal response. They applied a step change to the liquid inlet temperature and obtained the analytical solutions of the outlet temperatures as a function of time and location using Laplace Transform method. The effect of NTU on the thermal performance of the heat exchanger was presented. Other geometry consideration of the serpentine coil was also considered, and they found that the tube bend possessed significant effect on some heat exchangers. Asgharpour et al. [10] studied analytically and experimentally the transient performance of coupled heat exchangers exposed to sudden change in inlet

temperature. The effect of the reduction in the air inlet temperature of an air cooler on fluid exit temperatures was examined. An air-cooler heat exchanger was subjected to the temperature change by means of using an evaporative cooling. A Matlab model with sets of partial differential equations were employed in the analytical solution and results were verified using the experimental data. Their work also investigated other parameters effect on the transition time such as: connecting pipes length, mass flow rate, and the heat transfer coefficient.

Zhang et al. [11] experimentally and numerically studied the transient heat transfer of a C-shaped rod bundle heat exchanger that is used in reactors as a passive residual heat removal. To analyze the heat transfer, they used empirical equations along with the numerical turbulent model. Different turbulence models and eddy simulation were investigated then results were validated by experimental data. Higher heat transfer rate is found in the vertical section than in the horizontal section. Adding to that, flow velocity, turbulent mixing, and flow resistance showed an effect on the heat transfer of the heat exchanger. A minimum capacity rate fluid in a single pass cross flow heat exchanger was selected for step changes in temperature, Syed and Idem [12]. Numerical analysis based on the finite difference method was used to present the prediction of changing the grid size and time steps in the study. Their observation was that transient time was reduced with smaller capacity rate ratio for both fluids outlet temperatures. A compared case of the minimum and maximum capacity rate ratio led to the conclusion of smaller temperature change found in the maximum capacity rate ratio compared to the minimum. Adding to that, larger NTU values resulted in higher time needed to reach steady state condition.

Ataer [13] obtained an analytical method to predict the transient performance of a cross flow heat exchanger when the hot fluid is subjected to inlet temperature change in a step form. He took into consideration the heat capacity of fins, walls, and the fluids. Results of exit fluid temperatures were presented in terms of delay time, gain, and time constant. His model was compared with numerical and experimental results from a previous work by Ataer [14] and found good agreement.

Studied on the cross-flow heat exchanger was extended to include transient temperature response done by Mishra et al. [15]. They used numerical analysis on two unmixed fluids considering the finite wall capacitance with inlet temperature and flow rate variations. The hot fluid inlet temperature was changed in a step, exponential, ramp, and sinusoidal form. They concluded that for any case of step, ramp, or sinusoidal, the exit temperature variation depended on the magnitude of disturbance given to the fluid. For high disturbance in the hot fluid, the exit temperature found increasing while; it is the opposite case for the cold fluid. Silaipillayarputhur and Idem [16] studied a model to predict the transient performance of a multi-pass cross flow heat exchanger. The fluids used were unmixed in the pass and mixed between the passes. Steps in the inlet temperature and mass flow rates of the fluids were considered. Results from their study were presented and compared to steady state predictions from the literature which yielded good agreement. A recent experimental investigation done by Valle et al. [17] used to validate a model created by them is performed. For their model and experiments, a cross flow water to air heat exchanger was used. The study included a single variation in the water inlet temperature and mass flow rates in a step, sinusoidal, and ramp changes. Their results showed a good agreement between experiments and numerical model.

49

The limitation of the work discussing the transient response of compact heat exchangers and the necessity to acquire experimental data were the motivations of this study. The advancement in technology systems and processes require an understanding of each component of the system while a change in the operating conditions may occur. For better representation of exchanger designs, a dynamic thermal response study of this equipment is essential as a step to enhance its performance. The work of this paper presents an experimental dynamic analysis of a cross flow meso heat exchanger as the inlet temperature of the hot fluid changes in a step form. Both fluids mass flow rates are held constant as well as the cold fluid inlet temperature. Heat is transferred from the hot DI water to the cold air. The heat transfer rates are calculated for both fluids and their behavior is presented with respect to time. The effect of step changes on the response of the exit temperatures of both fluids and the thermal performance of the heat exchanger is discussed. Uncertainty analysis for the experimental data is performed and accounted for when plotting the results. A final heat balance error to show the amount difference of heat transfer of the two fluids is demonstrated.

3.2. Experimental setup

The primary objective of this work is to investigate the transient behavior of a compact heat exchanger. To achieve this goal, a unique experimental setup as shown in Figure 3.1 is constructed and a schematic of the basic components of this setup is illustrated in Figure 3.2. The main working fluids used are Deionized (DI) water as the hot fluid and air as the cold fluid. The system comprises sections of fluid inlet, test section, and fluid outlet. Measurement devices are placed at each fluid inlet and outlet sections for temperature and pressure readings. To monitor, display, and record the data obtained from experiments, a

50

data acquisition is connected to the system equipped with LabVIEW software. Preliminary tests were carried out to check for the range of operating temperatures the fully instrumented system is capable of and its accuracy in repeating the same measurement. Considering the measured parameters along with the fluids and their instrumentations, the setup is divided into three cycles as in the following.

3.2.1   Air side cycle

The airside cycle comprises a thermal wind tunnel that provides the system with air at various flow rates and temperatures. The air cycle includes filters, strainers, and in-built heat exchanger to ensure uniform flow at a set temperature passes through the test section. Air is delivered to the test section using an upstream frequency variable blower while temperature is controlled through the use of an in-built heat exchanger. Constant air velocity and temperature are forced to flow by means of an air blower to the test section. For the current investigation, the inlet temperature and mass flow rates of air are held constant and their values with their uncertainties can be found in table (3.1).

3.2.2   Test section

The test section location is in the center of the wind tunnel and encompasses the meso heat exchanger. The fully insulated Polycarbonate sheet test section ensures no heat transfer between the heat exchanger and the surrounding. While air flows through the test section by the wind tunnel, DI water is also allowed to flow through pipes to the heat exchanger's channels. Some of the heat exchanger specifications are listed in table (3.2). The test section is designed in a way that different compact heat exchangers can be installed in it.

<div align="center">(a)</div>
<div align="right">(b)</div>
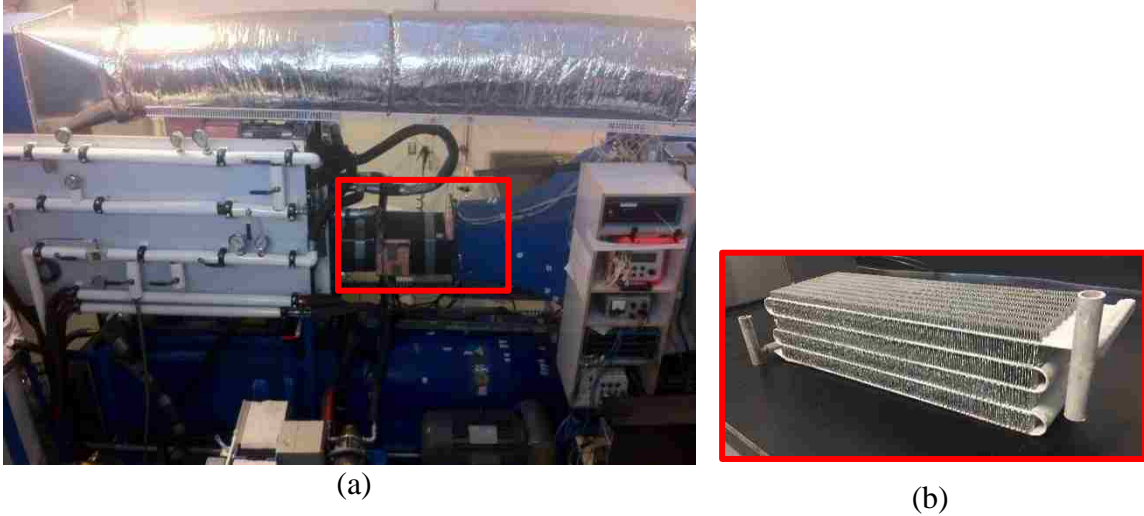
Figure 3.1 (a) Experimental set up, (b) Meso heat exchanger

Table 3.1 Heat exchanger Specifications

Heat exchanger specifications	Dimensions
Channel diameter (m)	*0.001*
No. of channels in a slab	*68*
No. of slabs	*5*
Slab thickness (m)	*0.002*
No. of serpentines	*4*
Channel length of (m)	*1.658*
slab length (m)	*0.305*
Slab width (m)	*0.1*
Slab height (m)	*0.102*
Fin density (fins per inch)	*12*

3.2.3 *Liquid side circuit*

The water cycle has two parts, main and secondary circuits. The main circuit provides the flow of DI water at constant inlet room temperature. Then a portion of this DI water is sent to exchange the heat with the secondary circuit that consists of plate heat exchangers while the rest bypasses these exchangers by means of a flow adjustment valve. Once the heat transfer between the two fluids occurs, the hot DI water flows through the small channels to the heat exchanger at a constant temperature. To force the flow of DI water through the heat exchanger, a gear pump is used. Several temperature and pressure gauges and RTDs are installed at the DI water flow line. As well as, a Coriolis mass flow meter to measure the DI water flow rate as it passes to the heat exchanger. To achieve the step change, the hot DI water is mixed with the cold DI water bypassed the plate heat exchangers to reach the desired inlet temperature value. The DAQ system allows the recording and monitoring the various data of temperature, pressure, and mass flow rates. The 20kW inline immersion heater, has an accuracy of controlling up to 0.1°C, is capable to provide a wide range of temperatures that can be used for applying the step changes.
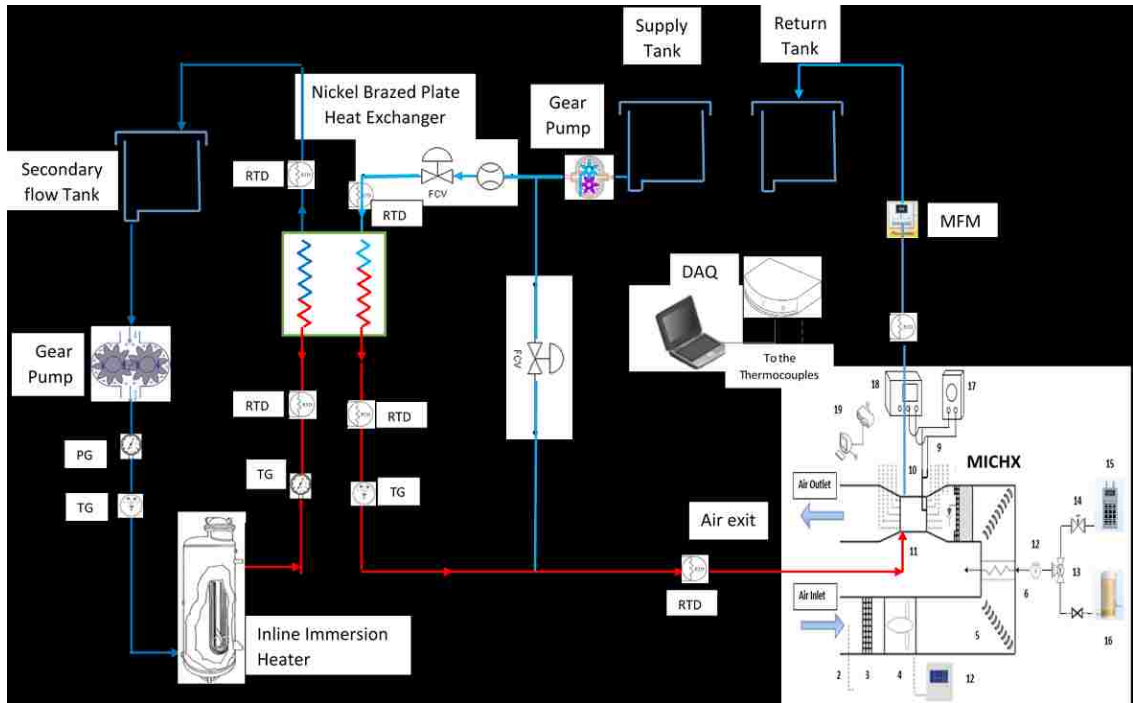
Figure 3.2 Schematic diagram of the experimental set up

3.2.4 Air temperature measurement

Figures 3.3a and 3.3b, illustrate the thermocouples arrangement at the upstream and downstream of the airside. Equally spaced 9 thermocouples at the inlet of the test section and 18 thermocouples at the outlet are installed inside the wind tunnel to measure the inlet and outlet temperatures of air across the test section.

The airside temperature in this work is maintained at a constant value throughout the whole experiment. The measurement readings obtained from the thermocouple grids is recorded by the data acquisition system (DAQ).
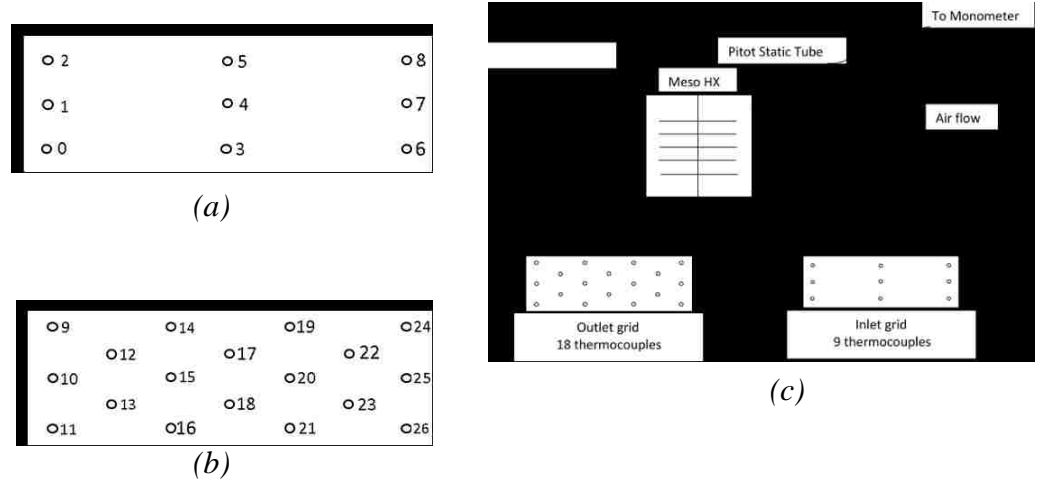
Figure 3.3 (a) Airside inlet thermocouples grid, (b) Airside outlet thermocouples grid, and (c) Cross section of the wind tunnel with the test section and the grids

3.3. Data Reduction

The process of data reduction uses the equations to find out the exit temperatures of both fluids and the thermal performance of the heat exchanger represented by effectiveness, heat transfer rate, and the heat balance. When analyzing results, some assumptions are made and are listed as follows: negligible axial heat conduction in the heat exchanger, no heat transfer from or to the environment, and no fluids phase change occur. Dimensionless parameters were also considered and are shown in the following equations.

Dimensionless outlet temperatures based on Gao [18] can be found as,

$$T_{h,o}^{*}(t) = \frac{T_{h,o}(t) - T_{c,in}(t)}{T_{h,in}(t) - T_{c,in}(t)} \qquad 3.1$$

$$T_{c,o}^{*}(t) = \frac{T_{c,o}(t) - T_{c,in}(t)}{T_{h,in}(t) - T_{c,in}(t)} \qquad 3.2$$

The residence time is defined as the length of the channel divided by the velocity of DI water which shows the time it takes the main hot fluid to pass through the heat exchanger,

$$t_{res} = \frac{nA_cL}{\dot{\forall}} = \frac{L}{V} \qquad \text{3.3}$$

When the time is divided by the residence time, a dimensionless time is reached as,

$$t^* = \frac{t}{t_{res}} \qquad \text{3.4}$$

Reynolds number for hot DI water is calculated based on the geometry of the heat exchanger used in this work. The DI water mass flow rate is kept constant at $Re_w \approx 1400$ and is given as,

$$Re_w = \frac{\rho_w v_w D_{h,w}}{\mu_w} = \frac{\dot{m}_w}{17\pi\mu_w D_{h,w}} \qquad \text{3.5}$$

The heat transfer effectiveness ε is defined as the ratio of the actual heat transfer rate to the maximum possible heat transfer rate Cengel [19] using the energy balance of the hot and cold fluids. The effectiveness can be expressed in terms of the heat capacity rate and the temperatures of the two fluids. The equations of effectiveness for the steady states are extended to include time under transient variation by Cima and London [20] as follows,

$$\varepsilon_h(t) = \frac{C_h\left(T_{h,in}(t) - T_{h,out}(t)\right)}{C_{min}\left(T_{h,in}(t) - T_{c,in}(t)\right)} \qquad \text{3.6}$$

$$\varepsilon_c(t) = \frac{C_c\left(T_{c,out}(t) - T_{c,in}(t)\right)}{C_{min}\left(T_{h,in}(t) - T_{c,in}(t)\right)} \qquad \text{3.7}$$

Normalized temperatures of both fluids based on their outlet temperature are defined in eqns. 3.8 and 3.9. These equations represent the ratio of the fluid outlet temperature

difference from initial to a certain time to the difference from initial to final time reaching

the steady state as seen in the following,

$$T'_{h,o}(t) = \frac{T_{h,out}(t) - T_{h,out}(0)}{T_{h,out}(\infty) - T_{h,out}(0)} \qquad 3.8$$

$$T'_{c,o}(t) = \frac{T_{c,out}(t) - T_{c,out}(0)}{T_{c,out}(\infty) - T_{c,out}(0))} \qquad 3.9$$

The heat transfer rate for each fluid is calculated using the equations provided as follows,

$$\dot{Q}_w = \dot{m}_w \, c_p \, \Delta T_w \qquad 3.10$$

$$\dot{Q}_a = \dot{m}_a \, c_p \, \Delta T_a \qquad 3.11$$

The percentage of error in the heat balance [HB] is found based on the heat transfer rate

difference of the two fluids to the average heat transfer rate as,

$$Error \ in \ heat \ balance \ HB\% = \frac{\dot{Q}_w - \dot{Q}_a}{\dot{Q}_{ave}} \qquad 3.12$$

3.4. Uncertainty analysis

Every measurement device used in the experiments such as RTDs, PTDs, velocity

measurements and mass flow rate devices, etc. has related instrumental errors supplied by

the manufacturer. These errors contribute to the error of the measured data and can be

evaluated using the RSS method as in Figliola and Beasley [22].

$$U_x = \pm\sqrt{B^2 + P^2} \qquad 3.13$$

The precision and bias errors are found from the subsequent equations,

$$P = \pm\sqrt{P_1^2 + P_2^2 + P_3^2} \qquad\qquad 3.14$$

$$B = \pm\sqrt{B_1^2 + B_2^2 + B_3^2} \qquad\qquad 3.15$$

The final uncertainties are conveyed in a 95% confidence level as,

$$U_{x(0.95)} = \pm\sqrt{B^2 + (t_{v,95\%}P)^2} \qquad\qquad 3.16$$

Taking into consideration the sources of errors that contribute to the final results of the experiments is very crucial. These can include: calibration, data acquisition DAQ, and data reduction errors. The uncertainty related to the data acquisition is comprised of the DAQ card and the signal conditioner SCXI and it is given as,

$$U_{DAQ\ system} = \pm\sqrt{B_{DAQ\ card}^2 + B_{SCXI}^2} \qquad\qquad 3.17$$

The final uncertainty associated with the temperatures of the fluids using the RTDs and the thermocouples for measurement is shown in eqns. 18 and 19,

$$U_{T,air} = \pm\sqrt{U_{DAQ}^2 + U_{Thermocouples}^2} \qquad\qquad 3.18$$

$$U_{T,water} = \pm\sqrt{U_{DAQ}^2 + U_{RTD}^2} \qquad\qquad 3.19$$

Reynolds number is calculated based on the mass flow rate, viscosity, and the hydraulic diameter and the total uncertainty that combines all the uncertainties of each parameter is found as,

$$U_{Re_h} = \pm \sqrt{\left(\frac{\partial Re_h}{\partial \dot{m}_h} U_{\dot{m}_h}\right)^2 + \left(\frac{\partial Re_h}{\partial \mu_h} U_{\mu_h}\right)^2 + \left(\frac{\partial Re_h}{\partial D_h} U_{D_h}\right)^2} \qquad 3.20$$

From equations 9 and 10, we found that the heat transfer rate is dependent on the mass flow rate, specific heat, and the temperature difference of the fluid. The total uncertainty of the heat transfer rate for any fluid side is calculated in the following equation,

$$U_{\dot{Q}_h} = \pm \sqrt{\left(\frac{\partial \dot{Q}_h}{\partial \dot{m}_w} U_{\dot{m}_w}\right)^2 + \left(\frac{\partial \dot{Q}_h}{\partial c_{p,h}(t)} U_{c_p}(t)\right)^2 + \left(\frac{\partial \dot{Q}_h}{\partial \Delta T,h(t)} U_{\Delta T}(t)\right)^2 + \left(\frac{\partial \dot{Q}_h}{\partial t} U_t\right)^2} \qquad 3.21$$

$$U_{\dot{Q}_c} = \pm \sqrt{\left(\frac{\partial \dot{Q}_c}{\partial \dot{m}_c} U_{\dot{m}_w}\right)^2 + \left(\frac{\partial \dot{Q}_c}{\partial c_{p,c}(t)} U_{c_{p,c}}(t)\right)^2 + \left(\frac{\partial \dot{Q}_c}{\partial \Delta T,c(t)} U_{\Delta T,c}(t)\right)^2 + \left(\frac{\partial \dot{Q}_c}{\partial t} U_t\right)^2} \qquad 3.22$$

Effectiveness as defined in eqns. 5 and 6 has uncertainty propagated through the temperatures of the fluids and is shown as,

$$U_{\varepsilon_h(t)} = \pm \sqrt{\left(\frac{\partial \varepsilon_h(t)}{\partial T_{h,in}(t)} U_{T_{h,in}(t)}\right)^2 + \left(\frac{\partial \varepsilon_h(t)}{\partial T_{h,out}(t)} U_{T_{h,out}(t)}\right)^2 + \left(\frac{\partial \varepsilon_h(t)}{\partial t} U_t\right)^2} \qquad 3.23$$

$$U_{\varepsilon_c(t)} = \pm \sqrt{\left(\frac{\partial \varepsilon_c(t)}{\partial T_{h,in}(t)} U_{T_{h,in}(t)}\right)^2 + \left(\frac{\partial \varepsilon_c(t)}{\partial T_{c,out}(t)} U_{T_{c,out}(t)}\right)^2 + \left(\frac{\partial \varepsilon_c(t)}{\partial t} U_t\right)^2} \qquad 3.24$$

Table 3.2 represents the estimated uncertainties of the main parameters

Table 3.2. Estimated Uncertainties

Parameters	Mean value	Uncertainties %
$T_{a,i}$ (°C)	*13*	*± 7.6*
Mass flow rate of air, $\dot{m}_a$, (kg/s)	*0.22*	*± 0.98*
Mass flow rate of DI water, $\dot{m}_w$ (kg/s)	*0.06*	*± 1.5*
D_h (m)	*0.001*	*± 3.48*
$A_{frontal,air}$ (m^2)	*0.03097*	*± 0.16*

3.5. Results and discussion

3.5.1. Step variations of temperature

Figure 3.4 shows the step variations of the DI water inlet temperature and the response of

the outlet temperatures of both fluids to the step change. The graph also displays the mass

flow rates of the fluids in an indication that no change happens to them with respect to

time. Three trials are investigated to check the system repeatability to demonstrate its

ability in repeating the same temperature reading within a certain amount of uncertainty or

deviation. The hot DI water inlet temperature steps tested are 1.5, 2.0, 2.5, 3.0 and 3.5 at a

fixed fluid inlet mass flow rates of 60g/s for hot and 232g/s for the cold fluid. Three sets

of experiments for data accuracy measurements are conducted. According to Fig. 3.5.2, the

steps are shown clearly, and the system is found accurate and repeatable in reading the inlet

DI water temperatures through all sets.
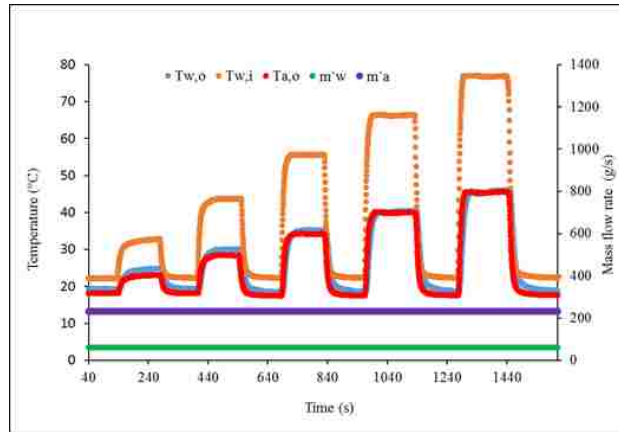
Figure 3.4 Fluid inlet temperature step change with time

3.5.2. *Step change effect on the fluids' outlet temperatures*

The effect of changing the inlet temperature of hot DI water on both fluids' outlet temperatures is presented in Figs. 3.5a and 3.5b including the uncertainty associated with each data measurement. The inlet temperature of the hot fluid changed into 5 steps while other operating conditions were kept constant. It is observed that both fluids outlet temperatures do not display an immediate response to the step change. For a step change of 1.5, the exit temperature of the hot DI water starts increasing after about 4s as the step is applied until it reaches the steady state at 24.5°C. The cold fluid outlet temperature for the same step change starts its increase after only 2s to reach its steady state value of 22.8°C. The time shown before a response in the temperatures occurs is called the initial delay time whereas the time it takes these temperatures to increase as a reaction to the step applied from one steady state to another is called the response time. A longer delay time is found on the hot fluid and can be due to the time required for the DI water to pass through the full length of the heat exchanger before the RTD reads the outlet temperature measurement. While in the case of air, once the DI water releases the heat, air exit temperature change is reflected by the thermocouples' readings.

61

As shown in Figs. 3.5a and 3.5b, the higher the step change, the higher outlet temperatures obtained for both fluids. In addition, as the inlet temperature step increases, its response time decreases. This is seen in both figures where a lower step change demonstrates longer time to reach steady state than a higher step change.

Figure 5c represents the outlet temperature measurements recorded by the airside thermocouple grid and the DI water RTD. The airside thermocouples grid (T-109 to T-126), and the RTD reading ($RTD_{w,o}$) are plotted for a step change of 1.5. The thermocouples show a faster response time compared to the hot DI water RTD temperature due to the length of the channels in the liquid side and the residence time that it takes the fluid to flush out of the heat exchanger. The reading and the delay time of each thermocouple is different and depend on its location in the grid, as shown in Figure 3.3.

The experimental condition of both fluids' temperatures at the highest step of 3.5, inlet and outlet, are shown in Figure 3.5d. For all the experimental runs, a constant air inlet temperature of 13°C was considered as shown in the figure while the DI water temperature experienced a step variation from 22 to 77°C. The increase of both fluid outlet temperatures is clear until a steady state is reached.

The response time at higher temperature steps becomes faster due to longer thermal entrance length. The longer thermal entrance length causes larger developing region with thinner boundary layer and higher heat transfer rate. Moreover, the liquid side Reynolds number increases with the higher temperature step changes, which enhances the molecular movements of the fluid.

(a)   (b)

(c)   (d)
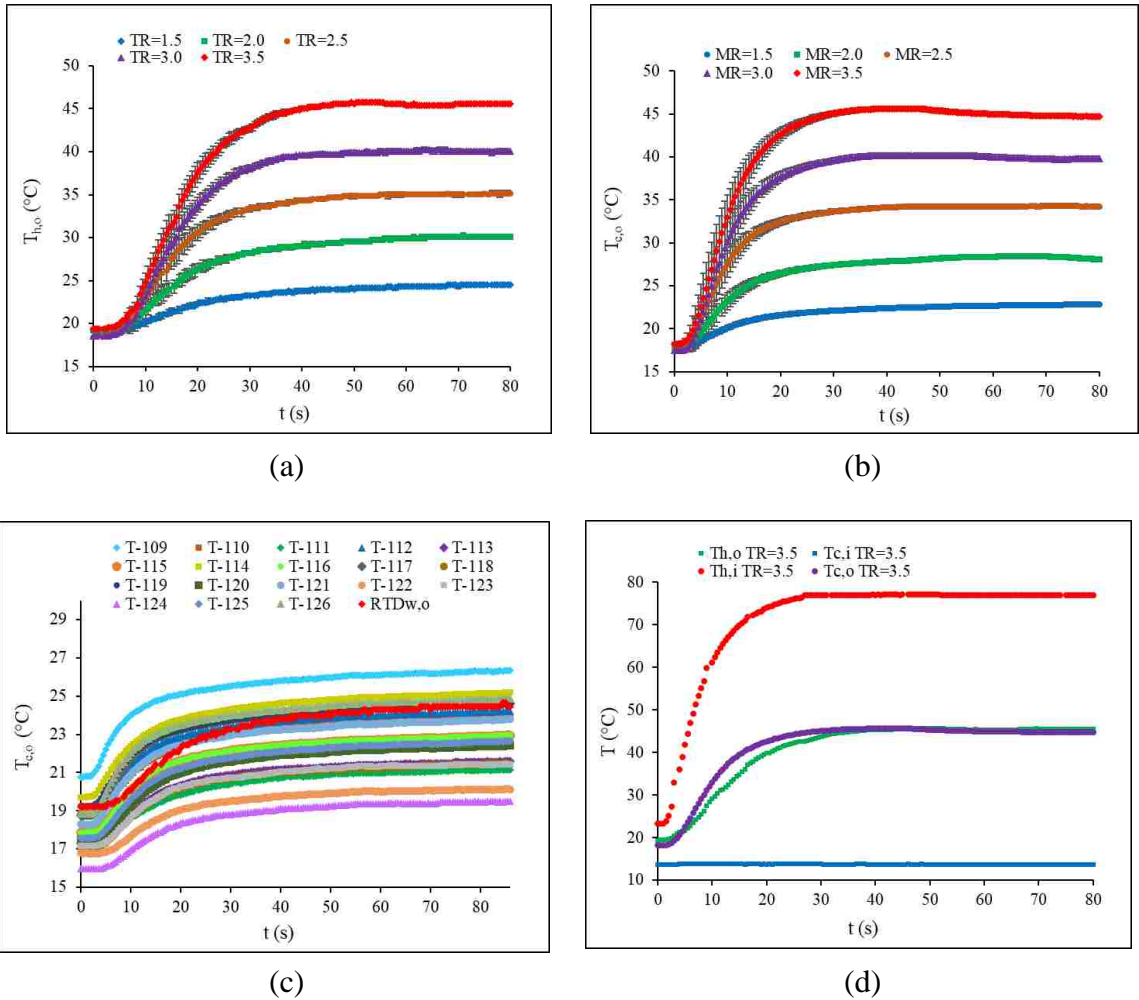
Figure 3.5 (a) Hot fluid outlet temperatures, (b) Cold fluid outlet temperatures, (c) Airside outlet thermocouples grid, and (d) Temperatures condition of both fluids at a step of 3.5

3.5.3. *Dimensionless temperatures and Response time*

For purposes of generalizing, dimensionless parameters of both fluids outlet temperatures with dimensionless time are shown in Figures 3.6a and 3.6b. The effect of the step magnitude on the fluid outlet temperature to reach steady state is seen in these figures however, when higher steps 2.5 and above are considered, this effect diminishes. The delay time presented in the response time and residence time leads to a decrease in the

dimensionless temperature of both fluids at each step change until it reaches the maximum lower value then an increase is noticed.

In Figure 3.6c, the response time at each step change is plotted. The decrease in the response time continues as the step variation increases, however, a diminished effect of the step change on response time is found when reaching higher step changes.
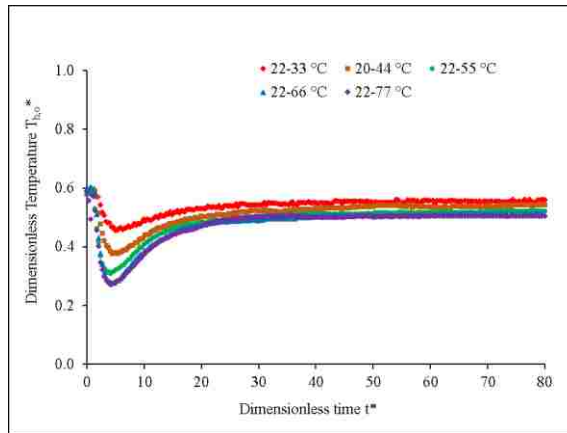
(a)
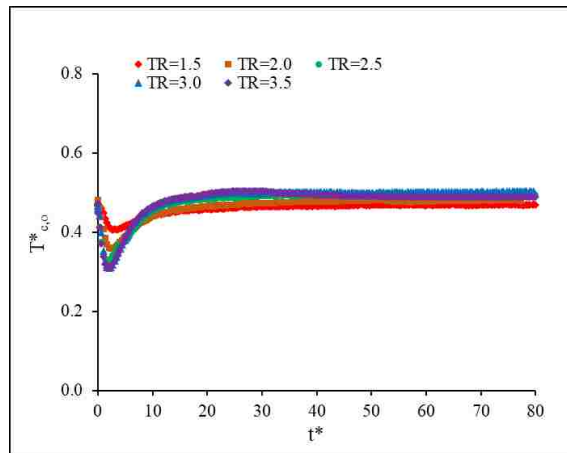
(b)
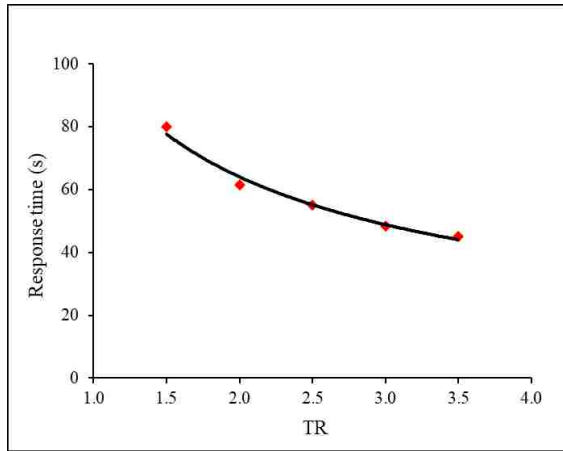
(c)

Figure 3.6 (a) Dimensionless hot fluid outlet temperature, (b) Dimensionless cold fluid

outlet temperature, and (c) Effect of step change on response time

3.5.4. *The Normalized temperature*

Another way to represent the transient results instead of using the outlet temperature of the

fluid is the normalized temperature. This temperature indicates the fraction of the outlet

temperature change from initial to the maximum outlet temperature change under a

transient step change until it reaches the next steady state. Figures 3.7a and 3.7b illustrate

the normalized temperature for each fluid under transient condition. The initial delay time

of the normalized temperature according to the hot fluid is seen higher than the cold fluid.

Furthermore, under the experimental operating conditions and the range of temperature

chosen for this study, a negligible influence of step variation is found at a step of 2.5 and

higher.
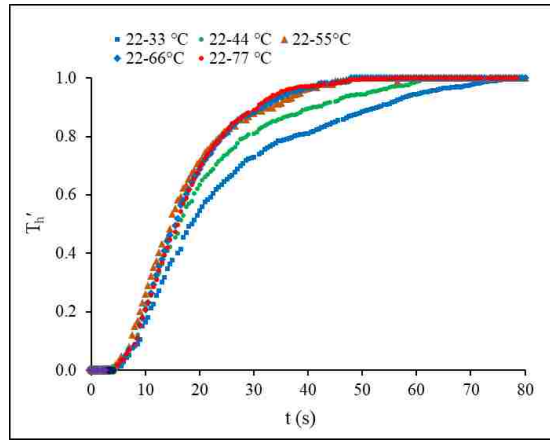
(a)
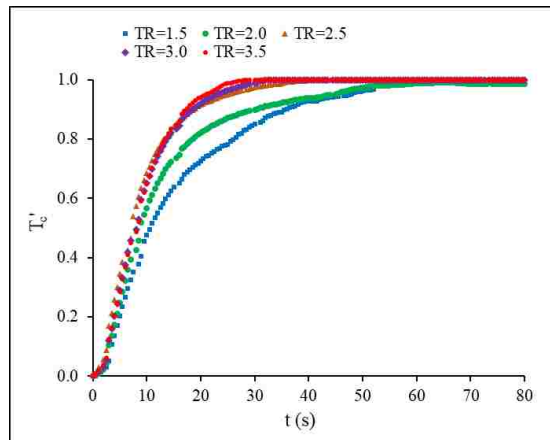
(b)

Figure 3.7 (a) Hot fluid normalized temperature and (b) Cold fluid normalized

temperature

3.5.5. *The heat transfer rate*

The heat transfer rate at different steps is illustrated in Figures. 3.8a and 3.8b for the period

of 0s to 80s. The increase in the heat transfer rate starts as the temperature step is applied

from a lower to a higher variation. Figure 3.8a shows that the heat transfer rate of the hot

fluid achieves its maximum value then drops down reaching its final steady state. The step

increase in temperature causes a rapid increase in the heat transfer rate of the hot fluid.

Initially, the DI water inlet temperature increases but its outlet does not show an immediate

66

response due to instrument response time and the residence time of the fluid. Simultaneously, an increase in the temperature difference between the inlet and outlet of the fluid leads to a peak in the heat transfer rate, keeping in mind that the mass flow rate of DI water is kept constant. The rise in the hot fluid outlet temperature after responding to the step change minimizes this temperature difference. For this reason, a drop in the heat transfer rate happens until the flow reaches the steady state where there is no change in the heat transfer rate with time. As expected, higher heat transfer is achieved at higher step changes. It is also noticed that the peak in heat transfer rate for the hot fluid happens at approximately 9s of the initial transient change.

This is not the case for the airside where a continuous increase in the heat transfer rate is seen with no peak values noted then reaches the steady state.
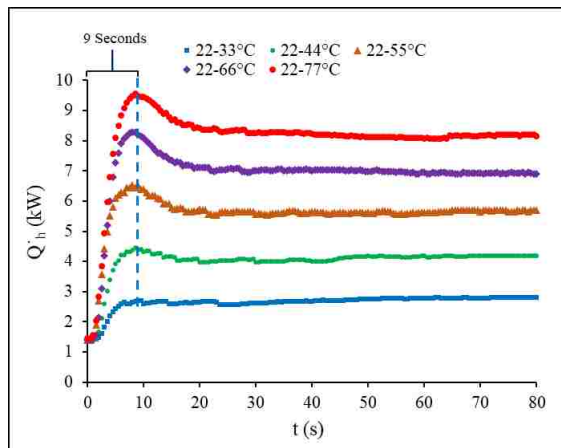
(a)
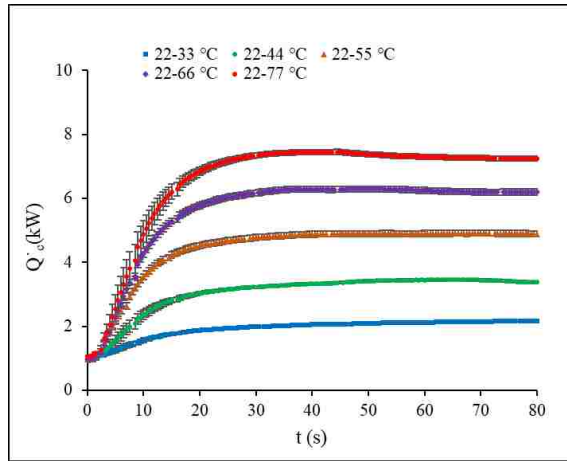
(b)

Figure 3.8 (a) Hot fluid heat transfer rate, and (b) Cold fluid heat transfer rate

3.5.6. *Transient effectiveness*

The transient effectiveness of the meso heat exchanger based on the two fluids is presented in Figures 3.9a and 3.9b as the hot fluid experiences a step change in its inlet temperature. Figure 3.9a shows a rise in effectiveness as the steps are applied before it drops and reaches steady state. Since effectiveness is calculated based on the heat transfer rate of the fluid divided by the maximum possible heat transfer rate, the inlet temperature of the hot fluid is included in the calculation of either fluid effectiveness. For this reason, an increase or drop in effectiveness happens due to step variation and the response time. For both fluids at final steady state, higher effectiveness values are observed for higher temperature steps. The cold fluid behaves adversely to the hot fluid in terms of effectiveness, when an increase of the DI water-based effectiveness is seen, a decrease in air-based effectiveness is noticed during transient condition. However, the highest increase or decrease in effectiveness ends at a step change of 2.5 and above. The steady state condition shows a similar behavior of effectiveness obtained from both fluids.

68

The hot side effectiveness during transient ranges is from around 0.44 to a maximum of 0.90 with higher response time while the cold side varies in about 0.45 to 0.24 with shorter response time when transient conditions are applied.
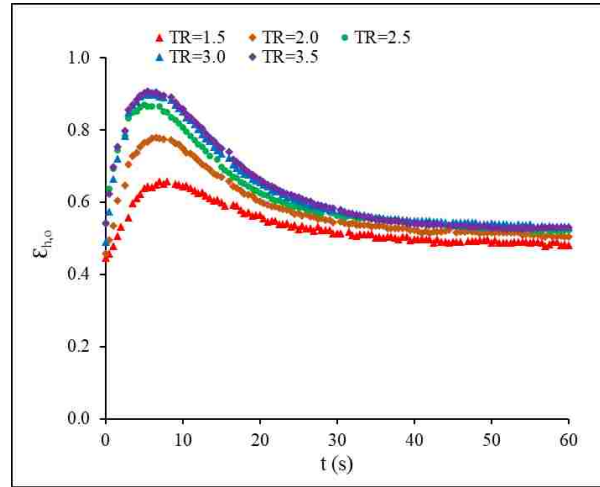
(a)
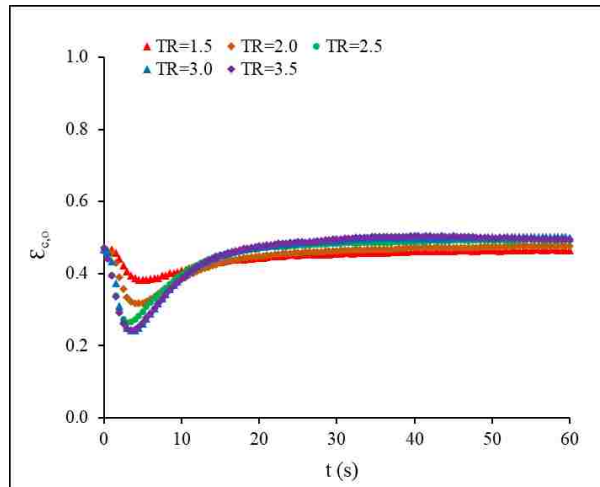
(b)

Figure 3.9 (a) Hot fluid based transient effectiveness & (b) Cold fluid based transient effectiveness

3.5.7. Transient Heat Balance (HB %)

The balance of heat transfer rate of both fluids in the heat exchanger is presented in Figure 3.10. As the transient condition is applied, the heat balance rate increases to a maximum value due to the increase in the hot fluid inlet temperature and heat transfer rate. The maximum values of heat balance reached under transient condition for a step of 1.5 and 3.5 are 49.7 to 109.3. The overall heat balance percentage at the steady state is found to be 2 to 8% from low to high step changes, respectively. This percentage is within the acceptable range set by [23].
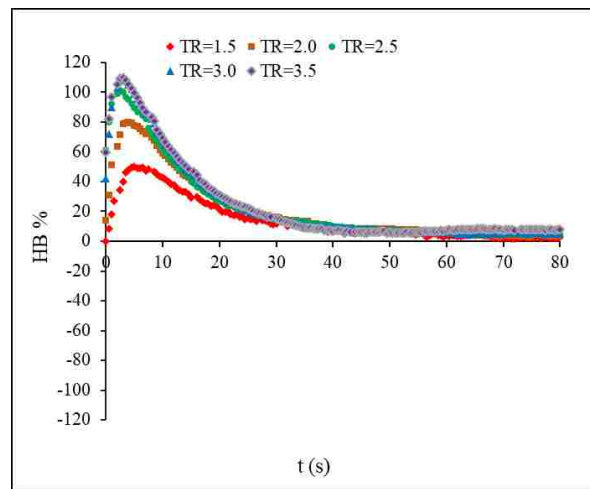
Figure 3.10 Heat balance (HB)

3.6. Conclusion

An experimental study on the transient response of a meso heat exchanger was examined. The transient characteristics of a cross flow liquid to air heat exchanger are studied based on the variation of the hot fluid inlet temperature while other operating conditions were held constant. Different 5 steps of changing the inlet temperature were applied as follows 1.5, 2.0, 2.5, 3.0, and 3.5 at constant mass flow rates of 60g/s for water, and 222g/s for air, with an air inlet temperature set to 13°C. The impact of the step change magnitude and significance on the transient performance of a compact cross flow heat exchanger as well

as, the fluids outlet temperature response was discussed. The results presented the behaviour of fluids exit temperatures, heat transfer rates, effectiveness, and heat balance as they vary with time. The main outcomes of the study are summarized in the following.

- The check for repeatability showed that the three tests performed confirmed the system repeatability and accuracy, where the experiments are found repeatable within 3%. Furthermore, from the heat balance error, a good agreement with the ASME PTC 30-1991 is found since steady state results are within the acceptable range specified.

- The hot fluid inlet temperature step variation increase led to a rise in the fluids' outlet temperatures, as expected, however, the cold fluid displayed a shorter response time than the hot fluid in reaching the steady state.

- The step change in the hot fluid inlet temperature caused an increase in both fluids' outlet temperatures, as expected. This increase is greater at higher step changes and it is found that the cold fluid reached the steady state faster than the hot fluid.

- A continuous decrease in the dimensionless temperature of both fluids is noticed up to a step of 2.5, after which no further decrease than the previous step occurred. The decrease in the dimensionless temperature is due to the response time and residence time associated with calculating the temperatures of both fluids.

- The normalized temperatures showed the final steady state reached by the two fluids at all step changes. It was observed that the step change has a significant influence at lower step changes and a negligible effect for higher step variations.

71

- A gradual decrease in the response time was seen as the hot fluid inlet temperature experienced a rise in a step form. While a negligible effect was noticed at higher step variation of 3.0 and above.

- Unlike the cold fluid, the hot fluid exhibited more heat transfer rate and showed a steeper increase with a maximum possible value reached after approximately 9s for all the step changes. This is not the case for the cold fluid, where, the gradual increase in its heat transfer ended when reaching the steady state.

- From effectiveness point of view, there is an adverse trend between the hot and cold fluids during the transient period. While the hot fluid showed a 38% increase, the cold fluid displayed a 37% decrease in effectiveness. These maximum increase and decrease values for both fluids are influenced by the step changes; however, the variation in the inlet temperature effect is found diminished at a step of 3.0 and higher. It was noted that for both fluids, highest effectiveness at steady state was achieved at the highest step change regardless of the fluid behaviour during the transient condition.

In conclusion, the work presented in this study provides a deep insight on assessing the dynamic performance of a compact cross flow heat exchanger subjected to a step change in the hot fluid inlet temperature. The insufficient experimental data on this subject makes it an attractive topic to enhance the database and explore the transient thermal performance of compact heat exchangers with temperature variation and the absence of flow maldistribution. The reported results can find an application in the design and selection of

a cross flow heat exchanger found in thermal management systems such as in automotive industry where compact heat exchanger is required for size and weight reduction.

Nomenclature

A_c *Channel cross section area, m^2*

D *diameter, m*

D_h *Channel hydraulic diameter, m*

HB *Heat balance*

L *Channel length along the water fluid, m*

$\dot{m}$ *Mass flow rate, kg/s*

Re *Reynolds Number*

T *Temperature, °C*

t *Time, s*

t_{res} *Resident time, s*

V *Fluid velocity, m/s*

$\dot{\forall}$ *Volume flow rate m^3/s*

∞ *Final*

0 *Initial*

Greek symbols

β *Area density, m^2/m^3*

73

ε *Effectiveness*

$\mathcal{E}^*$ *Generalized effectiveness*

μ *Dynamic viscosity*

ρ *Mass density, kg/m³*

Subscripts

a   *Air stream*

c   *Cold fluid*

f   *Final*

i   *Initial*

in   *Inlet*

h   *Hot fluid*

out   *Outlet*

w   *DI Water*

Superscripts

*   *Non-dimensional parameter*

References

[1]   R. Shah, and D. Sekulic′ "Fundamentals of heat exchanger design" John Wiley & sons, Inc., 2003, ISBN 0-471-32171-0.

[2]   G. P. Celata, G.L. Morini, V. Marconi, S.J. McPhail, and G. Zummo "Using viscous heating to determine the friction factor in microchannels – an experimental validation" experimental thermal and fluid science, 30(8): 725-731, 2006, ISSN 0894-1777.

[3]   H. Cao, G. Chen, and Q. Yuan "Thermal performance of crossflow microchannel heat exchangers" Industrial and Engineering Chemical Research, 49: 6215-6220, 2010.

[4]   M. Saadi, M. Ismail, S. Fotowat. A. Quaiyum, and A. Fartaj "Study of Motor Oil Cooling at Low Reynolds Number in Multi-Port Narrow Channels" SAE International Journal of Engines, 6(2):1287-1298, 2013, DOI: 10.4271/2013-01-1643.

[5]   A. Sridhar, A. J. King, and R. Narayanaswamy "Computational analysis of two-phase flow and heat transfer in parallel and counter flow double-pipe evaporators" International Journal of Heat and Mass Transfer, 104: 615-626, 2017.

[6]   S. Fotowat, M. Ismail, M. A. Quaiyum, S. Askar and A. Fartaj "Experimental study on air heating through a cross-flow minichannel heat exchanger" CSME Biennial International Conference, Winnipeg, Manitoba, Canada, P:1-6, June 2012, (1569554279).

[7]   F. E. Romie "Transient response of the counterflow heat exchanger" Transactions of ASME, Journal of heat transfer, 106: 620-626, 1984.

[8]   T. Gao, B. G. Sammakia, B. T. Murray, A. Ortega, and R. Schmidt "Cross Flow Heat Exchanger Modeling of Transient Temperature Input Conditions" in IEEE Transactions on Components, Packaging and Manufacturing Technology, 4(11): 1796-1807, 2014. doi: 10.1109/TCPMT.2014.2356202.

[9]   S. Abdallah, and S. Rooke "Transient Response of a Serpentine Finned-Tube Cross-Flow Heat Exchanger to a Step Change in Inlet Temperature" Journal of Heat Transfer Engineering 18(3): 51-60, 1997.

[10]   A. Asgharpour, E. Hajidavalloo and M. Taheri "Experimental and analytical investigation of transient behavior of coupled heat exchangers" Applied Thermal Engineering 60: 172-181, 2013.

[11]   Y. Zhang, D. Lu, Zheng Du, X. Fu, and G. Wu "Numerical and experimental investigation on the transient heat transfer characteristics of C-shape rod bundles used

in Passive Residual Heat Removal Heat Exchangers" Annals of Nuclear Energy, 83: 147-160, 2015, ISSN 0306-4549.99.

[12]   F. Syed, and S. Idem "Transient Performance of a Cross Flow Heat Exchanger Using Finite Difference Analysis" ASME. ASME proceedings, 10:1333-1342, 2008, Heat Transfer, Fluid Flows, and Thermal Systems, Parts A, B, and C doi:10.1115/IMECE2008-66274.

[13]   Ö.E. Ataer "An approximate method for transient behavior of finned-tube cross-Flow heat exchangers" International Journal Refrig, 27: 529–539, 2004.

[14]   Ö.E. Ataer, A. I˙leri, and Y. Go¨g˘u¨s "Transient behavior of finned-tube cross-flow heat exchangers" International Journal Refrigeration, 18(3):153–160, 1995.

[15]   M. Mishra, P.K. Das, and S. Sarangi "Transient behavior of crossflow heat exchangers due to perturbation in temperature and flow" International Journal of Heat and Mass Transfer, 49: 1083–1089, 2005.

[16]   K. Silaipillayarputhur, and S. Idem "Transient Performance Model for a Multipass Cross-Flow heat exchanger" Heat Transfer Engineering, 35: 15-24, 2014.

[17]   M. del Valle, C. Caceres and A. Ortega "Transient modeling and validation of chilled water based cross flow heat exchangers for local on-demand cooling in data centers" 15th IEEE Intersociety Conference on Thermal and Thermomechanical Phenomena in Electronic Systems (ITherm), Las Vegas, NV, pp. 727-736, 2016, doi: 10.1109/ITHERM.2016.7517619.

[18]   T. Gao, B. G. Sammakia, B. Murray, A. Ortega, and R. Schmidt "Data center crossflow heat exchanger study under different transient temperature boundary conditions" 30th semi-therm Symposium, IEEE, 2014, pp. 174-183, 978-1-4799-4374-6/14.

[19]   Y. A. Cengel "Heat Transfer: A Practical Approach" New York: McGraw-Hill Higher Education, 2006.

[20] R. M. Cima, and A. L. London "Transient Response of a Two-Fluid Counter-Flow Heat Exchanger-The Gas-Turbine Regenerator" Transactions of ASME, 80: 1169–1179, 1958, http://dx.doi.org/10.5772/67334.

[21] T. Gao, B. G. Sammakia, J. F. Geer, A. Ortega, and R. Schmidt "Dynamic analysis of cross flow heat exchangers in data centers using transient effectiveness method" IEEE transactions on components, packaging and manufacturing technology, 4(12): 1925-1935, 2014.

[22] R. S. Figliola, and E. B. Donald "Theory and Design for Mechanical Measurements" John Wiley & Sons, 5th ed., 2012.

[23]   ASME "An American National Standard, Performance Test Code (PTC) 30-1991, Air cooled heat exchangers" New York, 1991.

CHAPTER 4

A TRANSIENT RESPONSE COMPARISON OF A CONVENTIONAL AND A

MINICHANNEL HEAT EXCHANGER UNDER MASS FLOW AND

TEMPERATURE STEP VARIATIONS

4.1. Introduction

Heat exchangers are frequently comprising in the process of industrial and HVAC systems

and have an imperative role to play. Many researchers devoted themselves implementing

new innovative ideas to improve their efficient utilization and transfer of energy.

Refrigeration, air conditioning, and automotive heat and cooling system is an essential part

in the design of compactness in a structure and is provided to control the temperature,

humidity, and other process necessity. Limitation of size and/or special dimensions is

becoming progressively important in designing of these systems. The minichannel heat

exchangers which have higher heat transfer area per unit volume potentially lead to

compactness and better heat transfer performance. Mini-channel finned heat exchangers

are getting more importance for refrigeration systems, particularly while less charge of

refrigerant and compactness of heat exchanger is required, Kandlikar [1]. Along with the

use of small channels, enhanced surfaces are utilized in heat exchangers in the automotive

and refrigeration industries. Another approach to gaining more internal heat transfer is to

use serpentine bend. Aiming to examine the influence of serpentine in heat exchangers, the

thermo-hydraulic characteristics of a Serpentine meso-channel heat exchanger with

parallel channels were numerically studied by Dehghandokht et al. [2]. They modeled the

effect of serpentine on heat transfer and compared the results to the experimental data with

the same geometrical and operating test conditions. It was found that the adiabatic

serpentine in a meso-channel heat exchanger slab resulted in increasing the heat transfer.

This is due to the forming new entrance region and new temperature profile made by the flow U-turn and mixing of flow at the serpentine.

In a system, when changes occur to any parameter at the input, it takes time to reaching final state and getting stable. This short- term period is called transient. The focus on the transient behaviour of heat exchangers is increasing owing to the advances in the process control. Moreover, the dynamic responses of each component should be known to allow the full automation in the process plant. For this purpose, Guha et al. [3] numerically investigated a dynamic behaviour of heat exchanger network. They developed a finite difference numerical scheme and solution algorithm to solve the set of model equations. The nature of thermal dynamics in the heat exchanging streams was shown due to sinusoidal and periodic square wave variation of the inlet temperature. With the aim of improving the design of control strategies and energy efficiency, the characteristics of the heat exchangers in data centers focused on their transient performance was numerically investigated by Gao et al. [4]. They analyzed the effect of nonuniform fluid inlet temperature boundary conditions on the steady state and transient performance of cross flow heat exchangers. They examined the transient performance of the heat exchanger under different change functions such as step, ramp and exponential variation to the hot fluid inlet temperature. It was found that nonuniform inlet temperatures have expressively different effects on the performance of a cross flow heat exchanger for both the steady state and the transient circumstances. They also shown that transient nonuniform inlet temperatures affect both the steady state and transient results of cross flow heat exchanger performance, whereas the steady state nonuniform inlet temperature only affect the steady state performance. The dynamic temperature response of unmixed fluids in crossflow heat

exchangers, with finite wall capacitance with variations in both temperature and mass flow rate was numerically studied by Mishra et al. [5]. They applied the step and ramp changes in the mass flow of the both hot and cold fluids, and step, ramp, exponential and sinusoidal changes in hot fluid inlet temperature. They found a rise in mean exit temperatures once the larger disturbance is in the hot fluid, and a drop once the larger disturbance is in the cold fluid. Silaipillayarputhur et al [6] numerically examined the dynamic behaviour of a multi-pass cross flow heat exchanger under the temperature and mass flow rate changes. Using energy balance equations, an implicit central finite difference method was implied for both fluids and the heat exchanger wall. They found that owing to the finite propagation times related to the inlet variations and the storage of energy in the heat exchanger wall, the outlet temperatures of both fluids do not respond immediately. Syed et al. [7] examined the dynamic response of an unmixed, single pass, cross flow heat exchanger subjected to a step rise in temperature of the minimum capacity rate fluid using an implicit central finite difference method. They found a delay to the transient response of the minimum capacity rate fluid while, the immediate temperature response was for the maximum capacity rate fluid. Roetzel et al. [8] introduced a general mathematical model for anticipating temperature responses of one-dimensional flow heat exchangers. They assessed the transient parameters of heat exchangers used for the automatic control systems depending on the analytical and numerical analyses.

The transient responses of a water-to-air heat exchanger under transient condition that assist to optimize the control for an enhanced energy efficiency of a HVAC system was studied by Yao et al. [9]. They developed a dynamic model on the humidity, air and water exit temperature for the cases of start up the chiller, shut down the chiller and a rise in the

water flow rate. The results display that the input changes and the initial conditions will yield noteworthy effect on the proportionality coefficient of the response variables, but slight effect on the time constant of the response variables. Del Valle et al [10] experimentally measured the dynamic response of a 12"X12" single pass cross flow heat changer in a data center hybrid air–liquid cooling system. The test rig was able to produce step, ramp and frequency changes for temperature and flow rate of the water side. They found that the sinusoidal variation on the water flow rate was responsible for the delay angle between the inlet temperature variation and the both outlet temperatures. Moreover, shorter to no reaction was found between the inlet flow perturbation and the outlet temperature responses. Prabhakara Rao and Das [11] experimentally studied the effect of port to channel flow variation on the pressure drop across a Z and U-type plate heat exchangers. They found that under same conditions, the maldistribution was more drastic in the Z-type plate heat exchanger compared to the U type.

The listed previous work shows the lack in the experimental work and the need to analyze the behaviour of different heat exchangers such as compact ones due to the increasing demand of the industry for thus heat exchangers. This study aims to examine the dynamic response of a multiport slab finned mini-channel and a traditional heat exchanger with both subjected to variations in liquid temperature and flow rate when the mass flow rates and inlet temperature of the air are held constant. Different steps in a wide range of temperature and flow rate were applied using the well instrumented experimental setup. The outlet temperatures of the liquid and air, transient heat transfer rates, transient effectiveness, and time constant are presented and discussed.

4.2. Transient experimental setup

The fully instrumented experimental set up that is used in this study is shown in Figure 4.1

It is designed of investigate the steady state as well as the transient response of different

types of heat exchangers under variations of inlet mass flow and temperature. A detailed

description of the experimental set up and the schematic diagram can be found in [12]. The

test section is capable to encompass different types of heat exchangers and compare their

performance. The main working fluids used in these heat exchangers for the heat

exchangers are DI-water and air. The experimental data are monitored and recorded using

a data acquisition system (DAQ). The full instrumentation of the system includes having

differential pressure transducers and T type thermocouples on the air side, an inline

Coriolis mass flow meter, resistance temperature detectors (RTDs), pressure transducers

(PTDs), 10-ton chiller and 20kw inline heater on the liquid side.

Figure 4.1. Experimental setup

The test chamber that is placed in the center of the wind tunnel is made-up from transparent polycarbonate sheets with high thermal resistance. It has a rectangular shape with a cross section of 4"X 12" [0.1016 m X 0.3048 m] and a depth of 24" [0.6096 m]. For this study two different heat exchangers are situated inside the test chamber alternatively to study and compare their transient thermal behavior; a minichannel heat exchanger and a traditional radiator. For all the experimental runs, the inlet conditions of the airside are kept constant at 13°C and 222g/s or 6m/s for both heat exchangers. These fixed conditions are achieved using a thermal wind tunnel equipped with an inbuilt heat exchanger that provides a full control on the air inlet temperature through the heat exchange of cold water supplied through the use of a chiller with air at environment temperature through the inbuilt heat exchanger. Step changes in the liquid inlet temperature and flow rate are applied. The mass flow step changes varied from an initial value of 20 g/s to (10, 16, 30, 40, 50) g/s at a constant hot liquid temperature of 70°C. This constant hot liquid temperature is obtained through an inline heater and additional brazed and plate heat exchangers to supply the desired hot liquid temperature to flow inside the minichannel heat exchanger. On the other hand, the liquid step variation in temperature started from an initial value of 22°C to (33, 44, 55, 66, 77) °C at a constant hot liquid mass flow rate of 60g/s. Detailed explanation of the fluids circuits and the experimental procedure can be found in Fotowat et al. [12].

4.2.1. Tested heat exchangers

The heat exchangers used in this study are cross flow air to liquid heat exchangers have the same dimensions (height, length, and width) and made of aluminum material. Both has same fin density and thickness. The reason for this comparison is to compare the dynamic

behavior of the MICHX with a radiator in a car as a benchmark. The thickness of the slab

in MICHX is identical to the radiator.

Figure 4.2 shows a cross section of each heat exchanger while, Tables 4.1 and 4.2 display

specifications of the MICHX and conventional heat exchanger respectively.

(a)

(b)
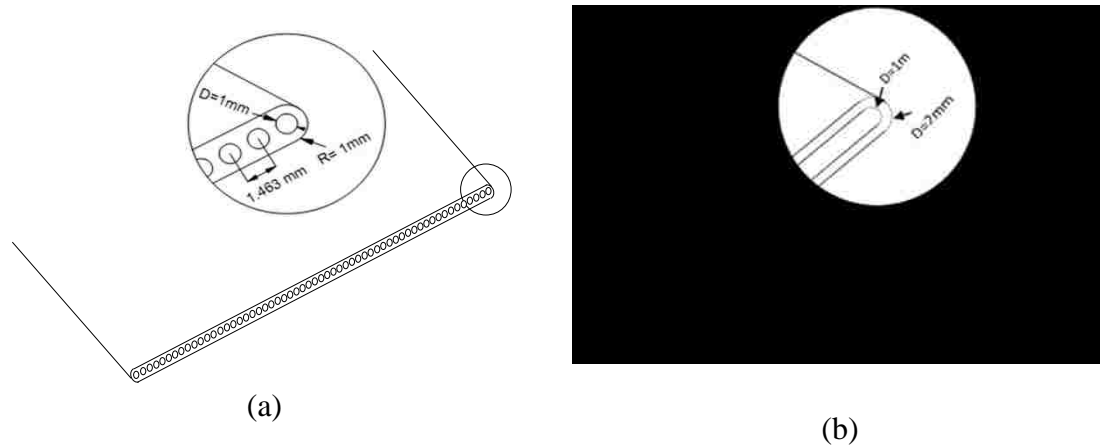
Figure 4.2. Schematic of (a) the MICHX (b) conventional radiator slabs cross section

Table 4.1 Specifications of the MICHX

Heat exchanger specifications	Dimensions
Channel diameter (mm)	1
No. of channels in a slab	34
No. of slabs	5
Slab thickness (m)	0.002
slab length (m)	0.305
Slab width (m)	0.102
Slab height (m)	0.102
Fin density (fins per cm)	5

Table 4.2 Specifications of the conventional heat exchanger

Heat exchanger specifications	Dimensions
Channel size, H x W (mm x mm)	1 x 50.6
No. of channels in a slab	1
No. of slabs	8
Slab thickness (m)	0.002
slab length (m)	0.305
Slab width (m)	0.102
Slab height (m)	0.102
Fin density (fins per cm)	5

4.3. Data reduction for the experiments

The outlet temperatures of both fluids and the thermal characteristics of the heat exchangers are evaluated by dimensional and non-dimensional parameters such as dimensionless temperature, heat transfer rate, and effectiveness.

$$T_{h,o}^* = \frac{T_{h,o}\,(t^*) - T_{c,in}}{T_{h,in} - T_{c,in}} \qquad 4.1$$

$$T_{c,o}^* = \frac{T_{c,o}\,(t^*) - T_{c,in}}{T_{h,in} - T_{c,in}} \qquad 4.2$$

The residence time defines the time it takes the hot liquid to pass through the heat exchanger and is presented as follows,

$$t_{res} = \frac{nA_cL}{\dot{\forall}} = \frac{L}{V} \qquad 4.3$$

By dividing time over the residence time, a dimensionless form of time is used for the generalization purpose as,

$$t^* = \frac{t}{t_{res}} = \frac{V_c}{L}t \qquad 4.4$$

Reynolds number is found for the hot fluid based on the diameter of the channel and the amount of mass flow rate as follows,

$$Re_h = \frac{\rho_h v_h D_h}{\mu_h} = \frac{\dot{m}_h}{2\pi \mu_{hD_h}} \qquad 4.5$$

Considering the geometry of the tested heat exchanger, MICHX, Reynolds number can be shown as,

$$Re_{h,MICHX} = \frac{2\dot{m}_h}{17\pi \mu_h D_h} \qquad 4.6$$

The heat transfer rates of both fluids are shown in the following,

$$\dot{Q}_h = \dot{m}_h \, c_{p,h} \, \Delta T_h \qquad 4.7$$

$$\dot{Q}_c = \dot{m}_c \, c_{p,c} \, \Delta T_c \qquad 4.8$$

Heat exchangers are characterized by the heat transfer effectiveness ε that is the heat transfer rate over the maximum possible heat transfer rate and is found using the energy balance of the hot and cold fluids Cengel [14]. The idea of the heat transfer effectiveness was extended to a time-dependent by Cima and London [15]. This expression was also used by Gao et al. [16] and Srihari Das [17]. Starting with the effectiveness definition,

$$\varepsilon = \frac{q}{q_{max}} \qquad 4.9$$

The maximum possible heat transfer rate is defined as,

$$q_{max} = (\dot{m}c)_{min}(T_{h,i} - T_{c,i}) \qquad 4.10$$

Where, $c = c_v = c_p$ refer to the fluid specific heat, the transient effectiveness is found as,

$$\varepsilon_h(t) = \frac{C_h \left(T_{h,i}(t) - T_{h,o}(t) \right)}{C_{min} \left(T_{h,i}(t) - T_{c,i}(t) \right)} \qquad 4.11$$

$$\varepsilon_c(t) = \frac{C_c \left(T_{c,o}(t) - T_{c,i}(t)\right)}{C_{min} \left(T_{h,i}(t) - T_{c,i}(t)\right)}$$

4.12

A measure of the accuracy of an experiment is given by its uncertainty. The uncertainty of the experimental data based on the uncertainty of all equipment and is analyzed and presented in appendix A.

Using Yin and Jensen analytical model [13], the hot liquid outlet temperature (x*= 1) is obtained as follows; (the derivation can be found in appendix B)

$$T_{h,o} = \left(T_c^\infty - T_{h,i}\right)\left[\left(1 - e^{NTU^0}\right) + \left(e^{NTU^0} - e^{NTU^\infty}\right)f(t^*)\right] - T_{h,i}$$

4.13

Then the $f(t^*)$ was found,

$$f(t^*) = 1 - \frac{(\lambda_2 + C_3)e^{\lambda_1 t^*} - (\lambda_1 + C_3)e^{\lambda_2 t^*}}{(\lambda_2 - \lambda_1)}$$

4.14

where,

$$C_3 = \frac{\varepsilon^0 \left(N_3^\infty / N_3^0 - 1\right)}{\left(\varepsilon^0 / NTU^0 - \varepsilon^\infty / NTU^\infty\right)}$$

4.15

$$\lambda_{1,2} = \frac{(C1 + D2) \pm \sqrt{(C1 + D2)^2 + 4(C2D1 - C1D2)}}{2}$$

4.16

$$C_1 = \frac{\frac{N_3^\infty \varepsilon^\infty}{N_2^\infty} - \left(\frac{N_3^\infty}{NTU^0} - 1\right)\varepsilon^0}{\frac{\varepsilon^0}{NTU^0} - \frac{\varepsilon^\infty}{NTU^\infty}}$$

4.17

$$C_2 = \frac{\frac{N_3^\infty \varepsilon^0}{N_2} - \left(\frac{N_3 \varepsilon^\infty}{N_2^\infty} - 1\right)\varepsilon^0}{\frac{\varepsilon^0}{NTU^0} - \frac{\varepsilon^\infty}{NTU^\infty}}$$

4.18

$$D_1 = \frac{N_3^\infty \left(\frac{\varepsilon^0}{NTU^0} - \frac{\varepsilon^\infty}{NTU^\infty} \right)}{N_1 \left(\frac{\varepsilon^0}{N_2^0} - \frac{\varepsilon^\infty}{N_2^\infty} \right)} \qquad 4.19$$

$$D_2 = -\frac{(N_2^\infty + N_3^\infty)}{N_1} \qquad 4.20$$

$$D_3 = \frac{N_3^\infty \varepsilon^0 \left(\frac{1}{NTU^0} - \frac{N_2^\infty \varepsilon^\infty}{N_2^0 NTU^\infty} \right)}{N_1 \left(\frac{\varepsilon^0}{N_2^0} - \frac{\varepsilon^\infty}{N_2^\infty} \right)} \qquad 4.21$$

Where,

$$e^0 = 1 - e^{NTU^0} \quad and \quad e^\infty = 1 - e^{NTU^\infty} \qquad 4.22$$

$$N_1 = \frac{m_w C_{p,w}}{m_h C_{p,h}} \qquad 4.23$$

$$N_2(x) = \frac{h_a(x) A_a}{m_h C_{p,h}} \qquad 4.24$$

$$N_3(x) = \frac{h_h(x) A_h}{m_h C_{p,h}} \qquad 4.25$$

$$NTU = \frac{N_2 N_3}{N_2 + N_3} \qquad 4.26$$

The analytical approach is simplified for the outlet temperature of the hot fluid and is independent of position along the heat exchanger.

4.4. Results and discussion

This section discusses the findings of the transient behaviour for two different heat exchangers as a results of step changes in the hot fluid inlet temperature and mass flow rate. The case of temperature change was performed under constant mass flow of both fluids and air inlet temperature. For this case, only the hot fluid inlet temperature was varied to steps of 1.5 to 3.5. The second case of varying the mass flow rate, steps of 0.5 to 2.5 were applied to the hot fluid inlet mass flow while keeping fluids inlet temperatures and air mass flow rate constant. The comparison of the two heat exchangers, MICHX and the radiator, were made for the two cases and the experimental results were used to compare and validate an analytical model in order to check its predictability of the experimental data.

4.4.1. Comparison of the outlet temperature of the MICHX and the radiator for the steps of 1.5 and 3.5 MICHX and Radiator

The effect of the inlet temperature steps on the outlet temperatures of the hot and cold fluids for both the MICHX and the conventional are presented in figure 4.3. A constant air inlet temperature of 13°C and mass flow rate of 0.222 kg/s were considered for the two type's heat exchanger with constant hot liquid mass flow rate of 60 g/s. The comparison is made for the lowest and highest hot liquid inlet temperature steps of 1.5 and 3.5. The conventional hot liquid outlet temperature is found 9% and 15% higher than the temperature of the MICHX for steps of 1.5 and 3.5 accordingly. Each step has its own response time, for the step of 1.5, the MICHX showed a 78s response time while the radiator was higher to 138s. As for the step of 3.5, the MICHX responded within 38s while the radiator response time was 76s. This concludes shorter response time of the MICHX that leads it to get to steady state faster compared to the radiator.

<div align="center">(a)   (b)</div>
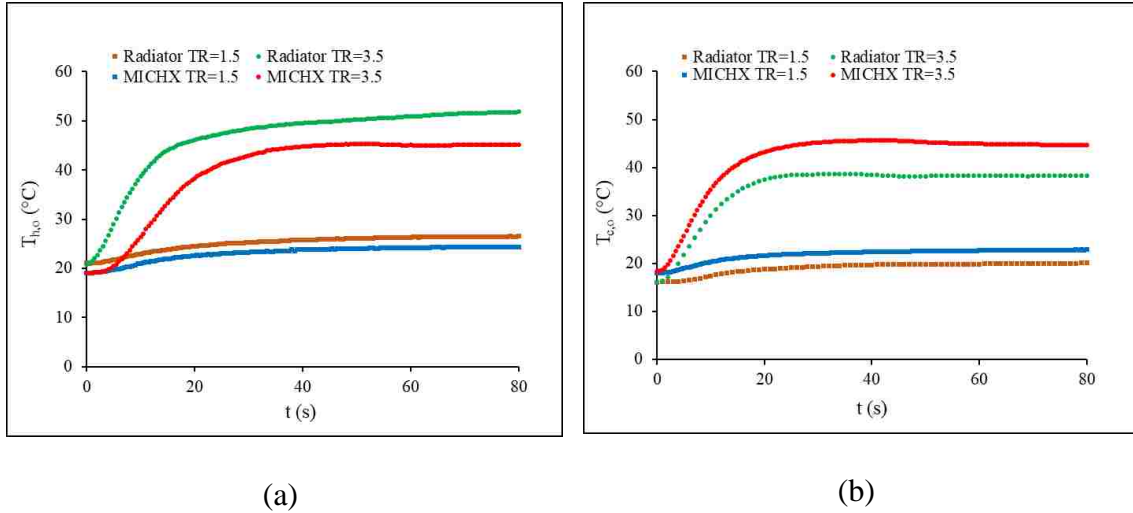
Figure 4.3 demonstrates the exit temperature response of the hot and cold fluids at the hot liquid inlet temperature variation for the conventional and MICHX

The effect of mass flow step change on the outlet temperatures of the MICHX and conventional heat exchanger are illustrated in figure 4.4. The MICHX hot liquid outlet temperature at a step of 2.5 is found 11% lower from the radiator and at a step of 1.5 it was 8% lower. That means lower heat transfer rate for the conventional radiator to the MICHX. Considering a mass flow step of 0.5, the MICHX provided faster response time at 83s compared to the radiator 178s. In the case of higher mass flow step change of 2.5, the response time was still better for MICHX at 50s compared to 143s for the radiator. While the MICHX recorded faster response time, its initial delay time was higher at 4.5s compared to the 0.7s of the radiator considering the case of a step change of 0.5. It is concluded that regardless of the value of the step change applied to the hot liquid inlet mass flow rate, the MICHX will respond faster to the change and record better response time to reach the steady state than a conventional radiator.

The reason for faster response time of the MICHX could be explained by the fact that the existence of the serpentine breaks the boundary layer, which elevates the heat transfer coefficient. Then, new boundary layer starts developing after each serpentine. Moreover, the MICHX has higher heat transfer surface area compared to the conventional one.

(a)   (b)
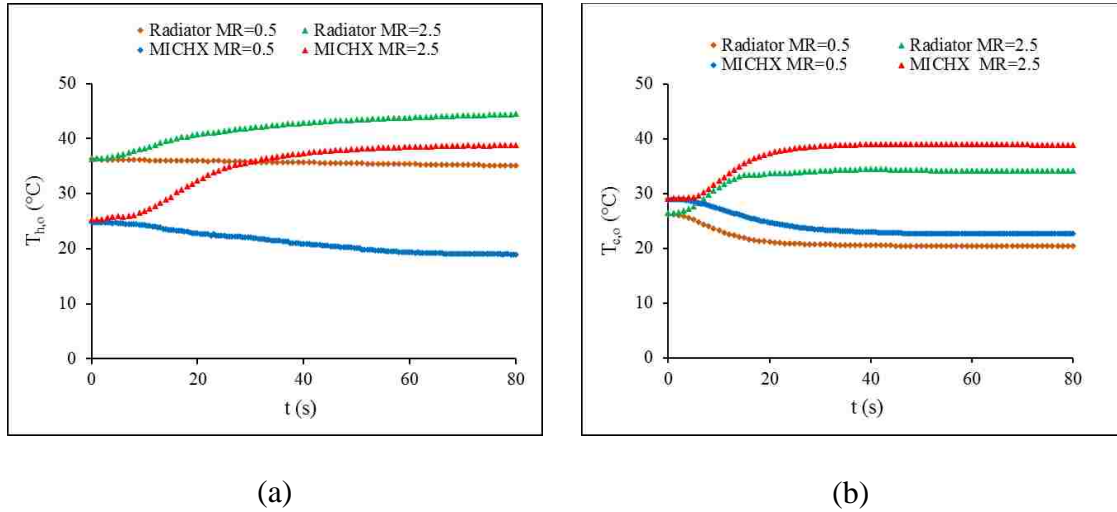
Figure 4.4 demonstrates the exit temperature response of the hot and cold fluids at the hot liquid mass flow step changes for the conventional and MICHX

4.4.2. Comparison of the Analytical model for dynamic heat exchanger response with the experimental data for a conventional heat exchanger

Figure 4.5 and 4.6 presented the outlet temperatures of a traditional tube and fin heat exchanger using the experimental data and analytical model. The experiment is conducted for the step up and down variation in mass flow rate of 0.5 to 2.5 at constant inlet temperature of 70°C for the hot fluid when the condition for the cold fluid kept constant at temperature of 13°C and mass flow rate of 0.222 kg/s. owing to appropriate comparison of

the experimental and analytical results, the initial delay and step time is removed from the figures. The outlet temperatures of hot fluid show more than 20% higher prediction for the analytical model compared to the experimental results. The possible reasons for the difference in prediction of the transient response are due to assuming the heat transfer coefficient to be constant along the heat exchanger to simplify solving the governing equations.

(a)   (b)
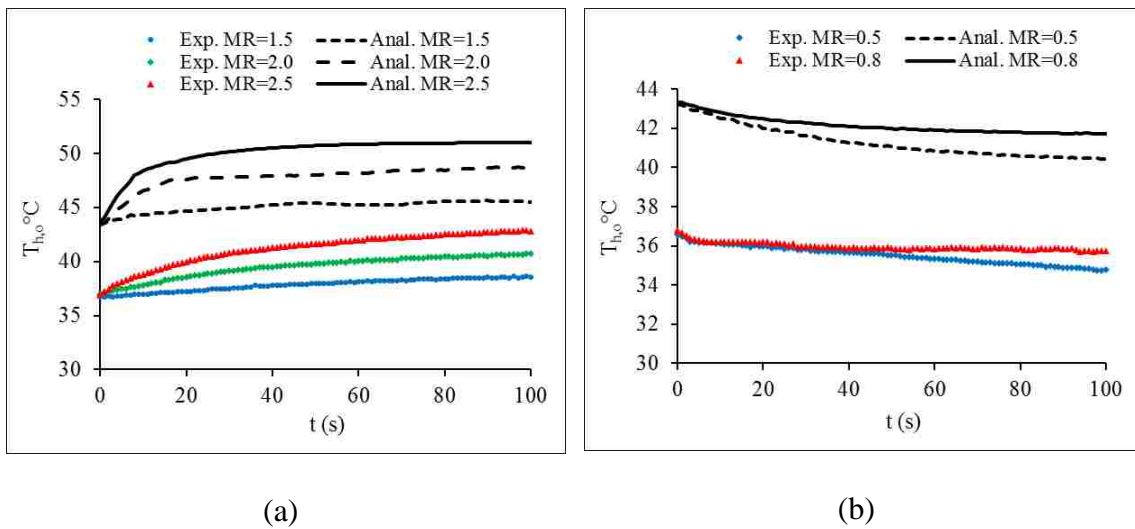
Figure 4.5 Comparison between the hot fluid outlet temperature prediction from experiment and analytical model for a conventional heat exchanger

<div align="center">(a)   (b)</div>
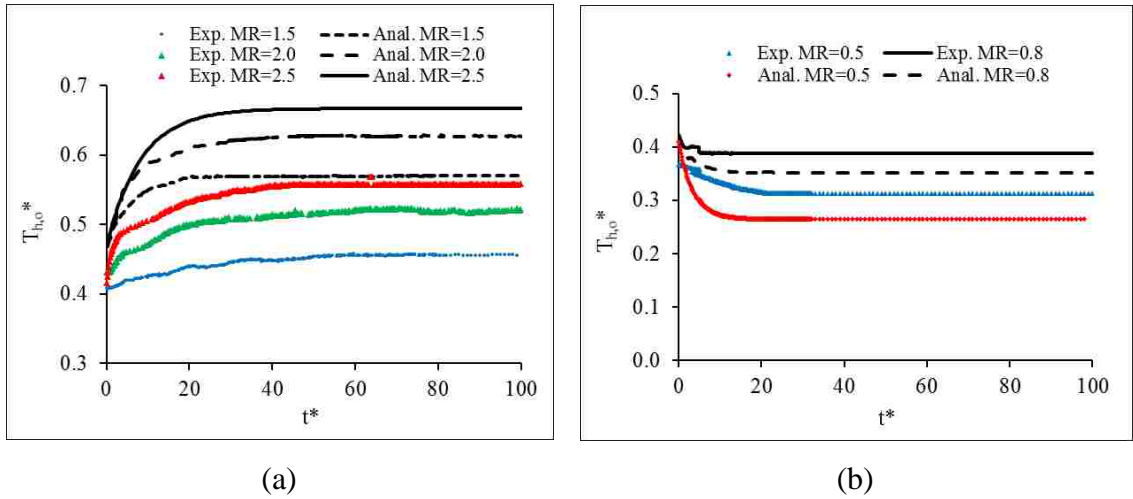
Figure 4.6 Comparison between the dimensionless hot fluid outlet temperature

prediction from experiment and analytical model for a conventional heat exchanger

4.4.3. *An empirical correlation for the temperature step variation*

Figure 4.7 shows variation in the ratio of the transient dimensionless hot fluid outlet

temperature on its steady state dimensionless temperature verses the dimensionless time.

The transient outlet temperature approaches quasi-steady-state for the non-dimensional

time greater than about 70. An empirical correlation is obtained by using an exponential

relation with power law effect of temperature step variations (Eq.4.27). The curve-fit

took the experimental data well, which can be seen from the root mean square values

more than 0.89.

$$T^*_{h,o}/T^{*,\infty}_{h,o} = 1 - 0.49 * TR^{0.3} * e^{(0.0004*TR - 0.06)t^*} \qquad 4.27$$
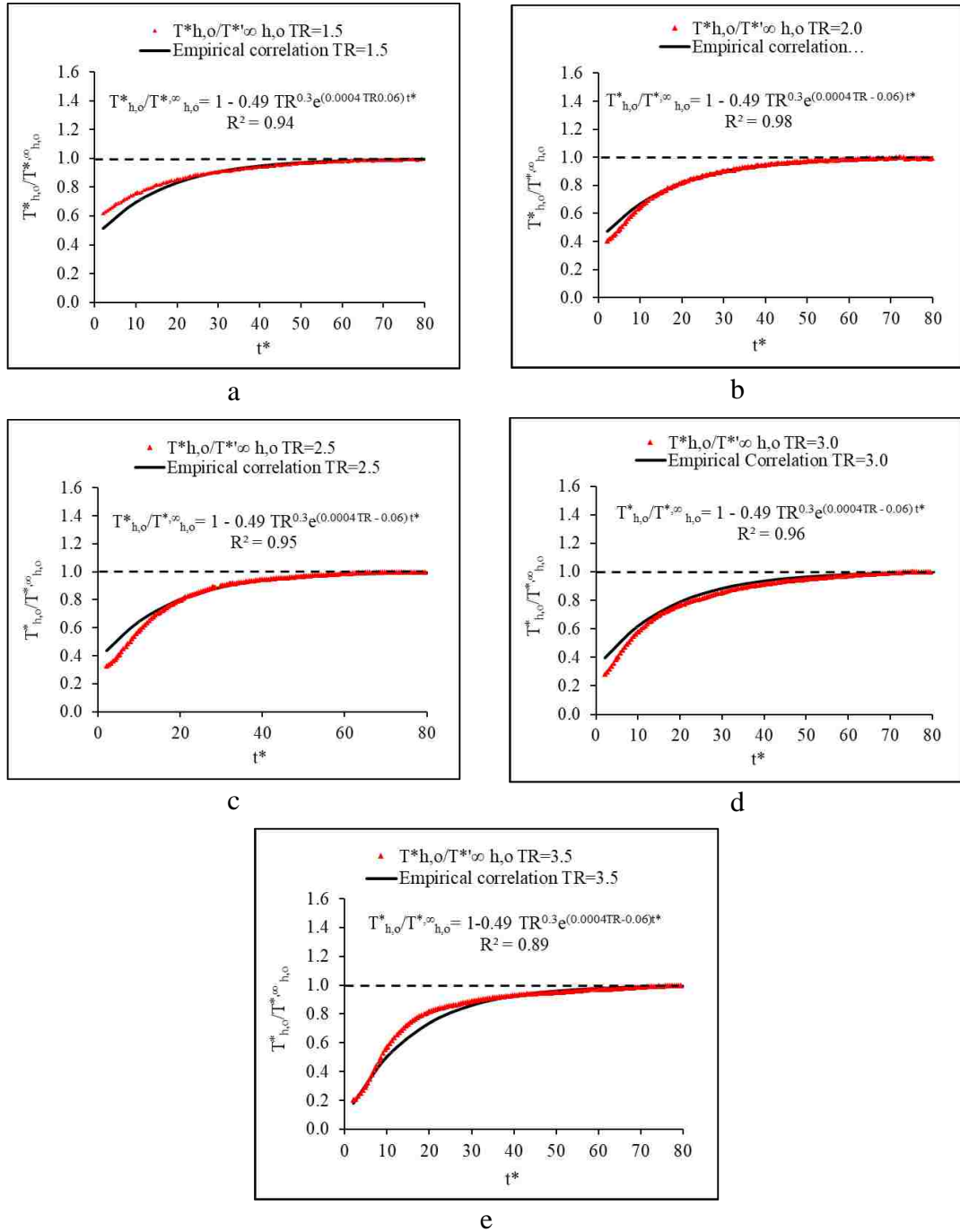
Figure 4.7 An empirical correlation for transient hot fluid outlet temperature by dimensionless parameters at a temperature step changes for a conventional heat exchanger

4.4.4. An empirical model for the mass flow step variation

The ratio of the transient dimensionless hot fluid outlet temperature on its steady-state verses the dimensionless time is presented in Figure 4.8. The transient outlet temperature approaches quasi-steady-state for the mass flow step variation at the dimensionless time larger than around 50. An empirical correlation is obtained for the step-up variation by Eq.4.28. The curve-fit measured current experimental data well, which can be seen from the root mean square values higher than 0.90.

$$T^*_{h,o}/T^{*,\infty}_{h,o} = 1 - (0.17\ MR - 0.1)\ e^{-0.05\ t^*} \qquad\qquad 4.28$$

a

b

c
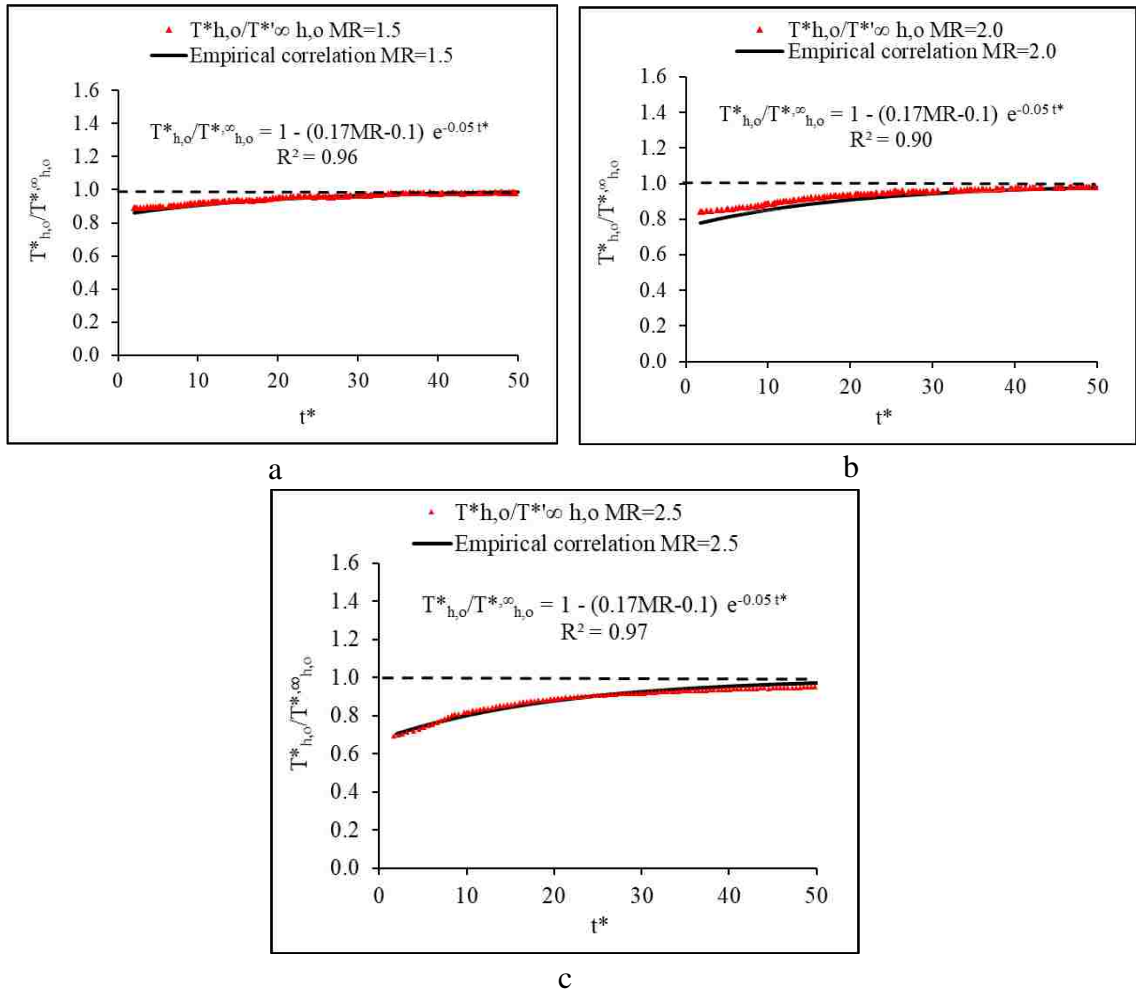
Figure 4.8. An empirical correlation for transient hot fluid outlet temperature by dimensionless parameters at a mass flow step changes for a conventional heat exchanger

4.4.5. *Comparison of heat transfer rate between the MICHX and cross flow conventional heat exchanger*

The transient effect of variation in the operating conditions of the presented heat exchangers on the heat transfer rates are shown in Figures 4.9 & 4.10. The changes are applied in the temperature and mass flow of hot fluid to study the dynamic effect in heat transfer rate for hot and cold fluids. When considering the hot liquid heat transfer rate of both exchangers, at temperature step of 3.5 and mass flow step of 2.5 the heat transfer rate shows a peak before reaching steady state. The MICHX among the two reaches higher peak at about 12% compared to the conventional for the temperature steps. For the case of mass flow, the peak is about 22% higher MICHX compared to the conventional on step of 2.5 while no peak is found for the case of negative step. This is due to the rapid change in temperature or mass flow rate from the base to the high value. The airside heat transfer rate of the two heat exchangers experienced a change with no peaks since the variation is applied on the hot liquid. The rate of heat transfer enhancement for the temperature step change is found about 30% for the MICHX than radiator whereas it is 21% for the case of mass flow steps. This is because of the higher heat transfer surface area, existence of serpentine, as well as secondary flow in the serpentine that causes the boundary layer to breaks and new boundary layer start developing.

(a)   (b)
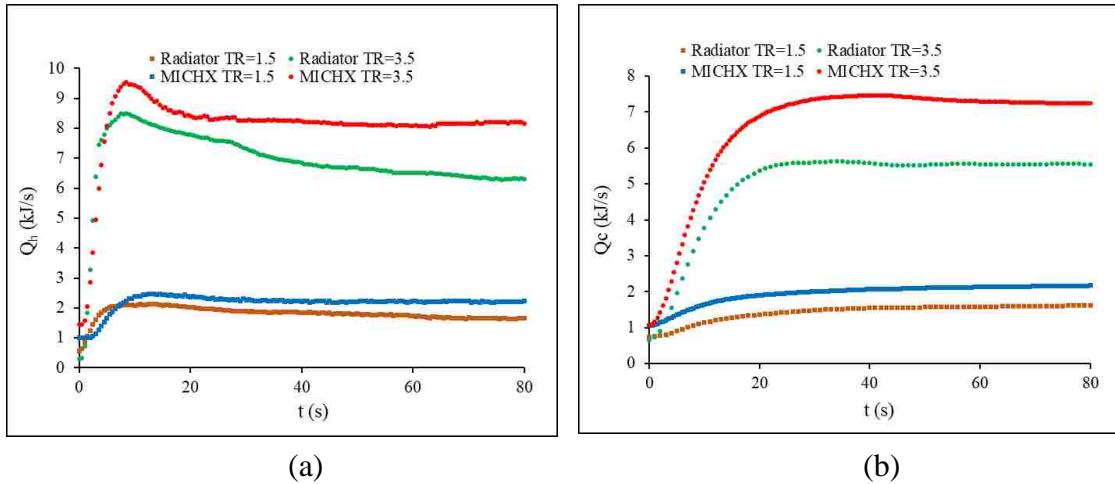
Figure 4.9 (a) shows the heat transfer rates of the hot and cold fluids at the hot liquid

mass flow step changes for the conventional and MICHX

(a)

(b)
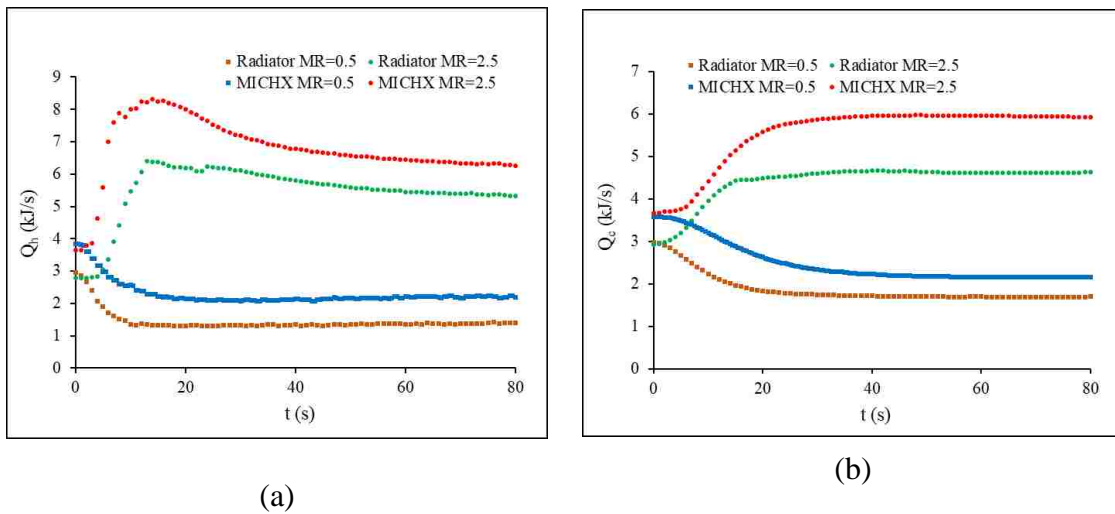
Figure 4.10 shows the heat transfer rates of the hot and cold fluids at the hot liquid inlet

temperature steps for the conventional and MICHX

4.4.6. Comparison of the transient effectiveness of the conventional and MICHX

The experimental data are demonstrated for transient effectiveness of the heat exchangers

in Figures 4.11a and 4.11b for the inlet temperature step changes, and 4.12a and 4.12b for

the mass flow step variation. The operating conditions experiences the same variations as

discussed above. The results show the reverse trend of transient effectiveness for the hot and cold fluid for both heat exchangers that is a positive peak for the hot fluid and negative peak for the cold fluid. Increase in effectiveness is found to be around 15% to 25% higher for the hot fluid transient effectiveness on the MICHX than the conventional for temperature steps and 11% to 35% for the case of mass flow changes. The transient effectiveness for the cold fluid is found to be 21% to 25% for the temperature step variation whereas 20% to 24% for mass flow step changes.

(a)

(b)
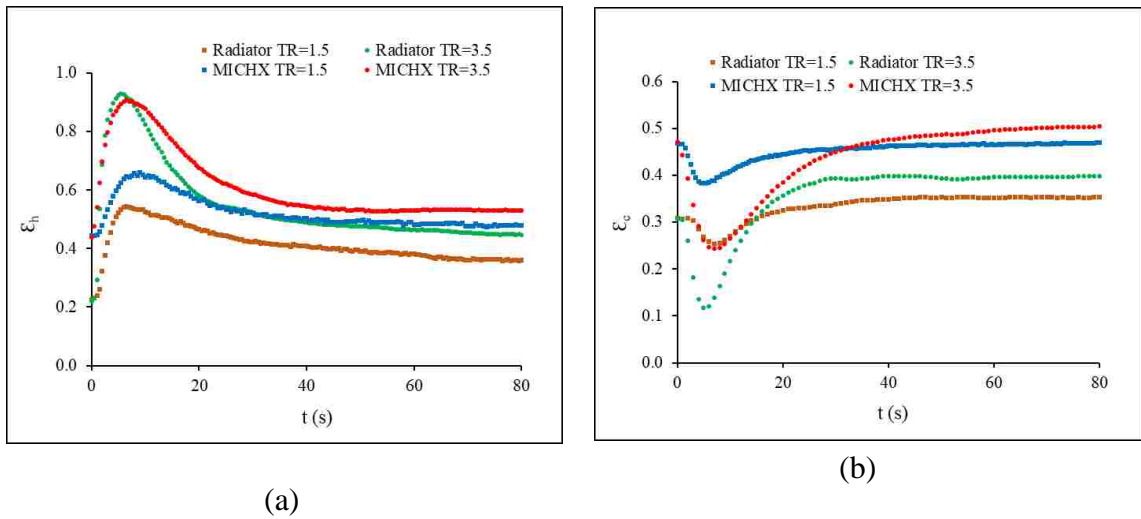
Figure 4.11 illustrates the effectiveness of the hot and cold fluids at the hot liquid inlet temperature steps for the conventional and MICHX

| (a) | (b) |
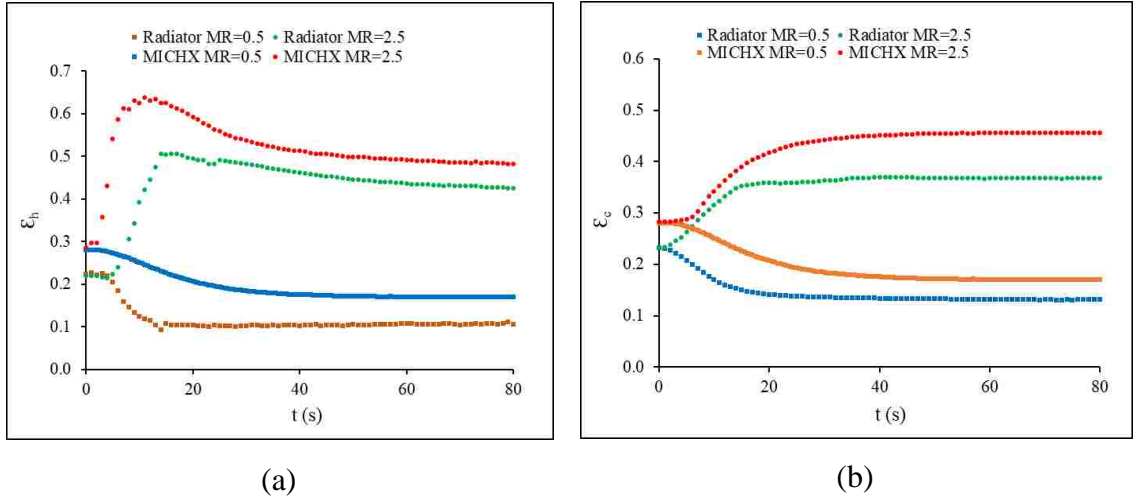
Figure 4.12 displays the effectiveness of the hot and cold fluids at the hot liquid mass flow steps for the conventional and MICHX

4.4.7. *Comparison of the dimensionless temperatures of the MICHX and conventional*

Figures 4.13a and 4.13b represent the behavior of dimensionless temperatures of both heat exchangers for the condition of inlet temperature variations. The trend of the charts displays the same negative dent for the hot and cold fluids. The enhancement of 17% to 18% is found for the hot fluid dimensionless temperature whereas 19% to 28% increase for the cold fluid. Figure 4.14a and 4.14b shows how the dimensionless temperature changes on time for mass flow step change. The dimensionless temperature for the case of the mass step changes decrease about 21% to 60% for the hot fluid side while experiences an increase about 18% to 21% for the cold side.

(a)   (b)
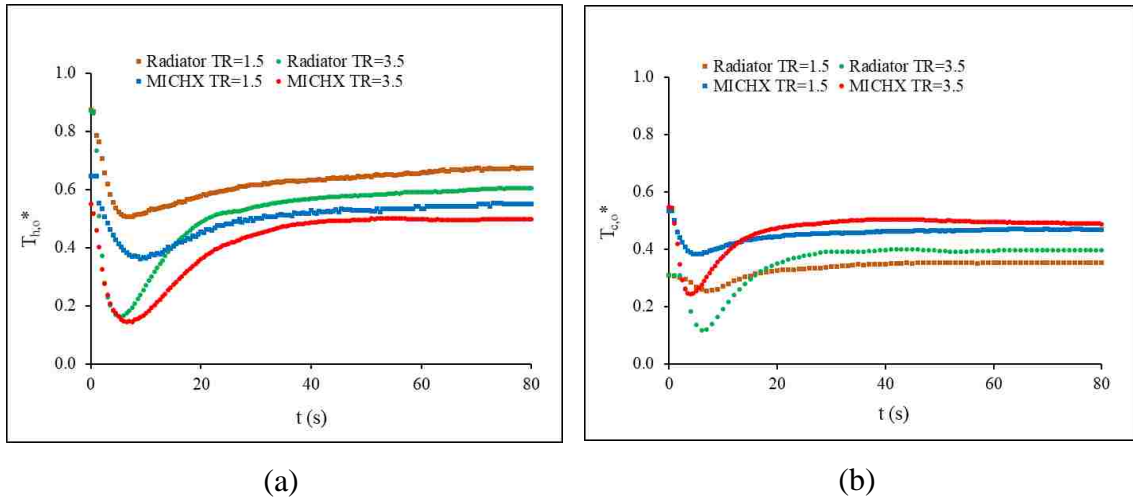
Figure 4.13 represent the dimensionless temperatures of the hot and cold fluids at the

hot liquid inlet temperature steps for the conventional and MICHX

(a)   (b)
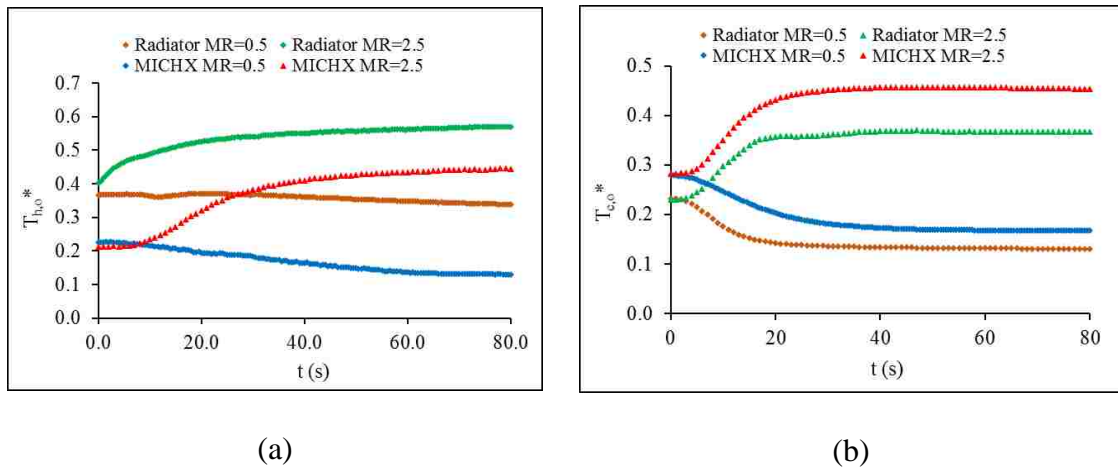
Figure 4.14 represent the dimensionless temperatures of the hot and cold fluids at the

hot liquid mass flow steps for the conventional and MICHX

4.4.8. Comparison of the dimensionless temperatures on Re for the MICHX and the radiator for the steps of 1.5 and 3.5

The dimensionless outlet temperatures of the heat exchangers of our study are represented

over the Reynolds number for the conditions of the temperature and mass flow variations

on figures 15a, 15b, 16a and 16b. The step variation of this experiment ranges between the

Reynolds number of about 550 to 3356 for the MICHX and about 1460 to 8295 for the

conventional cross flow heat exchanger for mass flow variation ranging between 5025 to 11057 for the MICHX and about 2290 to 4835 for the conventional on the temperature step variations. The trends show a negative peak for all the conditions of the temperature step variations. For the same mass flow rate Re is lower for the MICHX compare to the radiator. Nonetheless, dimensionless temperature for the mass flow changes show different trend to the temperature step changes. The initial delay increases as the step change increase and it is higher for the MICHX than the Radiator.

(a)   (b)
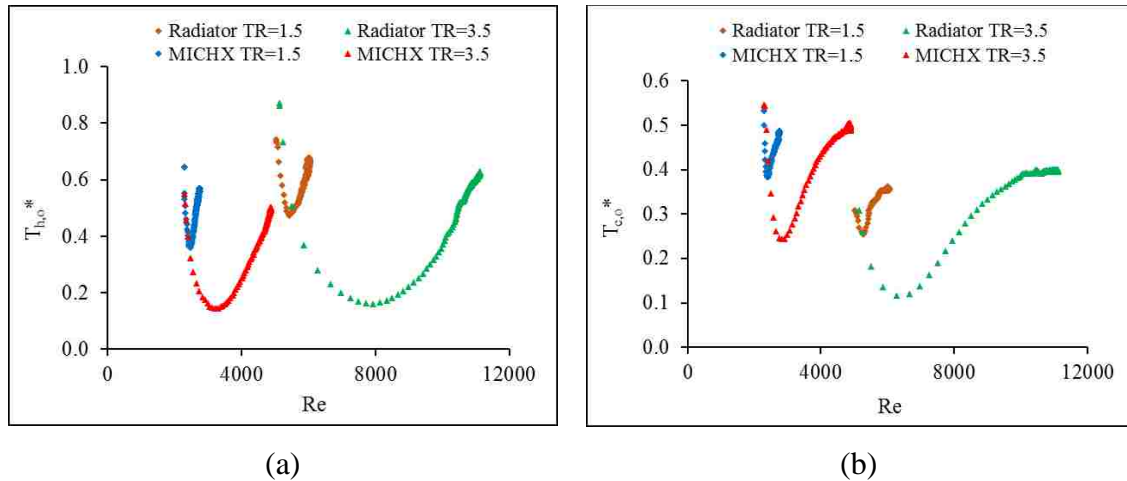
Figure 4.15 demonstrate the dimensionless temperatures of the hot and cold fluids on Reynolds number for both heat exchangers

(a)   (b)
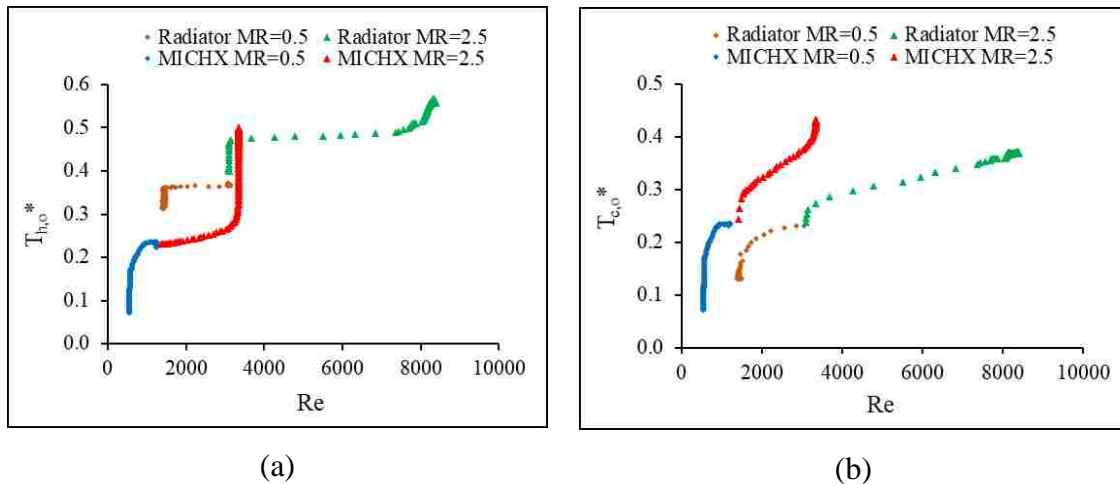
Figure 4.16 show the dimensionless temperatures of the hot and cold fluids on

Reynolds number at the hot liquid mass flow steps for the conventional and MICHX

4.5. Conclusion

Heat exchangers are one of the critical devices of the thermal systems. Increasing demand in thermal energy leads to enhance the efficiency of the systems by improving in heat exchanger performance. In this work the dynamic response of different heat exchangers was investigated experimentally to evaluate the transient performance of heat exchangers under mass flow step of 0.5 to 2.5 and inlet temperature step variations of 1.5 to 3.5. The results also are used to assess the predictability of the analytical model available in the literature.

- The shorter response time is found for the MICHX compared to the cross flow conventional one. The response times are found to be 38s and 76s on the temperature step variation and 83s and 178s on the mass flow step changes of 2.5 for the MICHX and conventional heat exchanger accordingly.

- The trend of transient response in hot fluid experienced a higher peak of 12% for the MICHX compared to the conventional heat exchanger.

102

- Response time is shorter for the MICHX compared to the conventional heat exchanger.

- The larger initial delay time is found longer for the MICHX then the conventional heat exchanger due to the higher resident time for the MICHX. The initial delay time is found 4.5s for the MICHX compared 0.7s for the cross flow conventional.

- It was found that the prediction of analytical model has over 20% overestimation compare to the experimental results. The possible reason for this difference could be due to the assumptions made such as constant heat transfer coefficient to simplify solving the governing equations.

- Two empirical correlations (Eqs. 4.27 and 4.28) are obtained to predict the hot fluid outlet temperature in the dimensionless parameters for the temperature and mass flow step variations for a conventional heat exchanger.

- The hot fluid shown a 30% increase in heat transfer rate for temperature step of 3.5 and 21% for the mass flow step of 2.5 for MICHX compare to the conventional heat exchanger at the steady state conditions.

- Hot fluid effectiveness is found to be around 15% to 25% higher for the MICHX then the conventional cross flow heat exchanger for temperature steps and 11% to 35% for the case of mass flow changes.

Nomenclature

A_c *Channel cross section area, m^2*

$A^{'}$ *Surface area per unit length of the channel, m^2*

B *Bias*

D   *diameter, m*

D_h *Channel hydraulic diameter, m*

DAQ   *Data Acquisition*

L   *Channel length along the water fluid, m*

MICHX   *Minichannel Heat Exchanger*

$\dot{m}$ *Mass flow rate, g/s*

min   *Minimum*

P   *precision*

PTD   *Pressure Transducer and Transmitter*

RTD   *Resistance Temperature Detector*

Re   *Reynolds number*

RSS   *Root of sum of squares*

SCXI   *Data acquisition module and terminal block*

Q   *Heat transfer rate, W*

T   *Temperature, °C*

t   *Time, s*

U   *Uncertainty %*

t_{res} *Resident time, s*

V   *Velocity, m/s*

$\dot{\forall}$ *Volume flow rate m^3/s*

Greek symbols

ε   *Effectiveness*

μ   *Dynamic viscosity*

ρ *Density, kg/m^3*

Subscripts

a   *Cold fluid, Air stream*

c   *Cold fluid*

i   *Inlet*

h   *Hot fluid, water stream*

o   *Outlet*

Superscripts

*   *Dimensionless parameter*

References

[1]   S. G. Kandlikar "A Roadmap for Implementing Minichannels in Refrigeration and Air-Conditioning Systems— current Status and Future Directions" Heat transfer engineering, 28(12):973-985, 2007.

[2]   M. Dehghandokht, M. G Khan, A. Fartaj, s. Sanaye "Numerical study of fluid flow and heat transfer in a multi-port serpentine meso-channel heat exchanger" Applied Thermal Engineering, 31: 1588-1599, 2011.

[3]   C. Guha, and A. Chaudhuri "Transient analysis of heat exchanger network" Journal of the Institution of Engineers, Chemical Engineering Division, v 87, PP. 51-59, March 2007, ISSN: 00203351.

[4]   T. Gao, B. Sammakia, J. Geer, A. Ortega and R. Schmidt "Transient Effectiveness Characteristics of Cross Flow Heat Exchangers in Data Center Cooling Systems" 14th IEEE ITHERM Conference PP.688-697, 2014.

[5]   M. Mishra, P.K. Das, and S. Sarangi "Transient behaviour of crossflow heat exchangers due to perturbations in temperature and flow" International Journal of Heat and Mass Transfer 49:1083–1089, 2006.

[6]   K. Silaipillayarputhur, and S.A. Idem, "Transient response of a cross flow heat exchangers subjected to temperature and flow perturbations" Proceedings of the ASME, international mechanical engineering congress and exposition, Houston, Texas, Nov. 2015.

[7]   F.H. Syed, and S. Idem "Transient performance of a cross flow heat exchanger using finite difference analysis" ASME, Proceedings of International Mechanical Engineering Congress and Exposition, IMECE2008, Boston, Massachusetts, USA, Oct-Nov 2008.

[8]   W. Roetzel, M. Li, and X. Luo "Dynamic behaviour of heat exchangers" Advanced Computational Methods in Heat Transfer, 451-460, 2002, ISBN 1-85312-906-2.

[9]   Y. Yao, M. Huang, J. Mo, and S. Dai "State-space model for transient behavior of water-to-air surface heat Exchanger" International Journal of Heat and Mass Transfer 64: 173–192, 2013.

[10]   M. Del Valle, and A. Ortega "Experimental Characterization of the Transient Response of Air/Water Crossflow Heat Exchangers for Data Center Cooling Systems" International Technical Conference and Exhibition on Packaging and Integration of Electronic and Photonic Microsystems, InterPACK, 1 – 9, 2015.

[11]   B. Prabhakara Rao and K. S. Das "An Experimental Study on the Influence of Flow Maldistribution on the pressure drop across a plate heat exchanger" Transactions of the ASME 126: 680-691, JULY 2004.

[12]   S. Fotowat, S. Askar, and A. Fartaj "Experimental transient response of a minichannel heat exchanger with step flow variation" Experimental thermal and fluid science, 89: 128-139, 2017, doi.org/10.1016/j.expthermflusci.2017.08.004

[13]   J. Yin, M. K. Jensen "Analytic model for transient heat exchanger response" International journal of heat and mass transfer, 46: 3255-3264, 2003.

[14]   Y. A. Cengel "Heat Transfer: A Practical Approach" New York: McGraw-Hill Higher Education, 2006.

[15]   R. M. Cima, and A. L. London "Transient Response of a Two-Fluid Counter-Flow Heat Exchanger-The Gas-Turbine Regenerator" Transactions of ASME, vol. 80, PP. 1169–1179, 1958. http://dx.doi.org/10.5772/67334.

[16]   T. Gao, B. Sammakia, J. Geer, A. Ortega, and R. Schmidt "Dynamic Analysis of Cross Flow Heat Exchangers in Data Centers Using Transient Effectiveness Method" IEEE Transaction of Component Packaging and Manufacturing Technology, vol. 4, no. 12, PP. 1925–1935, Nov. 2014. DOI: 10.1109/TCPMT.2014.2369256.

[17]   N. Srihari, and S. K. Das "Experimental and theoretical analysis of transient response of plate heat exchangers in presence of nonuniform flow distribution" J. of heat transfer, vol. 130, PP. 051801-1–9, 2008.

CHAPTER 5

A STUDY ON CORROSION EFFECTS OF A WATER BASED NANOFLUID FOR

ENHANCED THERMAL ENERGY APPLICATION

5.1. Introduction

Nanotechnology is gaining a huge attraction nowadays due to its widespread use ranging from agriculture, biomedical, water treatment to energy storage. The recent advancement in nanotechnology made it possible to disperse nanosize particles into a base liquid to enhance its thermodynamic properties. The resultant fluid is called a nanofluid. The nanoparticles used in nanofluids can be metals, oxides, carbon nanotubes, etc. The first study on a two-component mixture fluid was done by Maxwell [1]. He analytically studied conduction through suspended micro size particles. The Maxwell equation represented thermal conductivity for low particle volume concentration mixtures.

A later development in nano technology attracted the attention to investigate nanosize particles dispersed in a base fluid. Experimental effects of nanofluid flow on different type of materials is studied by Celata et al. [2] highlighting the importance of studying the effect of the nanofluid on the surface of the material used in the facility before adopting it as a heat transfer fluid. Experimental study was performed by Bubbico et al. [3] where metallic targets were exposed in a flow of nanofluid. Their results show that the damage on the metals was due to the effect of corrosion more than erosion and that the pH level of the suspension is very important. Carbon nanotubes (CNTs) effect on corrosion of different metals (Al, SS, and Cu) using different types of fluids was studied by Rashmi [4]. They reported the highest corrosion occurred for Aluminum regardless of the fluid used. They also extended their investigation to compare a standard radiator with a conventional fluid

to a smaller radiator with a CNT-nanofluid. Their finding was the last showed enhanced heat transfer over the conventional.

Applications of nanofluids include but not limited to HVAC, electronics, automotive, and biomedical. In heat transfer applications, studies on the use of nanofluids to enhance the heat exchange process have been done. Substitution of cooling and heating water with nanofluids in industrial cooling systems was examined by Routbort et al. [5]. The study found around 300 million kWh in energy saving every year in the electric power industry field in the unified conditions of the United States using nanofluids, this is equal to the energy required by 50,000 – 150,000 families. Furthermore, the stability of several nanofluids was examined by Hwang et al. [6] with UV–vis spectrophotometer. Stability of nanofluid means that to prevent the nanoparticles in dispersion stick together and form aggregate at a significant rate and settle out due to gravity. Many types of nanoparticles have been used to prepare nanofluids to investigate the thermal properties of such fluids.

Their findings were the stability of nanofluids was affected by the characteristics of the suspended particles and base fluids, the stability of the fluid can be improved by adding a surfactant, and the thermal conductivity depends on the volume fraction of nanofluids. In addition, Li et al. [7] studied the dispersion behavior of water-based copper nanofluid to have a superior comprehension of its stability. Results based on the sediment photographs and particle size distribution show better dispersion characteristics in the suspension when adding dispersant. Additionally, a significant impact of pH on the stability of the copper suspension was found.

Das et. al. [8] examined the increase of thermal conductivity of nanofluids with temperature having water as the base fluid and two types of particles, Al2O3 & CuO. Their main results yielded an increase of thermal conductivity enhancement with temperature. Buongiorno et al. [9] measured the thermal conductivity of identical samples of nanofluids using various experimental approaches over 30 organizations worldwide. Different base fluids and nanoparticles were used at a variety of concentrations. Results showed that the nanofluids thermal conductivity increases as the particle concentrations increase. Li et al. [10] experimentally measured the thermal conductivity and viscosity of aqueous magnetic fluids. A ferrofluid is a colloidal liquid made of nanoscale ferromagnetic particles suspended in a carrier fluid that becomes strongly magnetized in the presence of a magnetic field. Their study included the presence and absence of an external magnetic field. Their conclusion was that the thermal conductivity of the magnetic fluid is higher than that of a pure fluid. The effect of the magnetic field on thermal conductivity was found to be increasing when it is parallel to the temperature gradient and no effect was found when it is perpendicular. Water based aluminum oxide nanofluid was used to study its effect on enhancing the heat transfer performance of heat exchangers by Issa [11]. With two types of exchangers used, results showed an enhancement of effectiveness of about 49%. Furthermore, adding low concentration caused a noticeable improvement in the thermal performance of the system.

Additional investigation on the safe handling of nanoparticles or nanofluids is important since the particles used in nanofluids are very small and are within a range of (1-100nm). The presence of nanoparticles in the base fluid has a positive effect on the energy exchange process, however, the occupational exposure limit proposed by the National Institute for

110

Occupational Safety and Health or equivalent organizations should be taken into account. Studies on health effect of the exposure to various nanofluids are still behind the continuous growth of nanotechnology. Up to date, no record of harmful effects of working with nanofluids on health is found, however, a high level of precaution is to be followed when dealing with nanofluids due to the incomplete information on their safety and further studies are to be considered in order to identify a proper safety procedure. The research organizations in US and Europe as well as the National Science Foundation (NSF) and the National Toxicology Program have been investigating the toxicology of nanoparticles. They proposed the use of safety measures introduced by Massachusetts Institute of Technology (MIT) [12] for handling nanoparticles on nanofluids. From the open literature, there is no noticeable hazardous issue observed using nanofluids but due to the safety precautions of using nanoparticles, high safety measures, standards, and precautions should be followed in handling nanofluids. Nowadays, nanofluids, especially water-based nanofluids, are being used safely and successfully in industrial, biomedical engineering, and bioscience applications Wong [13].

This paper presents the pH impact of aluminum oxide/water (Al_2O_3/W) nanofluid on aluminum (Al), copper (Cu), and stainless steel (SS) which are used in common applications. Experiments on the most common materials will be performed to show the highest and lowest corrosive metals to be used. Two different solutions of same pH level of (3.7) of the Al_2O_3/W nanofluid are prepared with H_2SO_4+NaOH and HCl+NaOH. The effect of the solutions on the materials in a long term is examined with Scanning Electron Microscope/Energy Dispersive Spectroscopy (SEM/EDS) and WiTec system with an accelerating voltage of 5.0 kV. The effect of adding nanoparticles to a base fluid on the

111

thermal conductivity of the fluid is also presented at various temperatures (20, 30, and 40°C). After measuring the thermal conductivity, it is presented as a function of temperature and fluid concentration. In thermal systems for example, nanofluids are used to enhance the heat transfer. Results from this study will provide insight on the interaction of these nanofluids with the contact materials. Understanding the interaction of these fluids with the contact material used to serve as an important parameter when designing a thermal system with a nanofluid as the working fluid.

5.2. Experimental Procedure

The corrosive effect of a nanofluid on three different materials is investigated. An experiment is conducted using aluminum oxide/water (Al2O3/W) as the nanofluid and aluminum (Al), copper (Cu), and stainless steel (SS) as the targeted materials. The mentioned materials are chosen as the test cases due to their wide use in thermal systems such as automotive, HVAC, and power plants. The nanoparticles are known with their agglomeration and sedimentation in the base fluid, therefore, special methods are used to prepare nanofluids.

The presented nanofluid for this study Al2O3 is prepared using a 2-step method where nanoparticles are purchased and then are dispersed into the base liquid. The nanoparticles size used is 50nm of aluminum oxide (Al2O3), (AL- 0405, 99.5%), dispersed into the base fluid which is DI-water. The preparation procedure included adding surfactant and using rod sonication technique to improve the uniformity and stability of the nanofluid. This method led to a change in the pH value of the nanofluid to about 3.7. The material samples used in this study are immersed in beakers containing solutions of sulphuric acid (H2SO4)

and hydrochloric acid (HCl) of pH=3.7. These solutions are prepared by adding sodium hydroxide (NaOH) to the acids. The samples are left for a period of 8 months to see the long-term effect as shown in Figure 5.1. Deionized water (DI) is used to wash the samples, after that, they are gold coated using the sputter coater machine. A thin layer of gold helps to have clear images while using Scanning Electron Microscope and Energy Dispersive Spectroscopy (SEM/EDS) machine. Map notes, images, and analysis of all the surfaces of the samples captured are put together for final interpretation.

(a)   (b)

Figure 5.1 samples of (a) Al2O3 nanoparticles (50nm) and (b) Al2O3/W nanofluid (volumetric concentration = 5%)

Checking for the uniformity and stability of the nanofluid is also examined. The fluid is left aside for two weeks before performing the tests using the integrated WiTec Atomic Force Microscope (AFM) and Confocal Raman Spectrometer. It has a true surface profilometer and scanning near optical microscopy and is capable to achieve an optical resolution of 50-100 nm with a water-immersion objective lenses that can do analyses in liquids. Four different mass concentrations of the Al2O3 nanoparticles in the fluid are applied. These concentrations are 1.0, 2.0, 4.0, and 6.0%. Using the water-immersion

objective lenses of the Raman Spectrometer, an image of a very thin layer of the nanofluid is taken. This image is used to analyze the uniformity and stability of the nanofluid.

Figure 5.2 Thermal conductivity analyzer device (C-therm)

The thermal conductivity of the nanofluid at four different concentrations is tested by C-therm Figure 5.2, thermal conductivity analyzer device with a precision of better than 1%, at various temperatures (20, 30, & 40°C). An isotherm incubator was used to keep the temperature of the nanofluid constant to get better measurement of the thermal conductivity.

5.3. Results and Discussions

The study shows the corrosion effect that can occur on some chosen sample of materials used in many systems such as thermal system. It included copper, aluminum, and stainless steel. The samples left under environmental conditions and corrosion was captured using SEM/EDS. Then aluminum was chosen to be immersed in two different solutions, H_2SO_4 and HCL. The corrosion effect was also captured by SEM/EDS. Since thermal systems use these metals for their heat transfer equipment, the type of metal used is considered an

important factor when designing such equipment. Such a system requires a working fluid since it plays an important role in the heat transfer process. The enhancement of the thermal properties of the fluid such as in nanofluids, leads to higher heat transfer. Thus the choice of material when using a nanofluid as the working fluid has an essential effect on the heat transfer process.

Results are presented for different study cases; the effect of environment on the tested samples of metals, the effect of the acidic solution on the aluminum sample, study of the uniformity and stability of the nanofluid, and the thermal conductivity enhancement.

5.3.1 *Effect of environment on aluminum, copper, and stainless steel*
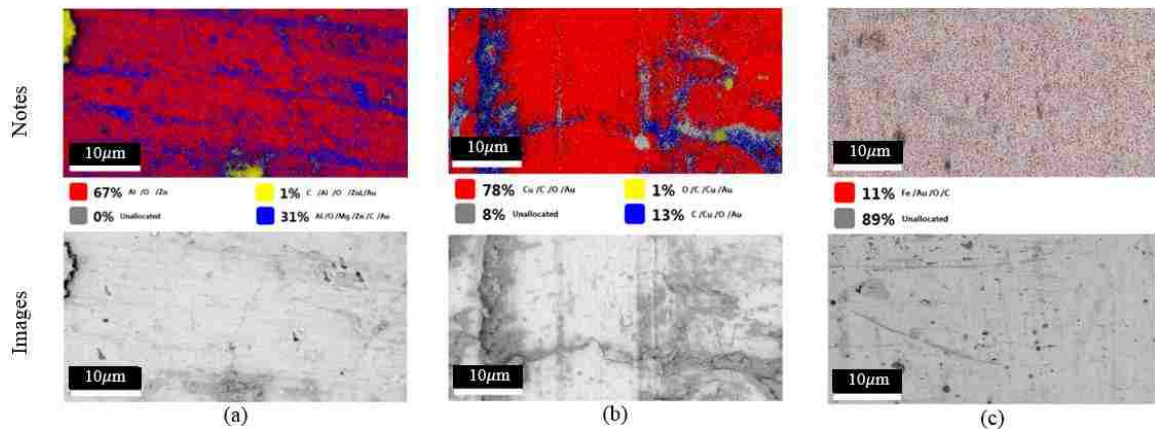
Figure 5.3 Maps and images of three different surfaces of (a) aluminum, (b) copper, and (c) stainless steel taken with an SEM/EDS

The images and surface map notes that represent corrosion of three different metals, aluminum (Al), copper (Cu), and stainless steel (SS), under environmental conditions are shown in Figure 5.3. The formation of Al_2O_3 and CuO on the surfaces of aluminum and copper respectively is noticed. The figure also shows, percentage wise, for each sample,the

115

amount of corrosion formed on its surface and its distribution. Negligible corrosion effect is noticed on stainless steel due to the thin protection layer of chromium oxide on its surface.

5.3.2   *Effect of acidic solution on aluminum*

(a)   *(b)*   *(c)*
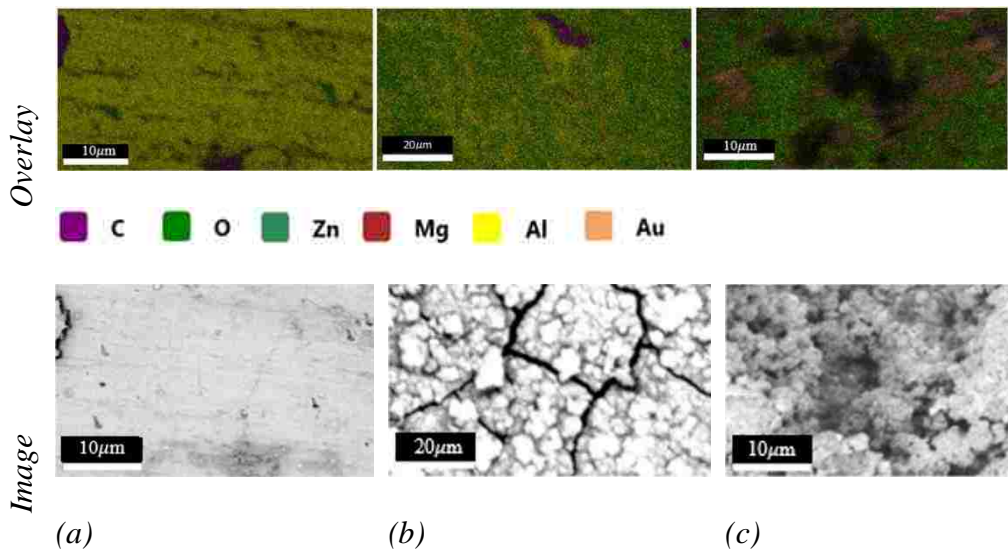
Figure 5.4 Overlay and images surfaces of (a) Aluminum under environment (Al), (b) Al in H2SO4 solution of pH=3.7, and (c) Al in HCl solution of pH=3.7

Out of the three metals chosen, aluminum sample is further investigated. Two different solutions of H2SO4 and HCL that have the same pH level of 3.7 are used. The aluminum sample is immersed in each of the solutions. Figure 5.4 represents the images captured of the (a) sample of aluminum taken under environmental conditions, (b) aluminum sample immersed in H2SO4, and (c) aluminum sample immersed in HCL. The figure shows the amount of oxygen on the aluminum sample contact surface if left under environmental conditions or immersed in any of the acidic solution and percentages were recorded as

116

follows, (a) 9.0%, (b) 47.0%, and (c) 42.0%. According to these percentages, higher partial pressure of oxygen is seen when aluminum sample is in the solution than when it is under environmental conditions. This means higher corrosion and cracks on the aluminum surface. Photos of all the metal samples in both acidic solutions are shown in Figure 5.5.

(a) Aluminum in H2SO4 solution	(b) Aluminum in HCl solution	(c) Copper in H2SO4 solution	(d) Copper in HCl solution	(e) Stainless steel in H2SO4 solution	(f) Stainless steel in HCl solution
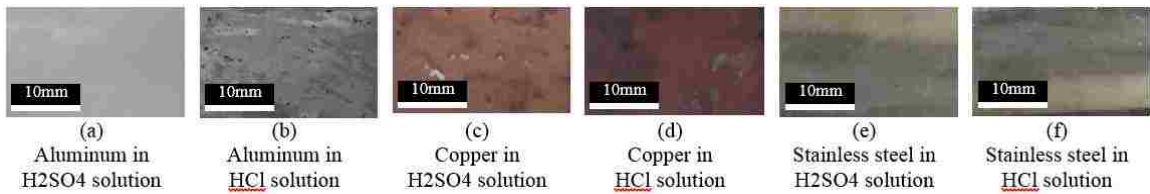
Figure 5.5 Photograph of different metal samples in acidic solutions of pH=3.7

(a)   (b)   (c)
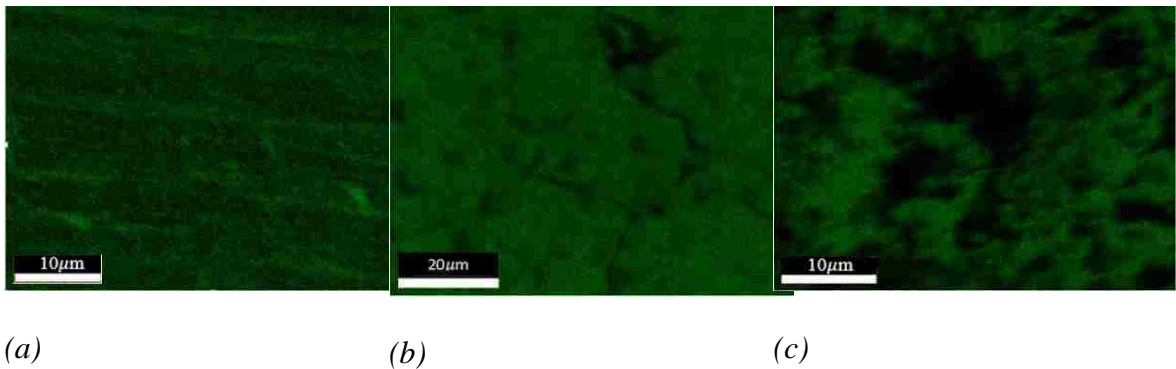
Figure 5.6 Mapping of oxygen on the surface of (a) Aluminum under environment, (b) Al in H2SO4 solution of pH=3.7, and (c) Al in HCl solution of pH=3.7

Figure 5.6 presents the oxygen mapping of (a) aluminum (Al), (b) Al in H2SO4 solution and (c) Al in HCl solution. The distribution of 9.0% oxygen on Figure 5.6a is found on the Al surface, which indicated the corrosion on the Aluminum. Figures 5.6b and 5.6c reveal that the percentage of oxygen on the surface increases to approximately 45.0%±2.0% for the samples that have been in contact with the solution. The level of oxygen pointed out the severity of corrosion and crack on the surface caused by the pH level of the solution.

117

There is a variation in the oxygen level produced by two different solutions, which is due to the effect of the acids in addition to the pH value.

5.3.3   *Uniformity of Al2O3/W nanofluid*

When using nanofluids in industry, nanofluid stability is important to achieve. In the present study, surfactants, which are chemical compounds added to the nanofluid, are used to increase the immersion of the particles leading to long term stability. Sonication was also used for the same purpose. These are easy and economical ways to increase the stability of the nanofluid. SEM/EDS map notes using Raman spectroscopy was used to check the stability and uniformity of the nanofluid for this study. The size of Al2O3 nanoparticles used in this study is 50nm with 99.5% purity. Figure 5.7 shows images taken for the nanoparticles and the DI-water separately, as well as, the produced nanofluid. Although, the powder is the composition of aluminum and oxygen only, the SEM map shows the presence of some unexpected carbon particles. In Figure 5.7b, the uniformity and purity of DI-water shown indicates no trace of any particles in it. When Al2O3 nanoparticles are dispersed in the base fluid, Figure 5.7c, a trace of particles can be seen clearly. However, the image still shows the uniformity distribution of nanoparticles within the base fluid. Uniformity and stability of nanofluids is important to avoid issues such as clogging or decreasing the thermal conductivity of the fluid.
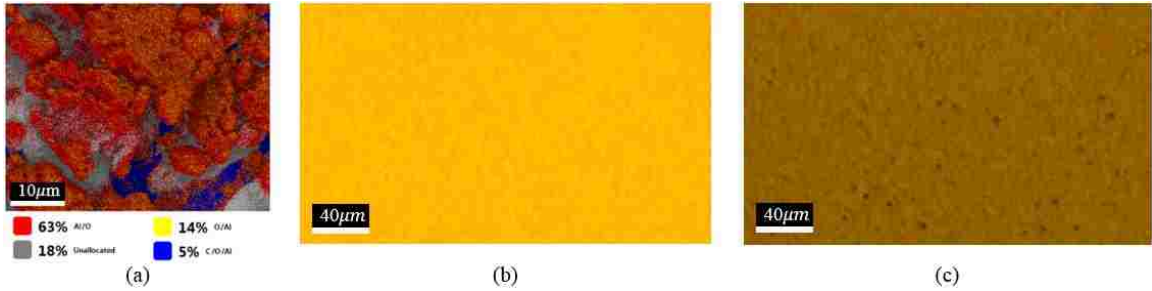
Figure 5.7 (a) SEM/EDS map notes of Al2O3 powder, (b) Raman spectroscopy of DI-water, and (c) Raman spectroscopy of Al2O3/W nanofluid

5.3.4 Enhancement of thermal energy

The effects of concentration, and temperature changes on the Al2O3/Water nanofluid thermal conductivity are illustrated in Figure 5.8. The thermal conductivity is plotted against different temperatures. For every set of temperature, four different concentrations were considered; (1.0, 2.0, 4.0 & 6.0) % as well as, pure water which is represented 0% concentration.
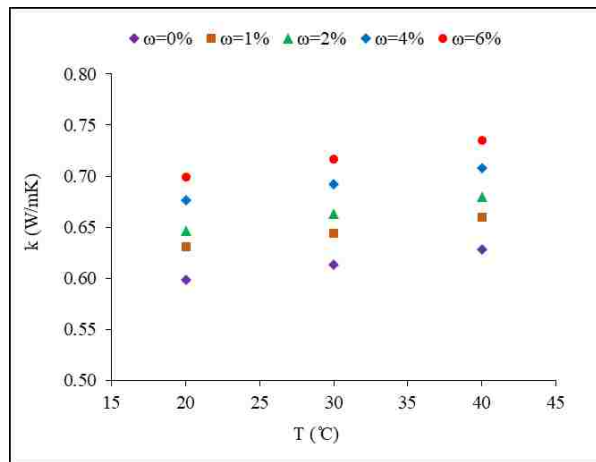
Figure 5.8 Thermal conductivity at different fluid concentration and temperatures

Compared to water, adding nanoparticles is seen to enhance the thermal conductivity of the fluid. Results show that increasing the temperature for a given concentration, thermal conductivity is found increasing. Compared to distilled water, higher temperatures of

119

nanofluid yield higher thermal conductivity. A thermal conductivity increases of 17% compared to DI water is found between temperatures of (20, 30, & 40) °C. This increase in the thermal conductivity of the nanofluid can be attributed to some reasons such as: as the temperature increases, the Brownian motion and collision between the particles increase resulting in a rise in the thermal conductivity. Also, the high surface to volume ratio of the nanoparticles due to the small size of particles used plays an important role as well. The nanoparticles concentration in the nanofluid plays an important role in the enhancement of thermal conductivity. It is noticed that the thermal conductivity of the nanofluid increases with the increase of the fluid concentration at a given temperature.
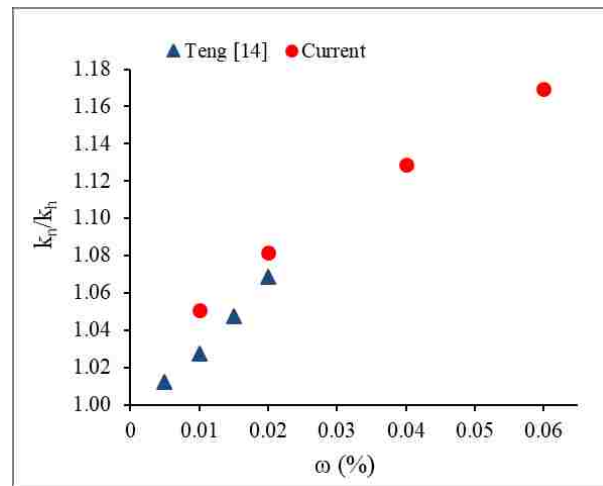
Figure 5.9 Thermal conductivity comparison at different fluid concentration and temperatures

Figure 5.9 represents the thermal conductivity ratio with weight fraction (ω) of nanofluid at a temperature of 30°C with nanoparticles size of 50nm. Results obtained are compared to Teng [14] and the comparison was made using the same size of nanoparticles 50nm with a range of weight fraction of (1, 2, 4 & 6) % for Al2O3/water nanofluid. The thermal conductivity is found to increase with the increase of the nanofluid concentration for a

given temperature. The increasing trend shows a good agreement with the compared experimental data, however, the current experimental results exhibit higher thermal conductivity compared to [14] as the temperature and concentration increase. The difference in the results might be due to particles shape, and the method of preparation of nanofluid.

5.4. Conclusions

The safety, chemical interactions of the nanofluid flow with common metallic surfaces used in various industrial applications are presented in the current study using SEM/EDS and WiTec machines with an accelerating voltage of 5.0 kV. The corrosion effect of three different materials (i.e. aluminum, copper and stainless steel) has been analyzed and its results are reported. The effect of corrosion on metallic surfaces is important to examine the long term effect of the exposure of different industrial system components to nanofluids if used instead of water. Additionally, nanofluid thermal conductivity is important in heat transfer processes and since many different results of thermal conductivity were documented with some discrepancies, an investigation of the experimental thermal conductivity at various temperatures and fluid concentrations is discussed in this paper and the results are as follows:

- Among the three materials used, Cu possessed the highest corrosion while SS showed the lowest corrosion at environmental condition. When these metals are submerged into acidic solutions, a considerable increase of oxygen is observed on all the metal surfaces due to the increase in the pH value.

- The higher amount of oxygen refers to higher oxygen partial pressure on the metals surface compared to the environmental condition which results in higher pitting and intergranular corrosion.

121

- The increase in thermal conductivity depends on the temperature and nanoparticles concentration. Other factors may play a role such as nanofluid preparation, nanoparticles shape and size, nanoparticle material, etc.

- Thermal conductivity increases as temperature increases. The increase rate depends on the nanoparticles concentrations in the fluid. The higher the concentration and temperature, the higher thermal conductivity obtained.

For future studies, further experiments including wider range of temperatures and nanoparticles concentration are needed in this field for better understanding of the behaviour of nanofluids. The interaction of various types of materials with nanofluids over time requires a further investigation to examine the applicability of nanofluids for many heat exchange processes.

References

[1]   J.C. Maxwell "A Treatise on Electricity and Magnetism" Clarendon Press, Oxford, UK, 2 (1873) 459.

[2] G.P. Celata, et al. "Experimental Results of Nanofluids Flow Effects on Metal Surfaces" chemical engineering research and design 9 2 (2 0 1 4) 1616–1628.

[3] R. Bubbico et al. "Experimental analysis of corrosion and erosion phenomena on metal surfaces by nanofluids" Chemical Engineering Research and Design, 104 (2015) 605-614, ISSN 0263-8762

[4] W. Rashmi, A. F. Ismail, M. Khalid, and T.F. Yusaf "Investigating corrosion effects and heat transfer enhancement in smaller size radiators using CNT-nanofluids" Journal of Materials Science, 49 (2014) 4544 – 4551. DOI 10.1007/s10853-014-8154-y

[5] J. Wallin, J. Claesson "Analyzing the efficiency of a heat pump assisted drain water heat recovery system that uses a vertical inline heat exchanger" Sustainable Energy Technologies and Assessments 8 (2014) 109–119C.

[6] Y. Hwang, et al. "Stability and thermal conductivity characteristics of nanofluids" Thermochimica Acta 455 (2007) 70–74

[7] X. Li, D. Zhu, X. Wang "Evaluation on dispersion behavior of the aqueous copper nano-suspensions" Journal of Colloid and Interface Science, 310 (2007) 456–463.

[8] S. Das, N. Putra, P. Thiesen, and W. Roetzel "Temperature Dependence of Thermal Conductivity Enhancement for Nanofluids" ASME, J. Heat Transfer 125.4 (2004) 567-574

[9] J. Buongiorno et al. "A benchmark study on the thermal conductivity of nanofluids" Journal of Applied Physics, 106, 094312 (2009), DOI:http://dx.doi.org/10.1063/1.3245330

[10] Q. Li, Y. Xuan, J. Wang "Experimental investigations on transport properties of magnetic fluids" Experimental Thermal and Fluid Science 30 (2005) 109–116.

[11] Roy Jean Issa. "Heat transfer investigation of aluminum oxide nanofluids in heat exchangers" European Scientific Institute, ESI

[12] V. Colvin "Nanomaterials Toxicity: potential risks of nanomaterials and how to safely handle materials of uncertain toxicity" Massachusetts Institute of Technology (2015).

[13] K. V. Wong and O. De Leon "Applications of Nanofluids: Current and Future" Advances in Mechanical Engineering, Article ID 519659 (2010) 1-11, doi:10.1155/2010/519659.

[14] T.P. Teng, Y.H. Hung, T.C. Teng, H.E. Moa, and H.G. Hsu "The effect of alumina/water nanofluid particle size on thermal conductivity" Applied Thermal Engineering 30 (2010) 2213-2218

CHAPTER 6

AN EXPERIMENTAL TRANSIENT RESPONSE OF A HEAT EXCHANGER WITH

THE AL2O3/WATER NANOFLUID MASS FLOW AND TEMPERATURE STEP

VARIATIONS

6.1. Introduction

The leading factor of a good design of a mechanical component is to minimize the size of

the component while keeping it efficient. Therefore, the advancement in technology

resulted in compact heat exchangers that have higher area density with reported high heat

transfer rates. Dehghandokht et al. [1] investigated the thermal performance of a compact

heat exchanger and studied the benefit of integrating a serpentine bend in a meso-channel

heat exchanger. They found that the existence of the serpentine bend in this resulted in an

increase in the heat transfer rate. Furthermore, the placing parallel channels inside the

meso-channel slab core led to a uniform distribution of the heat over the channels. In

addition to minimizing the size of equipment, the heat transfer fluid plays a crucial role in

the heat transfer performance. It is known that working fluids such as water and ethylene

glycol have low thermal conductivity compared to solids. Therefore, one way to increase

the thermal conductivity of fluids is by means of adding solid particles to the fluids.

Nanofluids are the new generation of nanotechnology fluids manufactured for better heat

transfer performance by introducing nanoparticles into the base fluid. The idea of using the

suspension of solids to enhance the heat transfer characteristics of fluids was explored more

than a century ago by Maxwell [2]. He was a front man who provided a theoretical basis

for computing the effective thermal conductivity of suspension. This was followed by

many theoretical and experimental investigations like Hamilton-Crosser [3], and Wasp [4].

Their model precisely anticipated the thermal conductivity of slurries. Nevertheless, the

particle size was limited on micro to macro-size with some reported disadvantages. Kang et al. [5] worked on measuring the thermal conductivities of three different nanofluids that have diamond, silver, and silica nanoparticles using transient hot-wire method. Experimental results were compared with values obtained from a theoretical model and found that the heat transfer mechanism should be taken into consideration when estimating the exact nanofluid thermal conductivity. Megatif et al. [6] studied the convective heat transfer coefficient of a TiO –CNT nanofluid using a shell-and-tube heat exchanger under different temperature and mass fraction. Their results showed a significant increase in the effective thermal conductivity and heat transfer coefficient of the nanofluid compared to the base fluid. Choi and Eastman1995 [7] provided a solution by dispersing nano size metallic and carbon nanotube particles into different working fluids to produce nanofluids. The enhancement in heat transfer is not only in the working fluids but also extends to study the dynamic response of heat exchangers as a result to any variation in their inlet conditions. Bunce and Kandlikar [8] presented a review of literature on the dynamic response of single pass parallel and counter flow heat exchangers. Three major types of transient inputs were classified, including step input i.e. a sudden change in temperature or flow rate, frequency input i.e. a periodic change in inlet conditions, and impulse input i.e. an infinite amplitude for an infinitesimal duration. The transient performance of heat exchangers affected by a random temperature and step flow changes was investigated by Xuan et al. [9]. The variations were occurred on either or both fluids, concurrently or individually. An industrial size heat exchanger with baffles was used to experimentally perform the transient analysis and to verify the feasibility of using Fourier series technique. Gao et al [10] analyzed the dynamic response of each component in an IBM data center

cooling facility. Their intention was to decrease the cooling energy use to less than 5% of the total energy consumption. A transient effectiveness method was presented to examine the heat exchangers performance experimentally and numerically. They found that the transient effectiveness curve is useful to study the transient response of heat exchangers in closed systems that consist of multiple heat exchangers. The dynamic performance of thermal environment in air cooled data centers was studied by Master et al. [11]. They developed a CFD/Experimental model to investigate the thermal response of data centers under particular situations of cooling disruption, server shutdown and cooling air flow changes. Erden [12] experimentally studied the transient response of the thermal environment in air cooled data centers. A CFD model was developed and validated by experimental results for specific condition of cooling to evaluate the thermal response of data centers. A quick increase of the temperature at key locations was found to rise beyond acceptable limits within a minute in case of complete fan failure scenario.

Along with the limited experimental investigations, numerical analysis that studied the dynamic behavior of different types of heat exchangers is reported. The dynamic response of a counter flow heat exchanger under a wide range of inlet temperature variations of one of the fluids was numerically studied by Bunce [13]. He used Thermonet, a commercial software, to model the heat exchanger transient response. Their findings include verifying that their solution agree well with other solutions found in literature and is valid for counter flow heat exchangers that are often used in industry owing to their thermal advantage. The effect of sudden change in flow rate of inlet fluids in double pipe and one pass shell and tube heat exchangers was numerically and experimentally investigated by Lachi et al. [14]. A simplified two parameter model with a time lag was presented to determine the time

127

constant of a double pipe heat exchanger. They obtained an analytical expression of the time constant using energy balance. About 10% variance was found between analytical and experimental results. In addition to that, the increase in the flow rate step change led to a drop-in time constant which resulted in a faster response of the heat exchanger. The effect of uniform and non-uniform flow distribution on the temperature transient response for U and Z-type plate heat exchangers was investigated by Srihari et al. [15]. They evaluated the transient outlet temperature response of heat exchangers for several transient conditions like initial delay and time constant. Their results showed that the Z-type flow configuration was highly affected by flow maldistribution compared to the U-type for both transient and steady state conditions.

The transient perturbations that occur in different types of heat exchangers in real life scenarios are approximated nearly by a step function according to Bunce and kandlikar [8]. In this research, a step variation is applied to the liquid side inlet conditions of mass flow rate and temperature while holding the other inlet parameters constant. The application of nanofluids in heat exchangers is very limited and mostly available for steady state conditions. This study focuses on investigating the transient behavior of a minichannel heat exchanger with nanofluid as the primary working fluid. The importance of this study lies in observing the response of the heat exchanger to the step variations as it goes from one steady state to the other. Additionally, the use of the nanofluid and its effect on heat transfer is discussed. Results in terms of outlet temperatures of both fluids, transient effectiveness, heat balance, and time constant are presented and analyzed for the thermal performance control of heat exchangers.

6.2. Transient experimental setup

A fully equipped experimental set up is designed and fabricated to study the dynamic response of different types of heat exchangers subjected to mass flow and temperature step changes as shown in Figure 6.1. Its schematic diagram, which consists of three circuits, can be seen in Figure 6.2. The working fluids are Al2O3/water nanofluid as the hot fluid and air as the cold fluid. A minichannel heat exchanger (MICHX) is placed in the test section to investigate its transient behavior. The MICHX consists of 68 channels of 1 mm diameter and 5 slabs with attached corrugated fins. The slabs and fins are made of aluminum 303. A 10-ton chiller with the aid of an inbuilt heat exchanger was mounted to control the airside inlet temperature. A data acquisition system (DAQ) with 96 channels is installed to monitor and record the data. Pressure transducers (PTDs), resistance temperature detectors (RTDs), T-type thermocouples and Coriolis mass flow meter are used to measure the fluids inlet and outlet pressures and temperatures as well as mass flow rates.

Figure 6.1. The experimental setup
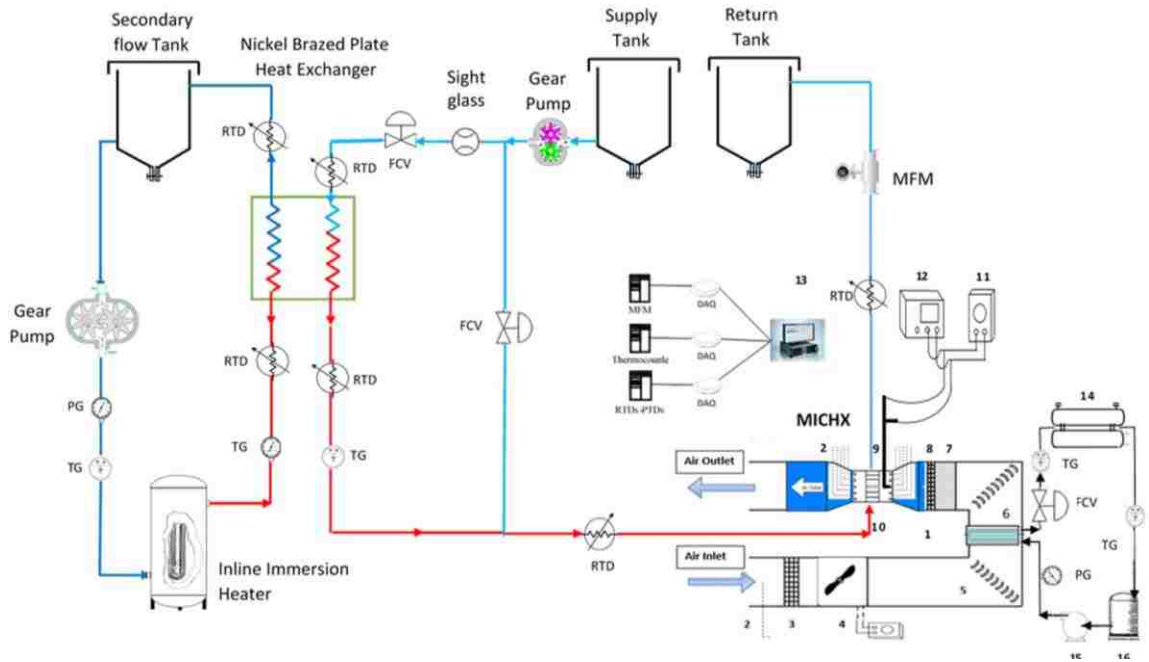
Figure 6.2. Schematic diagram of the experimental setup

6.2.1. Air side

The thermal wind tunnel is the essential part of the airside circuit as shown in Figure 6.3.

It is fabricated from high thermal resistance fiberglass, lined with a smooth surface that

protects the air flow against any disturbance and heat transfer to the environment. A 10-

ton chiller, 6 kW heater, and needle control valves are installed to accurately control the

inlet air temperature. The airside is equipped with 9 T-type thermocouples at the air inlet

of the test section and 18 T-type thermocouples at the air outlet to measure the air

temperatures. A thermocouple was also mounted at the inlet of the wind tunnel to monitor

the temperature of the supplied air. The constant temperature supplied air enters the tunnel

passing through a fine air filter to remove the dust particles that may affect the heat transfer.

Subsequently, the air passes through an inbuilt electrical blower controlled by a digital

processor panel to produce the required air velocity. Afterward, air flows to a well-

insulated in-built heat exchanger to achieve the desired inlet air temperature. Next, the

turning vane cascades, settling length, honeycomb, and screen pack straighten the air flow before reaching the test section. In this study, the airside inlet temperature and mass flow rate are maintained at a constant value during the entire experiment.
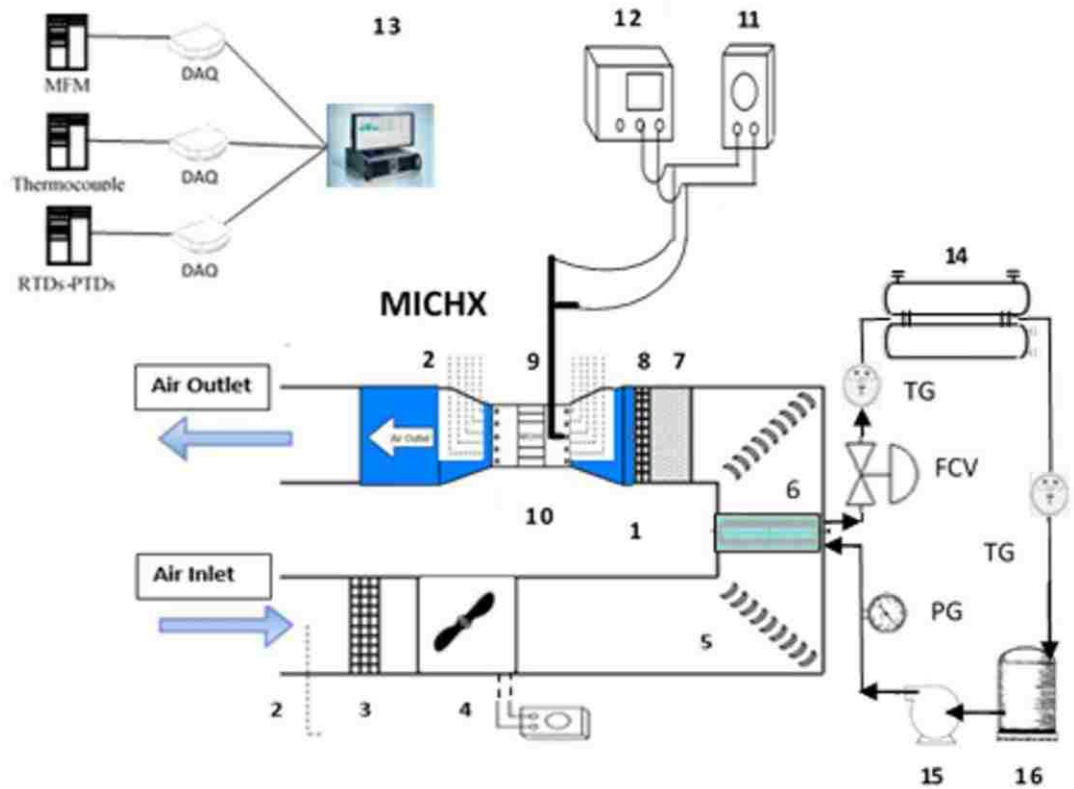
1	Thermal Wind tunnel	9	Pitot tube
2	T-type Thermocouple	10	Test section
3	Air filter	11	Differential Pressure Transducer
4	Air blower	12	Flow Kinetics Device FKT
5	Turning vanes	13	Data Acquisition System
6	Inbuilt heat exchanger	14	Chiller
7	Honeycomb - Straightener	15	Pumps - Centrifugal
8	Screen pack	16	Tank

Figure 6.3. Schematic diagram of the airside circuit and components

6.2.2. Liquid side

The liquid side consists of two circuits; the primary circuit delivers the 2.5wt% concentration Al_2O/water nanofluid at constant room temperature. Part of the fluid flows through a brazed plate heat exchanger and the other part bypass this heat exchanger using needle control valves. Later, the two fluids mix and exchange heat to supply the desired nanofluid temperature to achieve the temperature step changes and provide constant temperature for mass flow step changes. Two transient effects are studied, one due to mass flow rate variations and the other is due to temperature step changes. Each one of them is performed while holding the other inlet operating conditions constant. The mass flow steps vary from 20 to 10, 16, 30, 40, and 50 g/s at constant inlet nanofluid temperature of 70°C. Whereas, the temperature steps vary from 22 to 33, 44, 55, 66, and 77°C at constant inlet nanofluid mass flow rate of 60 g/s. A gear pump is used to force the main fluid to flow through the MICHX. An in-line Coriolis flow measurement device with the accuracy of 0.1% FS is used to measure and record the mass flow rate, density, and concentration of the nanofluid.

The secondary flow circuit consists of a brazed plate heat exchanger, a 20kW inline immersion heater, a heater temperature control panel with two microprocessors of 0.1°C accuracy, and a gear pump with a digital control panel. Step changes in temperature of the primary flow circuit are attained by sending part of the nanofluid through the brazed plate heat exchanger, Figure 6.4, then mixing it with the nanofluid at environmental temperature to obtain the desired nanofluid temperature.

Figure 6.4. The brazed plate heat exchanger

6.2.3. Test section and specimen

The test section was fabricated from 0.25" transparent polycarbonate sheets due to their thermal resistance, light weight, high impact, and transparency. The test section has a rectangular shape with dimensions of 4"X 12" and depth of 24". More details of the test section and the airside loop can be found in Fotowat et al. [16]. The minichannel heat exchanger has a volume density of 4000 m^2/m^3. Several thermocouples are installed on the insulated serpentines to monitor the temperature change along them. The specification of the minichannel heat exchanger is presented in table 6.1.

Table 6.1 Minichannel Heat Exchanger Specifications

Heat exchanger specifications	Dimensions
Channel diameter (m)	*0.001*
No. of channels in a slab	*68*
No. of slabs	*5*
Slab thickness (m)	*0.002*
No. of serpentines	*4*
Channel length of (m)	*1.658*
slab length (m)	*0.305*
Slab width (m)	*0.1*
Slab height (m)	*0.102*
Fin density (fins per inch)	*12*

6.3. Experimental procedures

There are two sets of the nanofluid transient steps that are considered for the experiment: mass flow and temperature steps. The airside inlet conditions are kept constant during the experiment at air inlet temperature of 13°C and mass flow rate of 222 g/s. The step changes in the liquid inlet temperature of 1.5 to 3.5 at a constant liquid mass flow rate of 60g/s yielded bulk Reynolds number of 1049 to 1288, 1532, 1803, 2094, and 2384. While, the step changes in mass flow rates of 0.5 to 2.5 at a constant liquid inlet temperature of 70°C yielded bulk Reynolds number of 636 to 339, 538, 987, 1346, and 1682.

➤ The secondary circuit is initialized by turning on the inline heater that is set to the desired value with a temperature accuracy of 0.1°C.

➤ The air inlet velocity is set by the blower to 6m/s using a digital controller. Afterwards, the hot and cold- water valves are opened to allow the flow of air to pass

through the wind tunnel inbuilt heat exchanger and achieve the required air temperature.

➤ The main circuit gear pump is initiated after the steady state condition is reached. The nanofluid flow rate varies by changing the accompanied pump frequency and the control needle valves regulate the nanofluid temperature.

➤ After reaching a steady state, a step change in temperature or mass flow rate is applied. Once the step change is performed, the system is left to reach the steady state before going to the next step. Each step is applied three times to check for repeatability. The data is collected using the data acquisition system equipped with LabView.

6.4. Data Reduction for the experiments

The thermal performance of the minichannel heat exchanger and the outlet temperatures of both fluids are characterized by dimensional and dimensionless parameters such as heat transfer rate, effectiveness, and the heat balance. The assumptions made for this study is listed below,

- Axial heat conduction in the MICHX is negligible.

- Heat transfer to or from the environment is insignificant.

- Both fluids are in a single phase.

- Thermophysical properties of both fluids are constant and calculated from the bulk temperature.

The dimensionless outlet temperature is defined by Gao et al. [17] as follows,

$$T_{h,o}^*(t) = \frac{T_{h,o}(t) - T_{c,i}(t)}{T_{h,i}(t) - T_{c,i}(t)} \qquad 6.1$$

$$T_{c,o}^*(t) = \frac{T_{c,o}(t) - T_{c,i}(t)}{T_{h,i}(t) - T_{c,i}(t)}$$

6.2

The residence time represents the length of the channel divided by the velocity of the Al$_2$O$_3$/water nanofluid that displays the time it takes the primary hot liquid to pass through the heat exchanger,

$$t_{res} = \frac{nA_cL}{\dot{\forall}} = \frac{L}{V}$$

6.3

The dimensionless time can be found using time divided by the residence time,

$$t^* = \frac{t}{t_{res}}$$

6.4

Reynolds number for the hot nanofluid is calculated according to the geometry of the MICHX and presented in eq. (6.3).

$$Re_h = \frac{\rho_h v_h D_h}{\mu_h} = \frac{\dot{m}_h}{17\pi\mu_h D_h}$$

The viscosity of the nanofluid is calculated using the Azmi et al correlation and measured using a falling ball viscometer.

The actual heat transfer rate to the maximum possible heat transfer rate is called effectiveness ε and is drawn from the energy balance of hot and cold fluids Cengel [18]. Cima and London [19] extended the idea of heat transfer effectiveness to a time-dependent which was also used by Srihari and Das [15], and Gao et al. [20].

$$\varepsilon_h(t) = \frac{C_h\left(T_{h,i}(t) - T_{h,o}(t)\right)}{C_{min}\left(T_{h,i}(t) - T_{c,i}(t)\right)}$$

6.5

$$\varepsilon_c(t) = \frac{C_c\left(T_{c,o}(t) - T_{c,i}(t)\right)}{C_{min}\left(T_{h,i}(t) - T_{c,i}(t)\right)} \qquad 6.6$$

The heat transfer rate for both fluids is calculated as follows,

$$\dot{Q}_h = \dot{m}_h \, c_p \, \Delta T_h \qquad 6.7$$

$$\dot{Q}_c = \dot{m}_c \, c_p \, \Delta T_c \qquad 6.8$$

The heat balance for this study is found as in the following equation,

Error in heat balance,

$$HB\% = \frac{(\dot{Q}_h - \dot{Q}_c)}{\dot{Q}_{ave}} \qquad 6.9$$

Normalized heat transfer rate is a non-dimensional heat transfer rate defined as the heat transfer rate of the hot fluid per frontal area of the heat exchanger and the temperature difference of the both fluids as follows;

$$Q^* = \frac{\dot{Q}_h}{A_f * \Delta T} \qquad 6.10$$

6.5. Uncertainty analysis

To assess the confidence in the experimental results, the uncertainty analysis is required. The error of the examination related to the heat exchanger dimensions, inlet and outlet fluid temperature, sensors of the instrumental devices such as mass flow meter, RTDs, thermocouples, and data acquisition system (DAQ) comprises DAQ card, and signal conditioners SCXI are computed.

Table 6.2 displays the estimated uncertainties of the main parameters. The RSS method is applied to calculate the errors of the measured data as in Figliola and Beasley [21].

$$U_x = \pm\sqrt{B^2 + P^2} \qquad 6.11$$

The precision and bias errors are measured from the following equations,

$$P = \pm\sqrt{P_1^2 + P_2^2 + P_3^2} \qquad\qquad 6.12$$

$$B = \pm\sqrt{B_1^2 + B_2^2 + B_3^2} \qquad\qquad 6.13$$

The total uncertainties could be calculated with a 95% confidence level as following,

$$U_{x(0.95)} = \pm\sqrt{B^2 + (t_{v,95\%}P)^2} \qquad\qquad 6.14$$

The overall uncertainty in data acquisition component is calculated from the RSS of the individual uncertainties as follows,

$$U_{DAQ\ system} = \pm\sqrt{B_{DAQ\ card}^2 + B_{SCXI}^2} \qquad\qquad 6.15$$

The uncertainty associated with the temperatures of the fluids using thermocouples and RTDs could be found in Eqs. (17) - (18),

$$U_{T,air} = \pm\sqrt{U_{DAQ}^2 + U_{Thermocouples}^2} \qquad\qquad 6.16$$

$$U_{T,nf} = \pm\sqrt{U_{DAQ}^2 + U_{RTD}^2} \qquad\qquad 6.17$$

Reynolds number is a function of mass flow rate, viscosity, and hydraulic diameter as shown in Eq. (5). The overall uncertainty in Re number is found as,

$$U_{Re_h} = \pm\sqrt{\left(\frac{\partial Re_h}{\partial \dot{m}_h}U_{\dot{m}_h}\right)^2 + \left(\frac{\partial Re_h}{\partial \mu_h}U_{\mu_h}\right)^2 + \left(\frac{\partial Re_h}{\partial D_h}U_{D_h}\right)^2} \qquad 6.18$$

The uncertainty associated with the transient effectiveness from Eqs. (6.6) - (6.7) is calculated as,

$$U_{\varepsilon_h(t)}$$

$$= \pm \sqrt{\left(\frac{\partial \varepsilon_h(t)}{\partial T_{h,in}(t)} U_{T_{h,in}(t)}\right)^2 + \left(\frac{\partial \varepsilon_h(t)}{\partial T_{h,out}(t)} U_{T_{h,out}(t)}\right)^2 + \left(\frac{\partial \varepsilon_h(t)}{\partial t} U_t\right)^2} \qquad 6.19$$

$$U_{\varepsilon_c(t)} = \pm \sqrt{\left(\frac{\partial \varepsilon_c(t)}{\partial T_{h,in}(t)} U_{T_{h,in}(t)}\right)^2 + \left(\frac{\partial \varepsilon_c(t)}{\partial T_{c,out}(t)} U_{T_{c,out}(t)}\right)^2 + \left(\frac{\partial \varepsilon_c(t)}{\partial t} U_t\right)^2} \qquad 6.20$$

The heat transfer rates of both fluids are a function of mass flow rate, specific heat, and the temperature difference of the fluids, as defined in Eqs. (8) - (9). The uncertainty of the heat transfer rate can be estimated as follows,

$$U_{\dot{Q}_h} = \pm \sqrt{\left(\frac{\partial \dot{Q}_h}{\partial \dot{m}_w} U_{\dot{m}_h}\right)^2 + \left(\frac{\partial \dot{Q}_h}{\partial c_{p,h}(t)} U_{c_p}(t)\right)^2 + \left(\frac{\partial \dot{Q}_h}{\partial \Delta T,h(t)} U_{\Delta T}(t)\right)^2 + \left(\frac{\partial \dot{Q}_h}{\partial t} U_t\right)^2} \qquad 6.21$$

$$U_{\dot{Q}_c} = \pm \sqrt{\left(\frac{\partial \dot{Q}_c}{\partial \dot{m}_c} U_{\dot{m}_h}\right)^2 + \left(\frac{\partial \dot{Q}_c}{\partial c_{p,c}(t)} U_{c_{p,c}}(t)\right)^2 + \left(\frac{\partial \dot{Q}_c}{\partial \Delta T,c(t)} U_{\Delta T,c}(t)\right)^2 + \left(\frac{\partial \dot{Q}_c}{\partial t} U_t\right)^2} \qquad 6.22$$

Table 6.2 Estimated Uncertainties

Parameters	Mean value	Uncertainties %
$T_{h,i}$ (°C)	70	± 1.1
$T_{a,i}$ (°C)	13	± 7.6
$\dot{m}_h$ Mass flow rate of nanofluid (kg/s)	0.01 to 0.06	± 1.5
$\dot{m}_c$, Mass flow rate of air (kg/s)	0.22	± 0.98
D_h (m)	0.001	± 3.48
$A_{frontal,air}$ (m^2)	0.03097	± 0.16
Velocity of air m/s	6	± 0.83
DAQ system	Peak to peak voltage	$6.33*10^{-6}$ V

6.6. Results and discussion

This section illustrates the results found when subjecting the heat exchanger to transient changes in inlet conditions of mass flow rate and temperature. The behavior and the dynamic response of the heat exchanger to these variations are reported. Dimensional and dimensionless parameters that include outlet temperatures of both fluids, heat transfer rates, heat balance, etc. are presented with respect to time. The main findings are listed, and a discussion is made based on the experimental outcome.

6.6.1. System repeatability for Step variation in the nanofluid mass flow rate and inlet temperature

The repeatability of the nanofluid inlet temperature and mass flow step variations with time is demonstrated in Figures 6.5a and 6.5b. The experiments were repeated 3 times for each step to find the precision and repeatability of the system. The inlet temperature of nanofluid was varied at steps of 1.5, 2.0, 2.5, 3.0, and 3.5 while keeping its mass flow rate at 60 g/s

and air mass flow rate of 222 g/s, and temperature of 13°C. The other experiments included changing the nanofluid mass flow rate at steps of 0.5, 0.8, 1.5, 2.0, and 2.5 while keeping its inlet temperature at 70°C, air inlet temperature of 13°C and a flow rate of 222 g/s. The system are shown truthfully and repeatability in reading all the data within less than 3% over all sets.

(a)   (b)
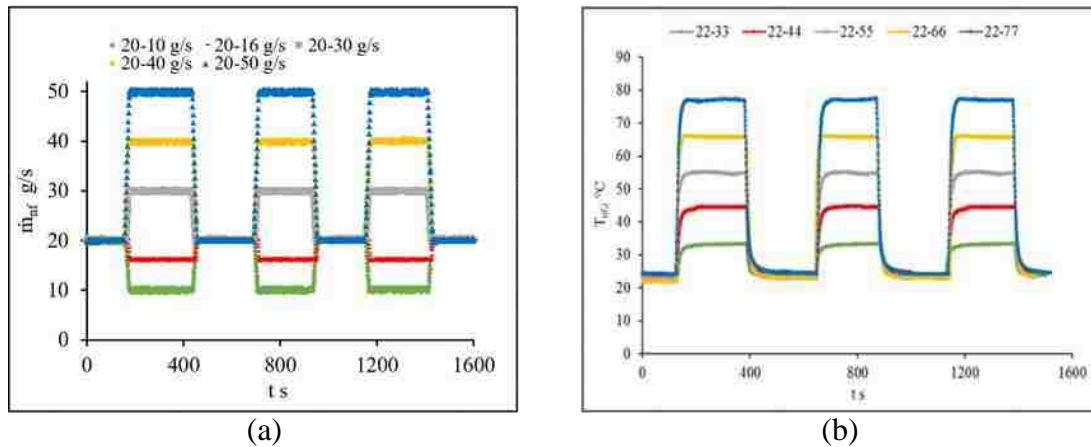
Figure 6.5 Repeatability of the experiments with time at step changes of nanofluid inlet (a) mass flow (b) temperature

6.6.2. *Effect of nanofluid mass flow step changes on fluids outlet temperatures*

Figures 6.6a and 6.6b illustrate the effect of nanofluid mass flow step changes on the outlet temperatures of both fluids. The uncertainties of the experimental data are calculated and represented with the data in the figures. The mass flow step perturbations vary from an initial steady value to steps of 0.5, 0.8 (step down) and 1.5, 2.0, and 2.5 (step ups) in 5 steps while all other parameters remain unchanged. The outlet temperatures do not show an instant response to the mass flow rate variations. The length of time it takes the outlet temperature to react to the inlet mass flow variation from one steady condition to another is called the response time. The response time for the hot nanofluid mass flow step change

141

is found to be 47.4, 42.1, 38.5, 53.2, and 64.1 seconds for steps of 1.5, 2, 2.5, 0.8, and 0.5, respectively. For step ups, the response time decreases as the step increases, while for a step down of 0.5 longer response time is shown compared to a step of 0.8. This difference in the negative steps can be explained by the longer residence time at a step of 0.5 of the hot liquid in the minichannel heat exchanger. However, the outlet temperature of the cold air starts changing after only 1.0s for the step of 1.5. The results indicate higher outlet temperatures for higher step changes. The higher the step change, the lower response time for step ups, while it is not the case for the step downs.

(a)   (b)
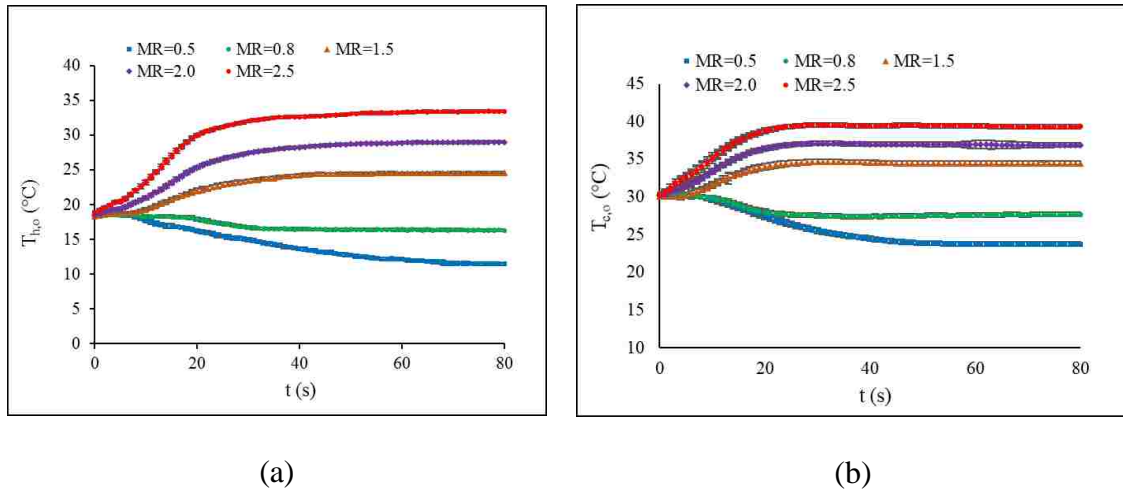
Figure 6.6 Effect of nanofluid mass flow change on outlet temperatures of (a) nanofluid (b) air

6.6.3.   *Outlet temperature responses to nanofluid inlet temperature step changes*

The effect of the nanofluid inlet temperature step variation on the outlet temperature. The effect of the nanofluid inlet temperature step variation on the outlet temperature of both fluids is demonstrated in Figures 6.7a and 6.7b. Uncertainty calculation of each

experimental data point is included in the figures. The hot fluid inlet temperature changed in 5 steps while keeping other inlet conditions of the fluids constant. The temperature is changed from a base value of 22 °C into steps of 1.5, 2.0, 2.5, 3.0, and 3.5 at a hot nanofluid constant mass flow rate of 60 g /s. The outlet temperatures did not show an immediate response to the temperature variations. The hot fluid showed a higher initial delay time however, the cold fluid exhibited shorter delay time. It can be seen from the figure that the response time falls as the step rises. For a step of 1.5, the response time for the hot and cold fluids are found to be 68 and 49 while, their initial delay time is found to be 6.0s and 2.0s, respectively.

(a)   (b)
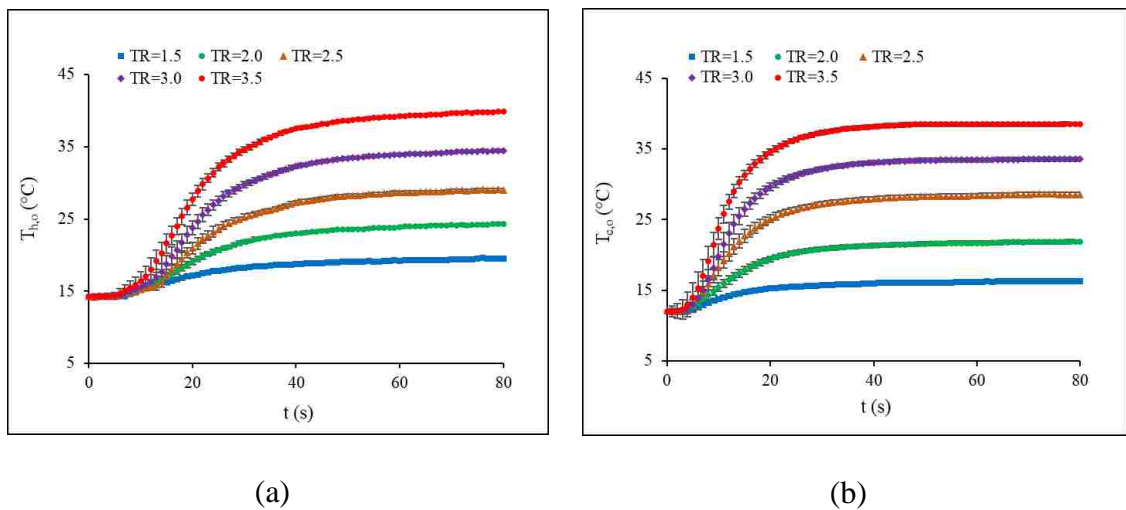
Figure 6.7 Outlet temperature responses at inlet nanofluid temperature steps for (a) nanofluid (b) air

6.6.4. *An empirical correlation for the nanofluid inlet temperature step variation in the MICHX*

The variation of the transient dimensionless outlet temperature over its steady state dimensionless temperature verses the dimensionless time for the Al2O3/water nanofluid is illustrated in Figure 6.8. The transient outlet temperature based on the inlet

143

temperature steps of 1.5 to 3.5 reaches quasi-steady-state for the non-dimensional time larger than about 50. The best-fit of the collected data obtained in the following empirical correlation (Eq. 6.24). The exponential relation with power law effect of temperature step variations captured the experimental data well, which can be seen from the R^2 values from 0.912 to 0.976 in Figures 6.8a to 6.8e. All the experimental data obtained are between $\pm 10\%$, which is in the good acceptance range.

$$T^*_{h,o}/T^{*,\infty}_{h,o} = 1 - 0.365\ TR^{0.8}\ e^{-(0.002*TR + 0.06)\ t^*} \qquad\qquad 23$$
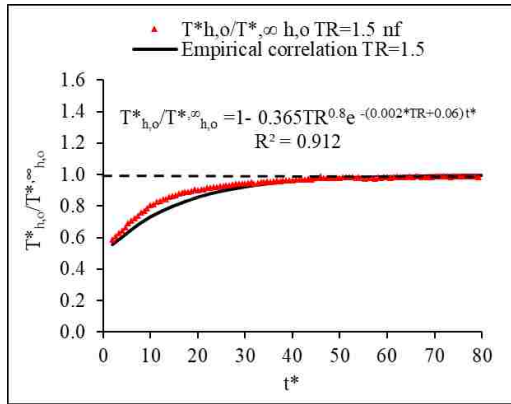
a
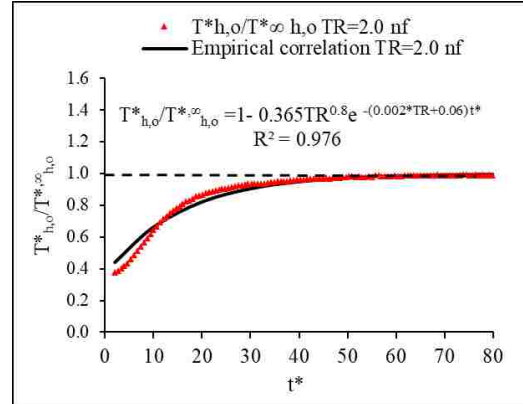
b
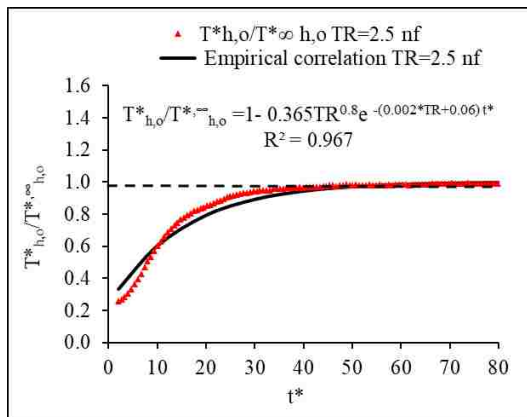
c
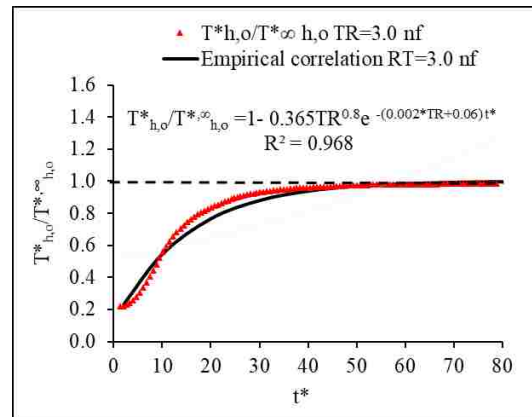
d
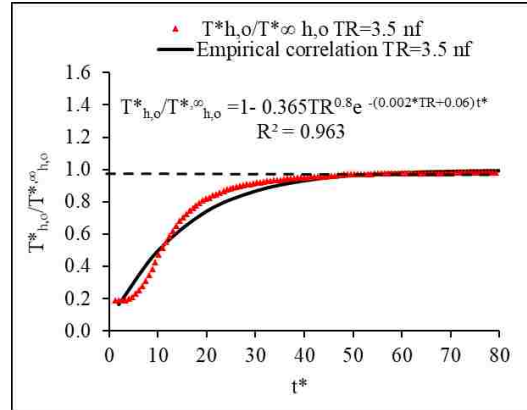
e

Figure 6.8 An empirical transient correlation for the nanofluid outlet temperature by dimensionless parameters at the temperature step variations in the MICHX

6.6.5. *An empirical correlation for the nanofluid inlet mass flow step variation in the MICHX*

Figure 6.9 a, b and c presents the ratio of the transient dimensionless outlet temperature over its steady-state of the Al2O3/water nanofluid on the dimensionless time. The transient outlet temperature approaches quasi-steady-state for the mass flow step variation of 1.5 to 2.5 at the dimensionless time higher than around 25. An empirical correlation is obtained for the mass flow step up variation (Eq. 6.25). All the experimental data collected are between ±15%, which is in the acceptance range.

$$T^*_{h,o}/T^{*,\infty}_{h,o}=1-1.67MR^{-1.7}e^{-(-0.105*MR+0.315)t^*} \qquad 24$$
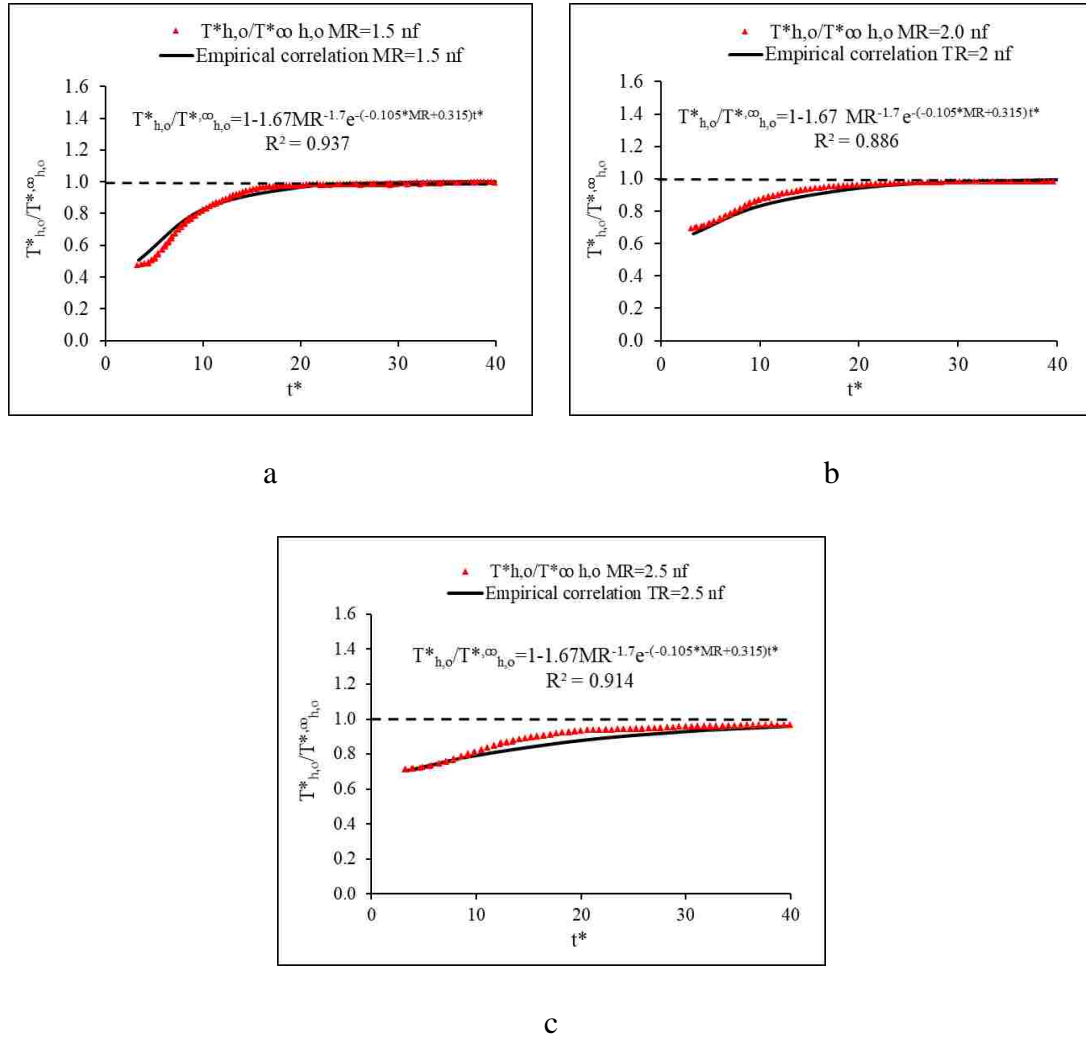
Figure 6.9. An empirical transient correlation for the nanofluid outlet temperature by

dimensionless parameters at the mass flow step variations in the MICHX

6.6.6. *Dimensionless outlet temperatures at different Re for nanofluid mass flow step changes*

Figure 6.10 illustrates the dimensionless outlet temperatures with respect to changes in

nanofluid Reynolds number in positive and negative steps. For the hot liquid positive step

changes, the initial delay time increases as Reynolds number increases. However, the initial

delay time has an opposing trend for the negative steps. The dimensionless temperature

rises at higher Reynolds number and reaches the highest possible. The smaller mass flow

steps led to lower changes in Reynolds number, which resulted in shorter initial delay time. When considering each step at a time, the effect of the residence time is observed through the change in Re until the end of the step change where the flow rate reached its steady state. However, the dimensionless outlet temperature continues to undergo a change due to the ongoing heat transfer that occurs from the liquid to the heat exchanger walls and then to the air. Once the heat transfer reached a steady state, the dimensionless outlet temperature stabilizes at its maximum point. For the cold air, Fig. 8b, initial delay time is observed as the mass flow step changes are applied. The response of the cold air to the flow steps is found lower than the hot liquid after the initial delay time due to the shorter residence time of the airside compared to the hot nanofluid. For all mass flow step changes, the initial Reynolds number started around 660 and varied in a step form to final values of (290, 550, 980, 1400, 1750) corresponding to steps of (0.5, 0.8, 1.5, 2.0, 2.5), respectively.

(a)   (b)
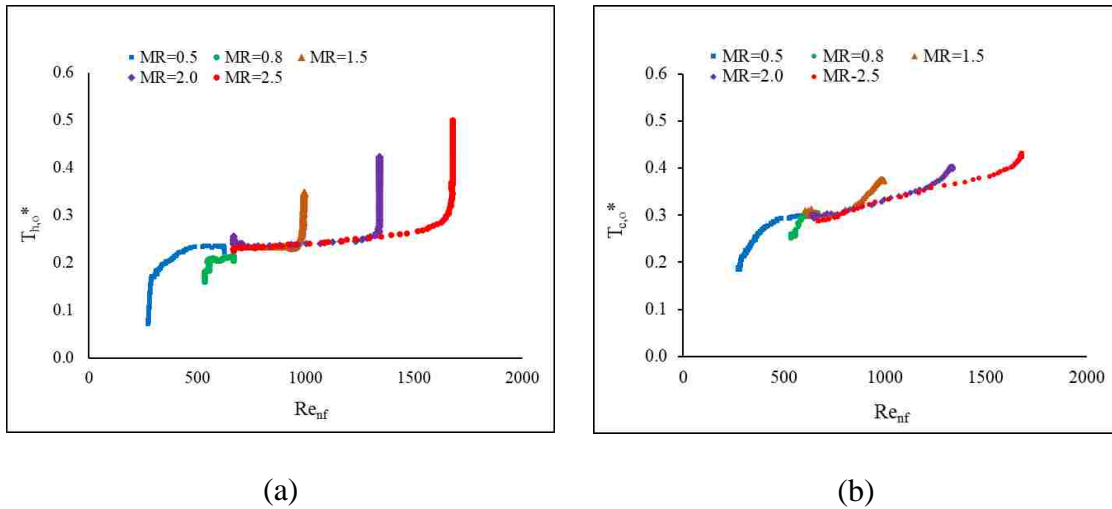
Figure 6.10. Dimensionless outlet temperature versus Re at nanofluid mass flow step changes for (a) nanofluid (b) air

6.6.7. *Dimensionless outlet temperatures at different liquid Re for nanofluid temperature step changes*

The effect of varying the nanofluid inlet temperature on its Reynolds number and dimensionless outlet temperatures is shown in Figure 6.11. Although the hot nanofluid mass flow rate is kept constant during the temperature step change, the nanofluid Re is found increasing. The step variations in the hot liquid inlet temperature from 1.5 to 3.5 yielded Reynolds numbers of 1094 to 2495. In Fig. 11a, an initial delay time is observed at the beginning of each step. According to eq.1 and since the inlet temperature of air is constant; the step change caused the ratio of the outlet to inlet liquid temperature to vary. At first, the inlet temperature change is higher than the outlet, which resulted in the fast drop in the dimensionless outlet temperature. When the inlet temperature reached its steady state value, the outlet liquid temperature continued to change until reaching its final value. The dimensionless outlet liquid temperature at the steady state is found higher for higher step change. In the case of airside, Fig. 11b, similar trend is observed. However, the changes in the dimensionless temperature are shorter compared to the liquid side. Moreover, the initial of the dimensionless temperature are almost the same as final value which is approximately 0.5.

(a)   (b)
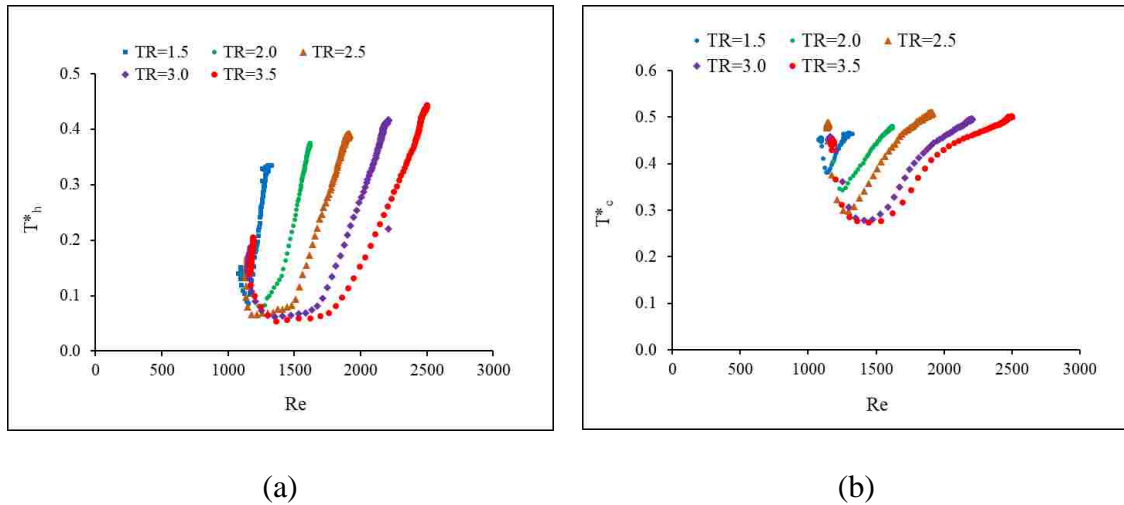
Figure 6.11. Dimensionless nanofluid outlet temperature vs. Re at temperature step

changes for (a) nanofluid (b) air

6.6.8.   *Effect of nanofluid mass flow step changes on heat transfer rate*

Figure 6.12 shows the effect of mass flow step changes on heat transfer rate for both fluids.

The hot liquid outlet temperature increased until reaching the highest maximum point

before it drops to reach the steady state. The heat transfer occurs from the liquid to the heat

exchanger walls then to air and due to the step in the liquid inlet temperature, the heat

exchanger walls absorb most of the heat first before they release it to air. At some point,

the rate of heat absorbed by the exchanger walls is higher than the rate of heat released to

air; this caused the peak. It is found that the peaks occur at 22s, 24s, and 26s for the positive

steps of 1.5, 2.0, and 2.5, and for the negative steps, they occur at 26s, and 32s for 0.8 and

0.5, respectively. In addition, the higher the mass flow step changes, the smaller the peak

time is in the case of positive steps. However, negative steps do not show any peak in heat

transfer. Fig. 12b shows an increasing trend for airside with no maximum peaks noticed.

149

6.6.9.   Effect of nanofluid inlet temperature step changes on heat transfer rate

The heat transfer rate at different nanofluid inlet temperature steps is presented in Figure 6.13. The heat transfer increases as the temperature step changes increase. However, it is observed that for all the step changes of the hot liquid, the highest maximum heat transfer reach is at time 13s. The heat transfer rate of the cold airside exhibited different behaviour with no peak recorded. A similar explanation as in the mass flow step changes can be used here for the reason behind forming the peaks and the drop until reaching the steady state. The initial delay time for the hot and cold fluids is 6.5, 1.5, respectively, which show a higher delay time for the hot liquid compared to cold airside.

(a)   (b)
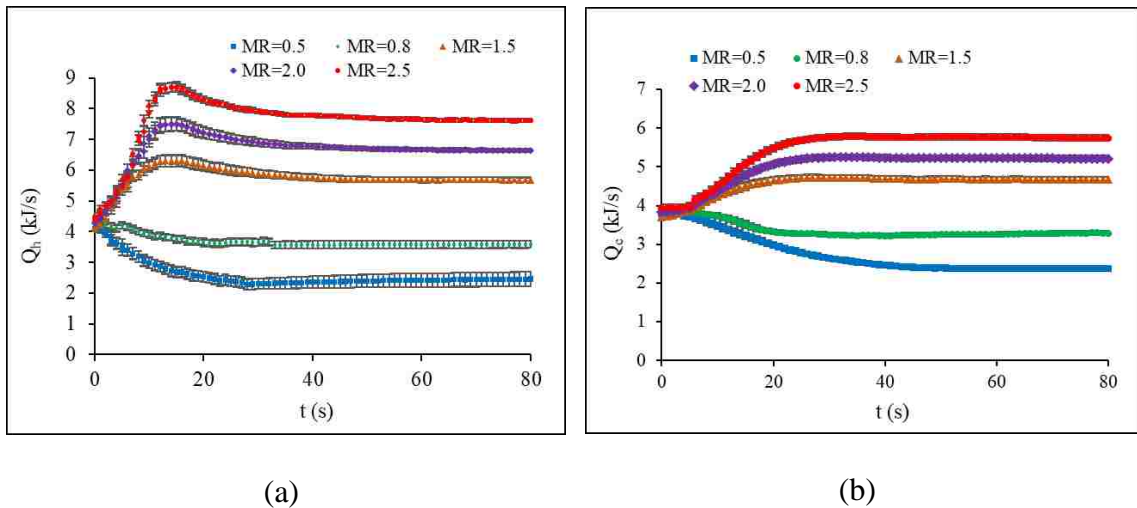
Figure 6.12. Heat transfer rate versus time at nanofluid mass flow step changes for (a) air (b) Al2O3/water nanofluid

(a)   (b)
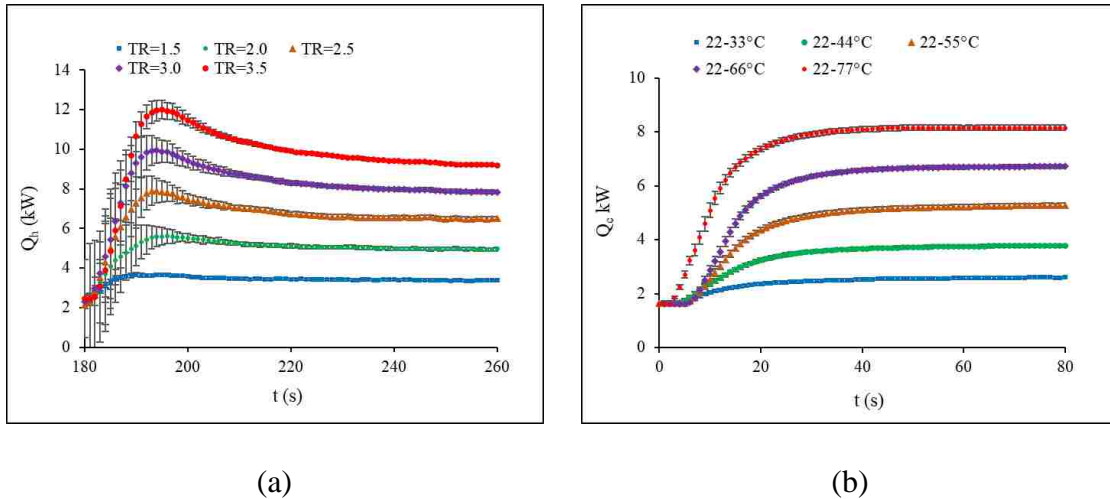
Figure 6.13. Heat transfer rate versus time at temperature step changes for (a)

nanofluid (b) air

6.6.10. Effect of nanofluid inlet temperature step changes on Normalized heat transfer rate

Normalized temperature is an alternative way to characterize the transient variation. It is

defined as the portion of the change in the nanofluid outlet temperature to the maximum

outlet temperature change until reaching the steady state. Normalized heat transfer where

the nanofluid is subjected to mass flow and temperature step changes is demonstrated in

Figure 6.14. The change in the liquid inlet temperature led to a change in the heat transfer

rate of both fluids and caused the heat transfer rate to vary. As seen in the previous

explanation for the heat transfer, the normalized heat transfer is following the same trend.

Peaks are formed due to rise of the heat in the exchanger walls before releasing it to air.

This conclusion is applied to the nanofluid temperature step changes and the positive mass

flow step changes. The negative mass flow step changes behaved differently than the hot

liquid and did not exhibit the same trend. The initial delay time is found noticeable in the

151

case of inlet temperature step changes compared to a negligible amount for the mass flow step changes.

(a)   (b)
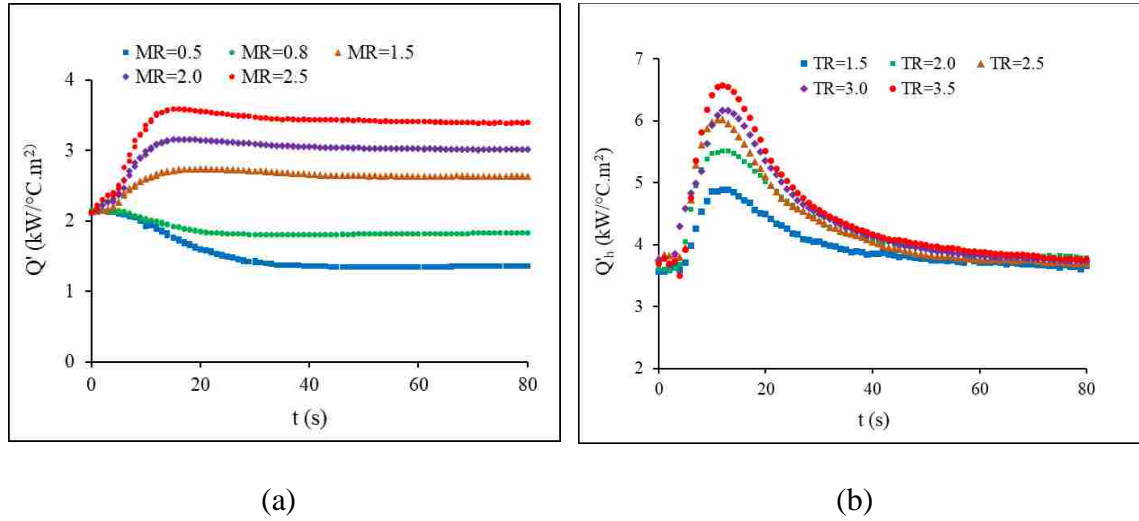
Figure 6.14. Normalized heat transfer rate at the nanofluid (a) mass flow and

(b)temperature step changes

6.6.11. Effect of nanofluid inlet temperature step changes on heat balance

The transient heat balance of both mass flow and temperature step changes is illustrated in Figure 6.15. The effect of the positive and negative step changes in mass flow is found to be adverse. The transient heat balance rose to a peak and dropped to reach the steady state condition for the positive step changes, meanwhile, an adverse trend is found for the negative step changes where it bottomed out to a maximum lowest then increased to the final steady state. Higher step changes resulted in higher change of the heat balance regardless of the direction of the step variations. The heat balance at the steady state is found to be around ±6% for the transient mass flow steps and up to 9% for the temperature step changes. The steady state heat balance is within the acceptable range according to the American society of mechanical engineers ASME [22].

152

(a)   (b)
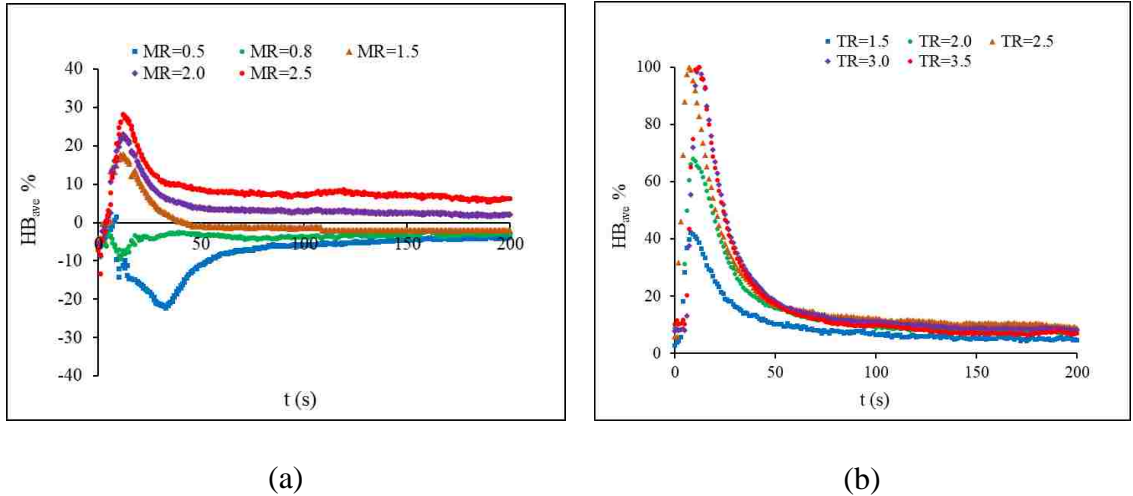
Figure 6.15. Effect of nanofluid (a) mass flow rate (b) temperature step changes on the heat balance

6.6.12. Effect of nanofluid mass flow step changes on effectiveness

Figure 6.16 present the transient effectiveness of the hot liquid and cold air due to the inlet mass flow step changes. Transient effectiveness increased with the increase in the mass flow step changes. Similar observation in the heat transfer rate is applied here, where the transient effectiveness increased to a peak and then dropped to reach steady state condition due to the fluctuation in the nanofluid mass flow and the effect of the residence time. At a step of 2.5, the nanofluid effectiveness reached a maximum value of 0.54 while the airside effectiveness reached with highest response time and airside effectiveness reached its highest at 0.46 with both at lower response time considering positive and negative steps. The response time of the hot liquid is found higher compared to the airside for the mass flow step changes.
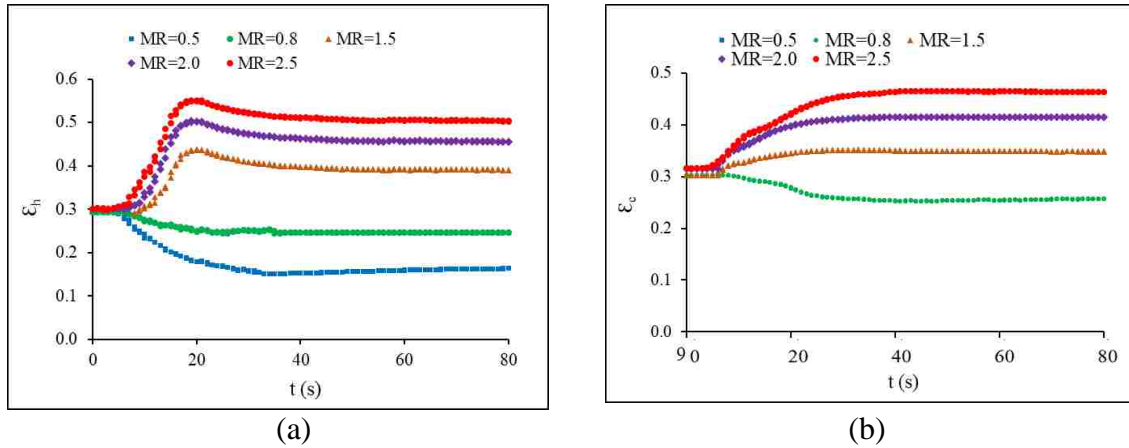
Figure 6.16. Effectiveness versus time at nanofluid mass flow step changes for (a)

nanofluid (b) air

6.6.13. Effect of the nanofluid temperature step change on transient effectiveness

The behavior of the MICHX under liquid inlet temperature step changes is found through

transient effectiveness as shown in Figure 6.17. Effectiveness is defined as the heat transfer

rate of the fluid over the maximum possible heat transfer rate. The maximum heat transfer

rate includes the inlet temperature of both fluids and the step changes of the hot liquid inlet

temperature. The transient effectiveness increased with the increase in the liquid

temperature step changes. A steeper highest possible peak is formed than the mass flow

step changes. The maximum effectiveness obtained from the hot nanofluid is 0.83 while a

value of 0.27 is calculated for the maximum lowest transient effectiveness of the cold

airside, which is found at a step of 2.5. The cold air showed a higher rate of change for the

lower step changes compared to the higher step changes. A negligible change in

effectiveness based on the airside is found in steps 2.5 and up.

154

(a)   (b)
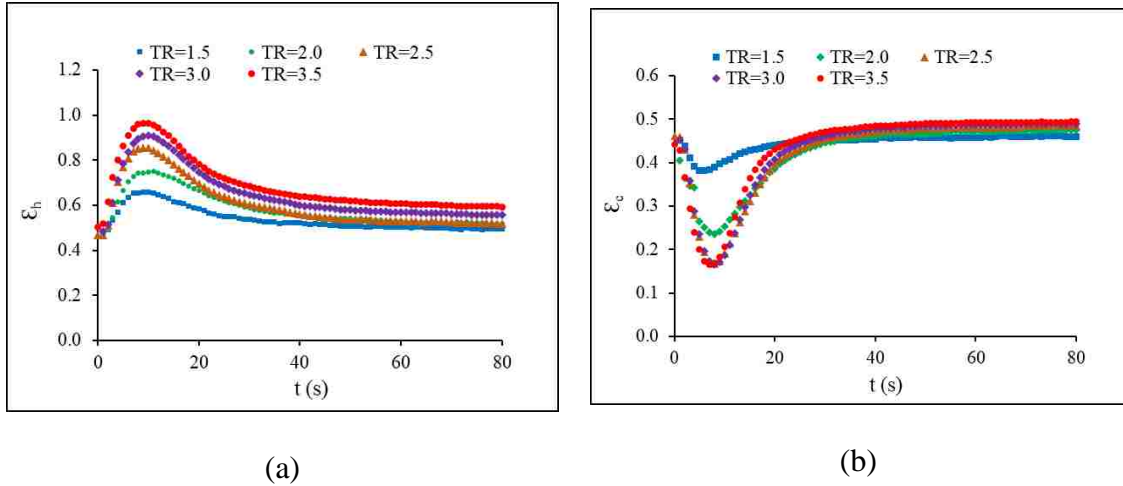
Figure 6.17. Effectiveness versus time at nanofluid temperature step changes for (a) nanofluid (b) air

6.6.14. Effect of mass flow step changes on dimensionless outlet temperatures

Figure 6.18 displays the outlet dimensionless temperature of both fluids with time at different nanofluid mass flow step changes. The dimensionless temperature expresses how the fluids outlet temperatures behave due to a sudden change in the liquid inlet temperature. Longer response times on the negative steps are found compared to the positive ones. In addition, the higher the negative step, the shorter the response time is. An asymmetric trend is found between the positive and negative steps for both fluids. Furthermore, longer initial delay time noticed for the hot liquid compared to air.

155

(a)   (b)
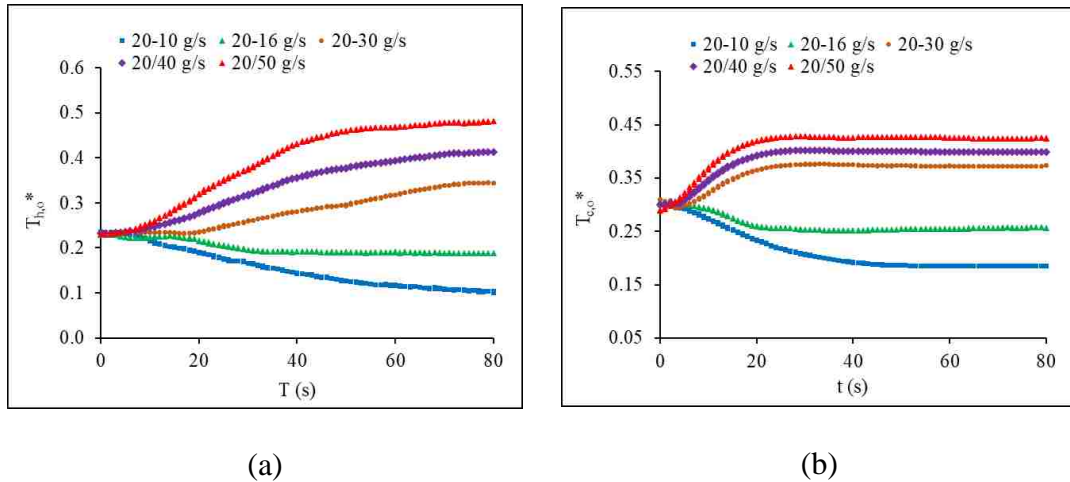
Figure 6.18 Dimensionless outlet temperature with time at liquid mass flow step

changes for (a) nanofluid (b) air

6.6.15. Effect of temperature step changes on the dimensionless outlet temperatures

The dimensionless outlet temperatures of the hot and cold fluids with time are shown in

Figures 6.19a and 6.19b at different nanofluid temperature step changes. Figure 6.19a

represents the hot liquid dimensionless outlet temperature with time. The higher step

changes resulted in lower dimensionless outlet temperature. The dimensionless outlet

temperature of air, Figure 6.19b, experienced a different trend than the liquid. The transient

region resulted in smaller temperature for higher steps. However, the steady state showed

higher temperature for higher steps. The rate of change in the lower step changes is higher

compared to the higher step changes for both fluids.
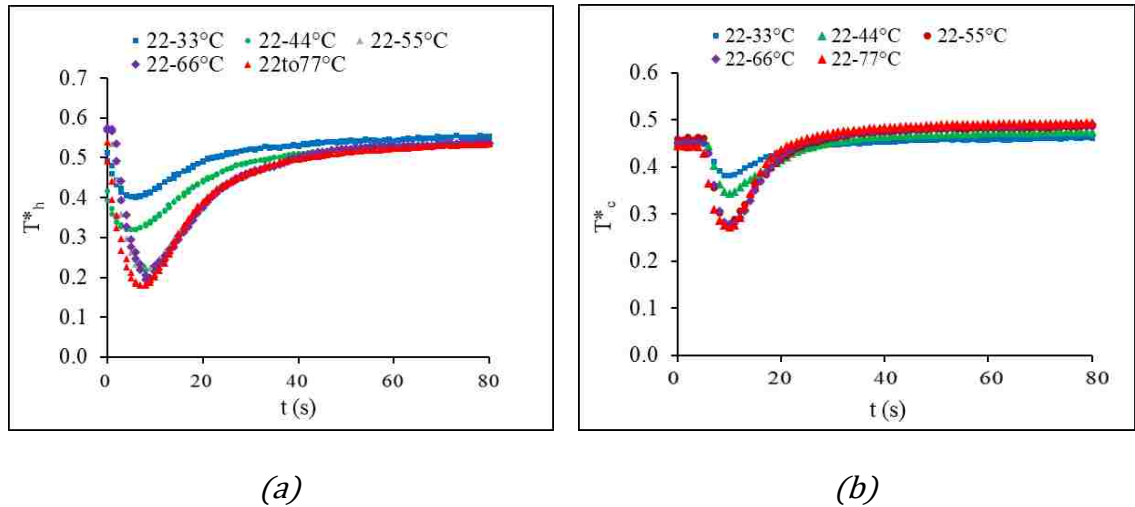
Figure 6.19. Dimensionless outlet temperatures with time at nanofluid temperature step changes of (a) nanofluid (b) air

6.6.16. Effect of nanoparticle dispersion on heat transfer rate for mass flow rate and temperature step changes

The benefit of using Al2O3/water nanofluid over water for the step variation in mass flow and inlet temperature is illustrated in Figures 6.20. The comparison between nanofluid and water for mass flow step changes of 0.5, 1.5 and 2.5 is demonstrated in Figure 20a. Meanwhile, Figure 20b, shows the nanofluid to water comparison at temperature step changes. It is shown that the response time for nanofluid is shorter compared to the base fluid. In addition, results show an increase of up to 19% in heat transfer rate with the use of nanofluid.

Shorter response time of the nanofluid for same operating condition can be interpreted by higher thermal conductivity and heat transfer rate of the nanofluid compared to water. Moreover, the increase in both mass flow rate and temperature step changes result in lower viscosity and higher Reynolds number of liquids. As a result, the thermal entrance length as well as heat transfer coefficient rise, and response time become shorter.

157

| (a) | (b) |
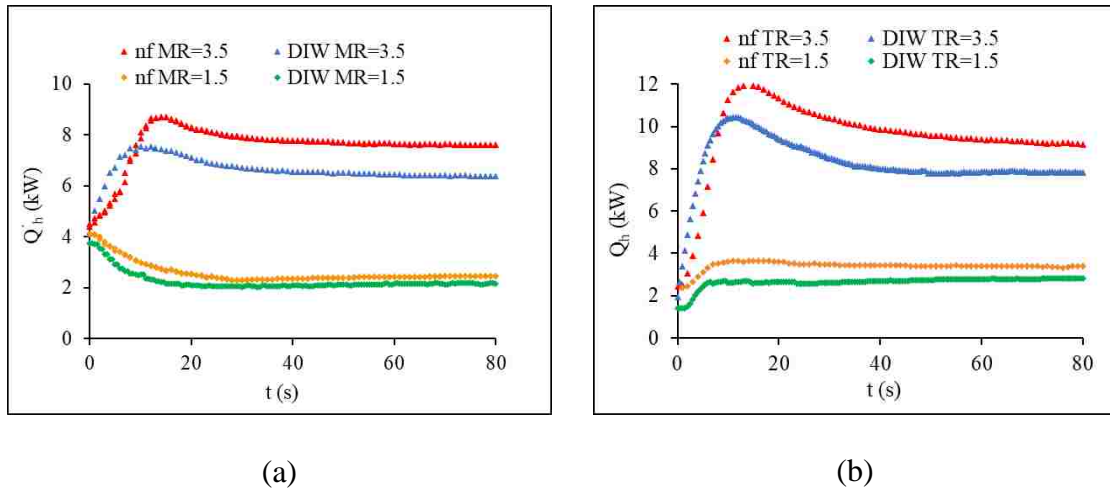
Figure 6.20 Comparison of the heat transfer rate for the nanofluid and water (a) mass flow rate (b) Temperature step change

6.6.17. TEM, EDS and DLS Analysis of the Al2O3/water nanofluid

A sample of Al2O3/DI-water nanofluid at a weight concentration of 2.5% is analyzed using the transmission electron microscopy (TEM). The images captured by TEM technique is used to visualize the distribution of nanoparticles in water as shown in Figure 6.21 at a scale of 20 nm. The spectrum analysis of the nanofluid is illustrated in Figure 6.22. Energy-Dispersive Spectrometry (EDS) analysis was performed to detect the elemental composition of the nanofluid solution and the purity of the nanoparticles. It was found that no other elements than Aluminum and Oxygen, as well as some Carbon exist, and the latter probably came from the grid. The size distribution of the nanoparticles dispersed into the nanofluid solution was analyzed using Dynamic Light Scattering (DLS) technique to control the size distribution profile in small particle suspension. The results are illustrated by intensity, number, and volume in Figure 6.23. The statistic graph of size measurements is illustrated in Figure 6.24. The test was repeated on three samples for accuracy. Table 3 displays the size distribution of nanoparticles dispersion by volume in nanofluid.

158

(a)   (b)   (c)
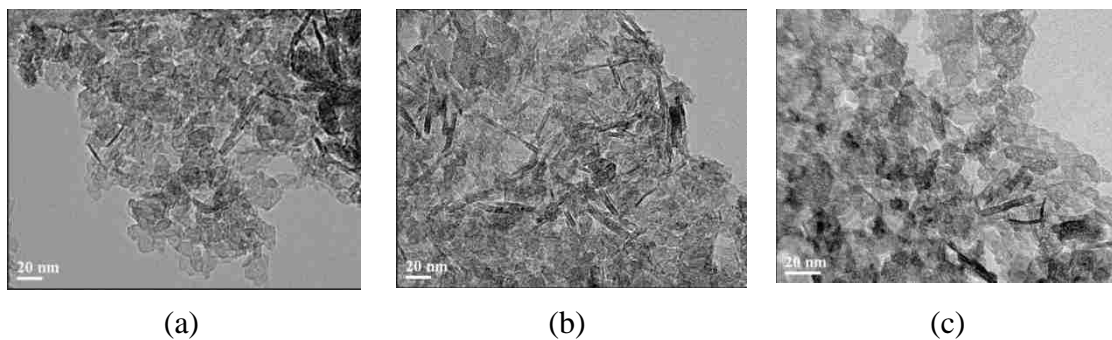
Figure 6.21. TEM spectrum for 20% dried Al2O3/water nanofluid

Figure 6.22 EDS Spectrum

(a) Intensity   (b) Numbers   (c) volume
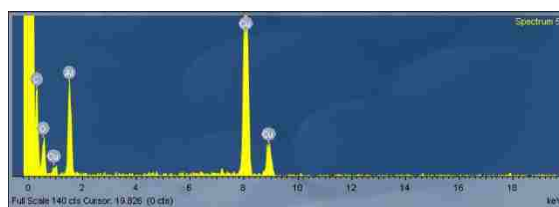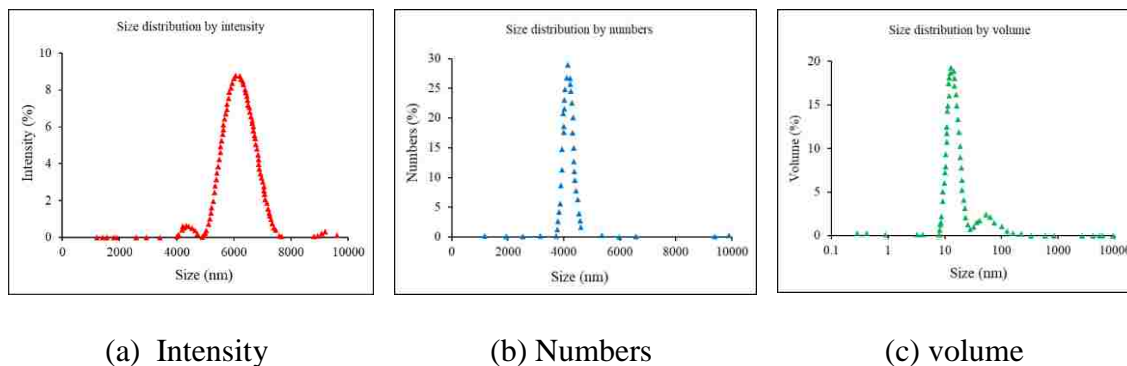
Figure 6.23. DLS report for nanoparticles size distribution

Table 6.3 Particle size distribution by volume in nanofluid

Size d.nm	Mean Volume %	Std Dev Volume %	Size d.nm	Mean Volume %	Std Dev Volume %	Size d.nm	Mean Volume %	Std Dev Volume %	Size d.nm	Mean Volume %	Std Dev Volume %
0.4000	0.0		5.615	0.0		78.82	1.6		1106	0.0	
0.4632	0.0		6.503	0.0		91.28	1.2		1281	0.0	
0.5365	0.0		7.531	0.0		105.7	0.9		1484	0.0	
0.6213	0.0		8.721	2.2		122.4	0.7		1718	0.0	
0.7195	0.0		10.10	9.4		141.8	0.6		1990	0.0	
0.8332	0.0		11.70	17.6		164.2	0.5		2305	0.0	
0.9649	0.0		13.54	20.0		190.1	0.4		2669	0.0	
1.117	0.0		15.69	15.9		220.2	0.3		3091	0.0	
1.294	0.0		18.17	9.4		255.0	0.3		3580	0.0	
1.499	0.0		21.04	4.2		295.3	0.2		4145	0.0	
1.736	0.0		24.36	1.5		342.0	0.2		4801	0.1	
2.010	0.0		28.21	0.7		396.1	0.1		5560	0.1	
2.328	0.0		32.67	1.1		458.7	0.1		6439	0.0	
2.696	0.0		37.84	1.8		531.2	0.0		7456	0.0	
3.122	0.0		43.82	2.2		615.1	0.0		8635	0.0	
3.615	0.0		50.75	2.4		712.4	0.0		1.000e4	0.0	
4.187	0.0		58.77	2.2		825.0	0.0				
4.849	0.0		68.06	1.9		955.4	0.0				
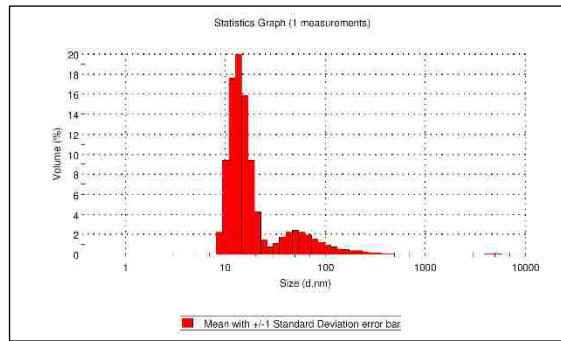
Figure 6.24. Statistic graph of size measurements on 2.5wt% Al2O3/water nanofluid

6.7. Summary and Conclusion

The rise in the total consumption of energy and the need for more thermal efficient system led to the search for enhanced devices that provide higher performance at lower cost, size, and material. The introduction of engineered fluids to replace the traditional working fluids is a great representative for this enhancement. They are known for their higher thermal

160

conductivity that improves the heat transfer rate. Nanofluids application includes increasing cooling or heating of heat exchanger devices, heat transfer efficiency of chillers, engine cooling, and cooling of electronics. A minichannel heat exchanger is selected in this study because of its higher volume density and thermal performance. This work investigated the thermal response of a minichannel heat exchanger where nanofluid and air are the main working fluids. The hot nanofluid was subjected to inlet mass flow and temperature step variations. The mass flow step changes varied from 0.5 to 2.5 while, the hot liquid temperature is kept constant at 70°C. Alternatively, the temperature step changes changed from 1.5 to 3.5 while, the mass flow rate was kept constant at 60 g/s. The Transmission Electron Microscopy (TEM), Energy- Dispersive Spectrometry (EDS) and Dynamic Light Scattering (DLS) analysis of the nanofluid are performed to demonstrate the particle size distribution, chemical characterization, stability and uniformity of suspension to show the distribution of the particles in the water. Results were shown in terms of transient dimensional and dimensionless hot and cold fluids outlet temperatures, heat transfer rates, heat balance, and effectiveness. The system repeatability in reading all the data showed a good confidence level within 3%.

➢ For the positive mass flow steps of 1.5 to 2.5, the hot liquid heat transfer rate had peaks at 22s and 26s, and for the negative steps of 0.8 and 0.5 the peaks were at 26s, and 32s, respectively. For both positive and negative steps, the higher the mass flow step changes, the peak time is smaller. Unlike the hot liquid, the cold airside had no peak for all the steps and had a continuous increase until reaching the steady state.

➢ Two empirical correlations (Eqs. 6.24 and 6.25) are obtained to predict the hot fluid outlet temperature in the dimensionless parameters for the temperature and mass flow step changes in a minichannel heat exchanger.

- ➢ The heat transfer of the hot nanofluid for all temperature step changes reached its maximum after 13s from the initial transient effect. The initial delay times is found higher for the hot liquid compared to the cold airside.

- ➢ The behaviour of the transient heat transfer rate in hot and cold fluids is not the same. The cold airside heat transfer rate showed a monotonic curve, while the hot liquid had a nonmonotonic trend with a resulted peak.

- ➢ The initial delay time of the normalized heat transfer is noticeable in the case of inlet temperature step variation while, it is negligible for the case of mass flow variation.

- ➢ Effectiveness based on the liquid side varied from 0.15 to 0.54 and on the airside ranged from 0.18 to 0.46. Higher rate of change in the effectiveness based on air is found at lower step changes compared to a negligible effect as steps of 2.5 and up.

- ➢ The rate of change of the dimensionless temperature is found higher for lower temperature step changes with a negligible effect for higher steps.

- ➢ Heat exchanger response time using nanofluid is shorter compared to water for both temperature and mass flow step changes.

- ➢ The use of nanofluid in a minichannel heat exchanger demonstrated up to 19% enhancement in heat transfer rate compared to DI water.

Institute for Environmental Research (GLIER) lab at the University of Windsor, the Western University, and the McMaster University.

Nomenclature

A_c *Channel cross section area, m^2*

B   *Bias*

D   *diameter, m*

D_h *Channel hydraulic diameter, m*

DAQ   *Data Acquisition*

HB   *Heat Balance*

L   *Channel length along the water fluid, m*

MICHX   *Minichannel Heat Exchanger*

$\dot{m}$ *Mass flow rate, g/s*

min   *Minimum*

P   *precision*

RTD   *Resistance Temperature Detector*

Re   *Reynolds number*

RSS   *Root of sum of squares*

SCXI   *Data acquisition module and terminal block*

Q   *Heat transfer rate, W*

Q'   *Normalized heat transfer*

T   *Temperature, °C*

t   *Time, s*

U   *Uncertainty %*

t_{res} *Resident time, s*

163

V	*Fluid velocity, m/s*
$\dot{\forall}$	*Volume flow rate m^3/s*
∞	*Final*
0	*Initial*

Greek symbols

ε	*Effectiveness*
μ	*Dynamic viscosity*
ρ	*Mass density, kg/m^3*

Subscripts

a	*Air stream*
c	*Cold fluid*
i	*Inlet*
h	*Hot fluid*
o	*Outlet*
w	*DI-Water*
nf	*Nanofluid*

Superscripts

*	*Dimensionless parameter*

References

[1]   M. Dehghandokht, M. G. Khan, A. Fartaj, and S. Sanaye, "Numerical study of fluid flow and heat transfer in a multi-port serpentine meso-channel heat exchanger" Applied Thermal Engineering, vol31, PP.1588-1599, 2011. https://doi.org/10.1016/j. applthermaleng.2011. 01. 035.

[2] J. C. Maxwell "A Treatise on Electricity and Magnetism" vol. 1, 2nd ed., Clarendon Press, Oxford, U.K., 1881.

[3] R. L. Hamilton, and O. K. Crosser, "Thermal Conductivity of Heterogeneous Two Component Systems" Industrial and Engineering Chemistry Fundamentals, vol1, no. 3, PP. 187–191, Aug1962, DOI: 10.1021/i160003a005.

[4] E. J. Wasp, J. P. Kenny, and R. L. Gandhi "Solid-Liquid Flow Slurry Pipeline Transportation, Series on Bulk Materials Handling" Trans. Tech. Publications, vol.1, no. 4, Clausthal, Germany, 1977.

[5] H.U. Kang, S.H. Kim, and J.M. Oh "Estimation of Thermal Conductivity of Nanofluid Using Experimental Effective Particle Volume" Journal of Experimental Heat Transfer, vol. 19, no. 3, PP. 181-191, 2006, https://doi.org/10.1080/08916150600619281.

[6] L. Megatif, A. Ghozatloo, A. Arimi, and M. Shariati-Niasar "Investigation of Laminar Convective Heat Transfer of a Novel Tio2–Carbon Nanotube Hybrid Water-Based Nanofluid" Journal of Experimental Heat Transfer, vol. 29, no. 1, PP. 124-138, 2016, https://doi.org/10.1080/08916152.2014.973974.

[7] S.U.S. Choi, and J.A. Eastman "Enhancing thermal conductivity of fluids with nanoparticles" International mechanical engineering congress and exhibition, San Francisco, CA, United States 1995. DOI: https://www.osti.gov/servlets/purl/196525.

[8] D.J. Bunce, and S.G. Kandlikar "Transient response of heat exchangers" Proceedings of the 2nd ISHMT-ASME heat and mass transfer conference, Surathkal, India, PP. 729–736, 1995.

[9] Y. Xuan, and W. Roetzel "Dynamics of shell-and-tube HX to arbitrary temperature and step flow variations" AIChE Journal, vol. 39, no. 3, PP. 413-421, Mar.1993. https://doi.org/10.1002/aic.690390305.

[10] T. Gao, B. Sammakia, J. Geer, A. Ortega, and R. Schmidt "Transient effectiveness characteristics of cross flow heat exchangers in data center cooling systems" 14th IEEE ITHERM Conference, 978-1-4799-5267-0/14/©2014 IEEE, pp688-697, 2014.

[11] B.L. Master, and K.S. Chunangad "Dynamic Performance of Heat Exchangers" Heat Transfer Engineering, vol. 29, no. 3, PP. 217-218, 2008. https://doi.org/10.1080 /01457630701755761.

[12] H. S. Erden "Experimental and Analytical Investigation of the Transient Thermal Response of Air-Cooled Data Centers" Ph.D. dissertation, Mechanical and Aerospace Engineering, Syracuse University, Syracuse, NY, U.S.A, 2013.

[13] D. Bunce "The Transient response of heat exchangers" MASc. thesis, Mechanical Engineering, College of engineering, Rochester institute of technology, May 1995.

[14] M. Lachi, N.El. wakil, and J. Padet "The time constant of double pipe and one pass shell-and-tube heat exchangers in the case of varying fluid flow rates" Int. J. of heat and mass transfer, vol. 40, no. 9, PP. 2067-2079, 1997. https://doi.org/10.1016 /S0017-9310(96)00274-8.

[15] N. Srihari, and S. K. Das "Experimental and theoretical analysis of transient response of plate heat exchangers in presence of nonuniform flow distribution" J. of heat transfer, vol. 130, PP. 051801-1–9, 2008.

[16] S. Fotowat, S. Askar, and A. Fartaj "Transient response of a meso heat exchanger with temperature step variation" Int. J. of Heat and Mass Transfer, vol.122, PP. 1172–1181, 2018. https://doi.org/10.1016/ j.ijheatmasstransfer. 2017.12.062.

[17] T. Gao, B. G. Sammakia, B. Murray, A. Ortega, and R. Schmidt "Data center crossflow heat exchanger study under different transient temperature boundary conditions" 30th semi-therm Symposium, IEEE, 2014. 174-183, 978-1-4799-4374-6/14.

[18]   Y. A. Cengel "Heat Transfer: A Practical Approach" New York: McGraw-Hill Higher Education, 2006.

[19]   R. M. Cima, and A. L. London "Transient Response of a Two-Fluid Counter-Flow Heat Exchanger-The Gas-Turbine Regenerator" Transactions of ASME, vol. 80, PP. 1169–1179, 1958. http://dx.doi.org/10.5772/67334.

[20]   T. Gao, B. Sammakia, J. Geer, A. Ortega, and R. Schmidt "Dynamic Analysis of Cross Flow Heat Exchangers in Data Centers Using Transient Effectiveness Method" IEEE Transaction of Component Packaging and Manufacturing Technology, vol. 4, no. 12, PP. 1925–1935, Nov. 2014. DOI: 10.1109/TCPMT.2014.2369256.

[21]   R. S. Figliola, and D. E. Beasley "Theory and Design for Mechanical Measurements" John Wiley & Sons, 5th ed., 2012.

[22]   ASME "An American National Standard, Performance Test Code (PTC) 30-1991, Air cooled heat exchangers" New York, 1991.

CHAPTER 7

SUMMARY AND CONCLUSION

This chapter aims to summarize the concluding remarks of the broadly discussed results starting chapter 2 to 6 followed by suggestions and recommendations for future researches. The main two objectives of the presented study were to enhance the heat transfer performance and characterize the dynamic behavior of different heat exchangers for their ultimate control. The increasing demand for more efficient, light weight, and low-cost thermal systems were the motivation to carry out this research.

This study investigated the effect of using a conventional and an engineered thermal fluid on the thermal performance of the heat exchangers. The enhanced thermophysical properties of the engineered fluid were considered and their influence on the heat exchanger performance was analyzed. The work was also extended to include a comparison between a conventional and a minichannel heat exchanger while both subjected to sudden changes in liquid side inlet conditions. A comprehensive well-equipped large-scale experimental setup was designed and assembled to examine the thermal performance of different heat exchangers under steady and transient changes. This setup was planned to accommodate accurate control of the fluid inlet parameters to accomplish transient variations in inlet conditions of the working fluids. The schematic of the main components of the experimental setup is demonstrated in Figure 3.2. The main observations and conclusions were discussed in the previous chapters and will be summarized in the following sections.

7.1. The dynamic behavior of heat exchangers

Heat exchangers analysis are commonly approximated by steady state solutions, however, in real life applications, heat exchangers undergo transient variations. An automotive thermostat is a great example of inlet conditions fluctuations. The opening and the closing of the thermostat valve creates a variation in the coolant temperature entering the radiator resulting in transient mode of the radiator. Another example can be seen in the refrigeration system with the expansion valve. The amount of liquid refrigerant injected into the evaporator is controlled by the expansion valve and any changes in the valve results in fluctuations in the evaporator inlet conditions which results in a transient behavior. For this regard, it is very important to characterize the dynamic behavior of heat exchangers for their effective control.

Researchers applied different forms of transient fluctuations in their investigation such as step, ramp, and exponential. However, the common type of transient variation that can be found in real applications is approximated nearly by a step function [1]. Heat exchangers do not rapidly respond to perturbations in fluid inlet mass flow rate or temperature, as a period of time is needed to reach the steady state after any disturbance. Fluctuations in inlet conditions will create a variation in the heat exchanger response, and consequently undesirable effect on the process [2]. Understanding the dynamic behavior of heat exchangers due to wide range of inlet condition fluctuations in one of the fluids and determining the factors that influence the transient response were pursued in this study.

A step change is chosen to be applied on the liquid side inlet conditions of mass flow rate and temperature to an unmixed-unmixed cross flow minichannel heat exchanger while

holding the other parameters constant. A wide range of step variations in mass flow 0.5 to 2.5 and in inlet temperature 1.5 to 3.5 was applied.

For the case of mass flow step change, the main concluding points are as follows:

- The fluid outlet temperatures did not respond instantly to the change in the liquid mass flow rate.

- Faster response time of the hot liquid for increased steps as Re is increased.

- An increase in the initial delay time with the increase of the mass flow rate step changes.

- An asymmetric trend for the heat transfer rate was found between the positive and negative step changes.

- Outlet temperature perturbation in a minichannel heat exchanger was found less compared to the limited experimental data found in literature.

For the case of hot liquid inlet temperature step change, the main concluding points are as follows:

- The system is confirmed repeatable and accurate within 3%.

- The heat balance error agreed with the ASME PTC 30-1991 specified acceptable range at the final steady state.

- Faster response time of the hot liquid than the cold air resulted in reaching steady state faster with higher rate of increase at higher step changes.

- A continuous decrease in the dimensionless temperature of both fluids up to a step of 2.5, after which no further reduction was noticed.

- Increasing the step change led to a gradual decrease in the response time up to a step of 3 where a negligible effect was observed afterwards.

- The heat transfer rate of the hot fluid was more than the cold with a steeper increase reaching a maximum possible value after approximately 9s for all the step changes compared to a gradual increase of the cold fluid.

- During the transient period, an adverse trend of effectiveness was found between the hot and cold fluids.

- Higher effectiveness at steady state was achieved for both fluids at the higher step changes.

When comparing a step of mass flow and temperature that have the same magnitude (1.5, 2.0, and 2.5) and holding air inlet conditions constant, the response time is found higher for the case of temperature than the mass flow step changes.

The listed results show that the heat exchanger performance depends on many factors; the response time that takes the heat exchanger to undergo a change from one steady state to another, the delay time that depends on the residence time which is a combination of the geometry of the heat exchanger and the responses of the measuring devices. Additionally, the operating conditions can play a role in the heat exchanger behavior. Some of the noted observations that can be drawn from this study that can affect the heat exchanger performance running under transient conditions are:

- Longer channel length as well as smaller channel size (physical geometry of heat exchanger) results in shorter residence time and consequently faster response time.

- Higher steps up results in shorter response time for mass flow and temperature variations. However, it is not the case for the mass flow step down where the response time is found to be 56s for a step of 0.5 and 45s for step of 0.8.

- Noticeable initial delay time for the normalized heat transfer was found in the case of inlet temperature step variation compared to negligible one for the case of mass flow changes.

7.2. Thermal performance of a Minichannel heat exchangers

The heat exchanger geometry plays a significant role in the design process of heat exchangers and its thermal performance evaluations. Different approaches have been under investigation to enhance the heat exchanger performance including improving their current design and introducing alternative geometries and working fluids. In the light of the search for reduced size, weight, and energy efficiency as well as improved performance, an enhanced surface area to volume ratio was presented. It is accomplished using mini size channels incorporated into a slab form. A heat exchanger with multiple slabs of minichannels was presented and is referred to as a minichannel heat exchanger. As proven in previous investigations, this design provides an increased heat transfer surface area to volume ratio and leads to savings in cost, weight, and size. The applicability of using minichannel to enhance the heat transfer performance of a heat exchanger for steady state is well established and discussed. The lack of the experimental data and research involving transient behavior of compact heat exchangers is one of the motivations for the current study.

A deep insight on assessing the dynamic performance of a compact cross flow heat exchanger based on the hot fluid inlet temperature and mass flow step changes was also

172

studied. The lacking experimental data on this subject makes it an attractive topic to enrich the limited existing database. In addition to investigating the effect of step changes in liquid inlet temperature and mass flow rate, the transient thermal response of different heat exchangers was also included and accounted for. Hence, the study was followed by the examination and comparison of transient response of a minichannel multiport slab and a traditional tube and fin heat exchanger when both were subjected to step variations in liquid flow rate and temperature. The outlet temperatures of both fluids, transient effectiveness, transient heat transfer rates, and time constant were presented and discussed.

Concluding remarks from the comparison are as follows,

- The response time of a MICHX was found shorter compared to the conventional heat exchanger.

- Longer initial delay time for the MICHX than the conventional heat exchanger due to higher residence time, 4.5s, for the MICHX compared to 0.7s for the cross flow conventional.

- Empirical correlations (Eqs. 4.27 and 4.28) are developed for the hot liquid temperature step as well as mass flow variations on the conventional heat exchanger, which displayed good agreement with the experimental data.

- The analytical model (Eq. 4.16) [3] overestimated the experimental results of the conventional heat exchanger study by more than 20%.

7.3. *Working fluid effect on the thermal performance of heat exchangers*

The enhancement of heat exchanger geometry improves the thermal performance of heat exchangers. However, the advancement in technology presents additional methods that lead to great improvement in thermal design of heat exchangers with enhanced thermal performance. Finding alternatives to the conventional working fluid or enhancing the

thermophysical properties of the existing one can lead to great improvement in the performance of heat exchangers. Currently, nanotechnology is obtaining a vast attraction owing to its extensive use in many applications such as agriculture, biomedical, water treatment to energy storage. The advancement in nanotechnology made it possible to disperse nano size particles into a base liquid to increase its thermal conductivity. The resulting fluid is called nanofluid.

Studying the interaction of nanofluid with the contact material is important to serve as a significant parameter while designing a thermal system with a nanofluid as the working fluid. The effect of the two different solutions (H_2SO_4+NaOH and HCl+NaOH) with the same pH level (3.7) of the Al_2O_3/W nanofluid on some common contact materials; Copper, Aluminum, and stainless steel, was tested with Scanning Electron Microscope/Energy Dispersive Spectroscopy (SEM/EDS) and WiTec system. Results from this study provides an insight on the interaction of these nanofluids with the contact materials. Cu possessed the highest corrosion while SS showed the lowest corrosion at environmental condition. This can be explained by a higher amount of oxygen which was found on the surface of the contact materials that referred to higher oxygen partial pressure on the metals surface compared to the environmental condition that resulted in higher pitting and intergranular corrosion.

The combination of the previous two studies investigating the transient effect and applying nanotechnology to advance thermal systems design and performance resulted in the following investigation of using nanofluid in a MICHX. A series of experiments were conducted to examine the effect of inlet mass flow and temperature perturbations in a MICHX with Al_2O_3/water nanofluid. Since most available studies including nanofluid

174

with heat exchangers running in a steady state, the importance of the current investigation lays emphases on exploring the dynamic behavior and the heat transfer enhancement of a MICHX with nanofluid subjected to step changes in liquid inlet conditions.

Once the thermophysical study and the interaction of the nanofluid with some common materials used in the heat exchanger design is accomplished, applying nanofluid to a MICHX is considered and tested. The outcome of this analysis yielded the following results,

- The use of nanofluid in a MICHX showed up to 19% enhancement in heat transfer rate compared to DI water.

- The response time of nanofluid was faster than water at both temperature and mass flow step changes.

- The heat exchanger with nanofluid experienced a maximum heat transfer rate after about 13s from the initial transient step before reaching the steady state condition for all temperature step variations.

The reported results can find an application in the design and selection of a cross flow heat exchanger found in thermal management systems such as in automotive industry where compact heat exchanger is required for size and weight reduction.

7.4. Future work recommendations

Although much effort has been made to highlight the most noteworthy data found from the test experimentation, there still a broad investigation remaining that can be further examined by future researchers.

- Advanced research can be extended to study the effect of transient response of heat exchangers due to the perturbation in the cold air side inlet mass flow rates and temperatures.

-       In-depth study is recommended to quantify the dynamic response of both liquid and air subjected to the temperature step down on liquid side perturbation.

-       A comprehensive understanding of the interactions between particles, stabilizers, the suspending liquid and the heating surface will be important for applications of nanofluid in heat transfer devices.

-       Further Investigation on the influence of viscosity and wettability of nanofluids on flow and heat transfer.

References

[1]   D.J. Bunce, and S.G. Kandlikar "Transient response of heat exchangers" Proceedings of the 2nd ISHMT-ASME heat and mass transfer conference, Surathkal, India, PP. 729–736, 1995.

[2]   K. Silaipillayarputhur, and S. A. Idem "Step response of a single-pass crossflow heat exchanger with variable inlet temperatures and mass flow rates" Journal of Thermal Science and Engineering Applications, Vol. 4, 044501 PP. 1-6, 2012.

[3]   J. Yin, and M.K. Jersen "Analytical model for transient heat exchanger response" International Journal of heat and mass transfer, vol. 46, 3255-3264, 2003. https://doi.org/10.1016/S0017-9310(03)00118-2

APPENDICES

APPENDIX A

UNCERTAINTY ANALYSIS

Error is defined as a variation between the true and recorded value of a measurement. Many sources of error occur in collecting data. Error can be categorized as systematic or random. Systematic error or bias error means that the error does not happen for random reasons only such as random variation, or 'noise in the system; otherwise, it is a random error or precision error, such as in repeatability. The combined error of two components, bias and precision errors, is calculated through the root sum square method, RSS. The measurement parameters are considered as independent and dependent parameters. The independent parameters are those measured through an experiment or directly recorded by data acquisition system (DAQ) i.e., temperature, pressure, time, mass flow rate, and dimensions of the heat exchanger. However, the dependent parameters are those that depend on independent parameters and would be calculated, like Reynolds number, heat transfer rate, and effectiveness.

Bias error

The Bias error can be assessed from the root sum square method (RSS) Figliola and Beasley [1] as below:

$$U_B = \pm\sqrt{B_1^2 + B_2^2 + \cdots + B_K^2} \qquad \text{A.1}$$

Where, i refers to the error source groups for example calibration error, i = 1, data acquisition error, i = 2, and data reduction error, i = 3,

Precision error

The precision error can be evaluated using the following formula:

$$U_p = \pm\sqrt{P_1^2 + P_2^2 + \cdots + P_k^2}$$

A.2

Repeatability error

The repeatability error for a device can be found as follows,

$$U_R = \pm\sqrt{R_1^2 + R_2^2 + \cdots + R_n^2}$$

A.3

The combination of these three errors can be evaluated from the following formula,

$$U_x = \pm\sqrt{B^2 + P^2 + R^2}$$

A.4

A.1 Uncertainty of the parameters

A.1.1 Uncertainty of the Independent Parameters

The uncertainty analysis in the independent parameters includes the absolute and relative uncertainties. For instance, if a measurement at a point is x, the absolute and relative uncertainties for the Bias and Precision may be calculated as below,

Absolute uncertainty

$$U_{XBP} = \sqrt{B^2 + P^2}$$

A.5

Relative uncertainty

$$\frac{UXBP}{X} = \frac{\sqrt{B^2 + P^2}}{X} \qquad \text{A.6}$$

The correlation between the dependents and the independents parameters can be determined as follows:

$$Y = f(X_1 + X_2 + X_3 + \cdots + X_n) \qquad \text{A.7}$$

Y denotes the dependent parameter and X_n denotes the independent parameters.

A.1.2 Uncertainty of dependent parameter

Hence, the absolute uncertainty of Y can be assessed from the following equation,

$$U_Y = \sqrt{\left(\frac{\partial Y}{\partial x_1} U_{x_1}\right)^2 + \left(\frac{\partial Y}{\partial x_2} U_{x_2}\right)^2 + \left(\frac{\partial Y}{\partial x_3} U_{x_3}\right)^2 + \cdots + \left(\frac{\partial Y}{\partial x_n} U_{x_n}\right)^2} \qquad \text{A.8}$$

$$Y \pm U_y$$

$$= Y$$

$$\pm \sqrt{\left(\frac{\partial Y}{\partial x_1} U_{x_1}\right)^2 + \left(\frac{\partial Y}{\partial x_2} U_{x_2}\right)^2 + \left(\frac{\partial Y}{\partial x_3} U_{x_3}\right)^2 + \cdots + \left(\frac{\partial Y}{\partial x_n} U_{x_n}\right)^2} \qquad \text{A.9}$$

Then, the relative uncertainty of Y can be shown as follows,

$$\frac{U_Y}{Y}$$

$$= \frac{\sqrt{\left(\frac{\partial Y}{\partial x_1} U_{x_1}\right)^2 + \left(\frac{\partial Y}{\partial x_2} U_{x_2}\right)^2 + \left(\frac{\partial Y}{\partial x_3} U_{x_3}\right)^2 + \cdots + \left(\frac{\partial Y}{\partial x_n} U_{x_n}\right)^2}}{f(X_1 + X_2 + X_3 + \cdots + X_n)} \qquad \text{A.10}$$

A.2 Uncertainties in the data collections and instruments

A.2.1 Uncertainty of data acquisition

DAQ Data Acquisition System (with chassis and all the accessories) model: 16-bit 6052E with capacity of -10 to+10VDC and accuracy of ± (29µV+0.035% of rdg) is used in the experiment.

A.2.2 Data reduction Uncertainty

The uncertainty of data reduction is owing to calculation truncation and curve fitting. The uncertainty of data reduction is insignificant.

A.3 Uncertainty of liquid side mass flow rate measurement and velocity

A.3.1 Uncertainty of the di-water mass flow rate

In this study, a Proline Promass 100 series inline mass flow measurement device with an integral display, an Ethernet IP output and a dispersion concentration measurement software, using universal tools for configuration devices, FieldCare , with an accuracy of ± 0.1% of the measurement mass is used.

A.3.2 Uncertainty of liquid side velocity

$$V_{L,ch} = \frac{\dot{m}_{L,ch}}{\rho_L A_{ch}} \qquad \text{A.11}$$

$$U_{V\,L,ch} = \pm \sqrt{\left(\frac{\partial V_L}{\partial \dot{m}_L} U_{\dot{m}_w}\right)^2 + \left(\frac{\partial V_L}{\partial \rho_L} U_{\rho_L}\right)^2 + \left(\frac{\partial V_L}{\partial A_{ch}} U_{A_{ch}}\right)^2} \qquad \text{A.12}$$

$$U_{V\,L,ch} = \pm \sqrt{\left(\frac{1}{\rho_L A_{ch}} U_{\dot{m}_L}\right)^2 + \left(\frac{\dot{m}_L}{\rho_L^2 A_{ch}} U_{\rho_w}\right)^2 + \left(\frac{\dot{m}_L}{\rho_L A_{ch}^2} U_{A_{ch}}\right)^2} \qquad \text{A.13}$$

A.4 Uncertainty of liquid side mass flow rate measurement and velocity

A.4.1 Uncertainty of the Air Mass Flow Rate

$$m_a = \rho_a \, v_a \, A_a \, \frac{kg}{s} \qquad \text{A.14}$$

$$U_{\dot{m}_a} = \pm \sqrt{\left(\frac{\partial \dot{m}_a}{\partial \rho_a} U_{\rho_a}\right)^2 + \left(\frac{\partial \dot{m}_a}{\partial v_a} U_{v_a}\right)^2 + \left(\frac{\partial \dot{m}_a}{\partial A_a} U_{A_a}\right)^2} \qquad \text{A.15}$$

$$U_{\dot{m}_a} = \pm \sqrt{\left(v_a A_a U_{\rho_a}\right)^2 + \left(\rho_a A_a U_{v_a}\right)^2 + \left(\rho_a v_a U_{A_a}\right)^2} \qquad \text{A.16}$$

A.4.2 Uncertainty of Air side velocity

The air flow velocity is measured from the following expression,

$$V_a = \pm \sqrt{\frac{2\Delta p_{dynamics}}{\rho_a}} \qquad \text{A.17}$$

The uncertainty of air flow velocity is calculated as below,

$$U_{V_a} = \pm \sqrt{\left(\frac{\partial V_a}{\partial \Delta p_{dynamics}} U_{\Delta p_{dynamics}}\right)^2 + \left(\frac{\partial V_a}{\partial \rho_a} U_{\rho_a}\right)^2} \qquad \text{A.18}$$

where,

$$\frac{\partial V_a}{\partial \Delta p_{dynamics}} = \frac{1}{\sqrt{2\rho_a \Delta p_{dynamics}}} \qquad \text{A.19}$$

$$\frac{\partial V_a}{\partial \rho_a} = -\frac{\sqrt{2\Delta p_{dynamics}}}{2\, \rho_a^{\frac{3}{2}}} \qquad \text{A.20}$$

Velocity of inlet air is measured at the centre of the test chamber by using a pitot static tube, a differential pressure transducer (DPT), and a data acquisition system (DAQ).

The uncertainty of Pitot tube: the Pitot tube should be installed parallel to the air flow within ±15°. However, the bias error of ±0.5% FS reading is introduced for misalignment installation. The total uncertainty of the Pitot static tube is calculated as follows,

$$U_{Pitot} = \sqrt{B_{Pitot}{}^2 + P_{Pitot}{}^2} = \sqrt{\left(\frac{0.05}{100}\right)^2 + (0)^2} = 0.05 \text{ volt} \qquad \text{A.21}$$

The accuracy of the DPT is supplied by the manufacturer as ±1% of FS. The transducer is set to 0-10 VDC. The total uncertainty of the transducer is calculated to be the following,

$$U_{PTDD} = \sqrt{B_{DPT}{}^2 + P_{DPT}{}^2} = \sqrt{\left(\frac{0.1}{100}\right)^2 + (0)^2} = 0.1 \text{ volt} \qquad \text{A.22}$$

Uncertainty of Data Acquisition System for the range of 0-10VDC is estimated for actual voltage as below:

$$U_{DAQ} = \sqrt{508365.62 + (318166 \, X \, V_{DAQ}{}^2)} \qquad \text{A.23}$$

Thus, the maximum uncertainty for the maximum voltage of 10VDC is found to be as below,

$$U_{DAQ} = 5.7 * 10^{-3} \text{ volt} \qquad \text{A.24}$$

A.5 Uncertainty of calibrator

An Omega dual thermocouple and RTD calibrator, Model # FDB140FK, with the RSS accuracy ± 0.03 °C are used in the lab. This dry block calibrator has a resolution of ±0.01C, and stability in 5 min ±0.05°C.

A.6 Uncertainty of RTDs and thermocouples

A.6.1 Uncertainty for water inlet and outlet temperature, RTDs

The bias error related to the inlet and outlet of the ultra precise RTDs has been supplied by the manufacturer. The bias error as a function of temperature is calculated based on the following formula,

$$B_{RTD} = \pm \frac{1}{10}[0.3 + 0.005|T(°C)|] \qquad \text{A.25}$$

The precision error in the liquid inlet and outlet temperature measurement is found through the following equation,

$$P_{RTD} = \pm t_{N,95}S_{\bar{T}} \approx \pm 1.96 \frac{S_{T,RTD}}{\sqrt{N}} \quad for \ N \geq 1000 \qquad \text{A.26}$$

The uncertainty of the RTDs based on the Bias and precision error is provided as follows,

$$U_{RTD} = \pm \sqrt{B_{RTD}^2 + P_{RTD}^2} \qquad \text{A.27}$$

$$U_{RTD} = \pm \sqrt{(\frac{1}{10}(0.3 + 0.005|T(°C)|))^2 + (1.96\frac{S_{T,RTD}}{\sqrt{N}})^2} \qquad \text{A.28}$$

A.6.2 Uncertainty for air inlet and outlet temperature _Thermocouples

Using the sensitivity of the T-type thermocouples, the uncertainty of the DAQ components can be translated from voltage to °C as follows,

$$U_{DAQ} = 6.033 \times 10^{-6}V \qquad \text{A.29}$$

The uncertainty related to the conversion of the voltage reading of the thermocouples to a °C reading which the sensitivity is found as,

$$\frac{\partial V}{\partial T_{Thermocouple}} = 43X10^{-6} \frac{V}{°C} \qquad \text{A.30}$$

$$U_{DAQ} = \frac{6.033 \times 10^{-6}V}{\frac{\partial V}{\partial T_{Thermocouple}}} = \frac{6.033 \times 10^{-6}V}{43 \times 10^{-6} \frac{v}{°C}} = 0.14°C \qquad \text{A.31}$$

A.7 Uncertainty of independent and dependent parameter

A.7.1 Uncertainty of independent parameter

Measured dimensions and the uncertainty of some lengths of the MICHX are acquired from the heat exchanger manufacturer. The reason is either that the measuring length is bigger than the range of the digital caliper or the bias error of the digital caliper stands higher than the uncertainty of the manufacturer. These dimensions contain heat exchange height, length, slab width, and fin thickness.

A.7.1.1 Uncertainty of the MICHX dimensions

$$B_{accuracy} = 2.54 \times 10^{-5} \ m \qquad \text{A.32}$$

$$B_{resolution} = 0.5 \times B_{accuracy} = 1.25 \times 10^{-5} \ m \qquad \text{A.33}$$

$$B_{caliper} = \pm\sqrt{\left(B_{accuracy}\right)^2 + (B_{resolution})^2} = \pm 2.84 \times 10^{-5} \qquad \text{A.34}$$

A.7.1.2 Uncertainty of height of the heat exchanger

$$S_{H_{HX}} = \sqrt{\frac{\sum_{i=1}^{N}(x_i-\bar{x})^2}{N-1}} = 0.008 \quad N{=}50 \qquad \text{A.35}$$

$$P_{H_{HX}} = \pm t_{v,95} S_{H_{HX}} \approx \pm 2 \frac{S_{H_{HX}}}{\sqrt{N}} \approx \pm 2.2 \times 10^{-4} \qquad \text{A.36}$$

$$U_{H_{HX}} = \pm \sqrt{(B_{caliper})^2 + (P_{H_{HX}})^2} = \pm 2.2 \times 10^{-4} \; (Absolute) \qquad \text{A.37}$$

$$U_{H_{HX}} = \frac{2.2 \times 10^{-4}}{1.016 \times 10^{-1}} \times 100 = \pm 0.22\% \; (Relative) \qquad \text{A.38}$$

A.7.1.3 Uncertainty of Width of the heat exchanger

Uncertainty of width of the heat exchanger is supplies by the manufacturer

$$U_{W_{HX}} = 0.15\% \qquad \text{A.39}$$

$$U_{W_{HX}} = 0.15 \times \frac{0.3048}{100} = \pm 0.00046 \qquad \text{A.40}$$

A.7.1.4. Uncertainty of length of the heat exchanger is received from the supplier

Uncertainty of length of the heat exchanger is supplies by the manufacturer

$$U_{L_{HX}} = \pm 2.2 \times 10^{-4} \qquad \text{A.41}$$

$$U_{L_{HX}} = \frac{2.2 \times 10^{-4}}{1.000 \times 10^{-1}} \times 100 = \pm 0.22\% \qquad \text{A.42}$$

A.7.1.5 Uncertainty of the channel hydraulic diameter

Description	Mean Value	Unit	Uncertainty (%)
Channel hydraulic diameter, $D_{h,c}$	1.0×10^{-3}	m^2	$\pm 3.48 \times 10^{-5}$

A.7.2 Uncertainty of dependent parameter

A.7.2.1 Uncertainty of MICHX surface areas

185

Uncertainty of the channel fluid cross section area is calculated as follows,

$$A_{CS,w} = \pi \, \frac{D_{h,w}^2}{4} = \pi \, \frac{0.001^2}{4} = 7.87 \times 10^{-7} \qquad \text{A.43}$$

$$U_{A_{CS,w}} = \pm \sqrt{\left(\frac{\partial A_{XS,w}}{\partial D_{h,w}} U_{D_{h,w}} \right)^2} \qquad \text{A.44}$$

$$U_{A_{Cs,w}} = \pm\pi \, \frac{D_{h,w}}{2} U_{D_{h,w}} = \pm\pi \, \frac{0.001}{2} \times 3.48X \, 10^{-5} \qquad \text{A.45}$$

$$= 5.66 \, X \, 10^{-8} m^2$$

Uncertainty of airside frontal area could be calculated from below formula

$$A_{fr,a} = H_{HX} \times W_{HX} = 0.3048 \times 0.1016 = 0.0310 \, m \qquad \text{A.46}$$

$$U_{A_{fr,a}} = \pm \sqrt{\left(\frac{\partial A_{fr,a}}{\partial H_{HX}} U_{H_{HX}} \right)^2 + \left(\frac{\partial A_{fr,a}}{\partial W_{HX}} U_{W_{HX}} \right)^2} \qquad \text{A.47}$$

$$U_{A_{fr,a}} = \pm \sqrt{\left(W_{HX} \times U_{H_{HX}} \right)^2 + \left(H_{HX} \times U_{W_{HX}} \right)^2} = \pm 1.6 \times 10^{-4} \, m \qquad \text{A.48}$$

$$U_{A_{fr,a}} = \frac{0.00016}{3.0907 \times 10^{-2}} \times 100 = \pm 0.52\% \qquad \text{A.49}$$

A.7.2.2 Uncertainties of the airside slab frontal area is found as

$$A_{fr,slabs} = N_{slab} \times (t_{slab} \times W_{slab}) = 3.048 \times 10^{-3} \qquad \text{A.50}$$

$$U_{A_{fr,slabs}} = \pm \sqrt{\left(\frac{\partial A_{fr,slabs}}{\partial t_{slab}} U_{t_{slab}} \right)^2 + \left(\frac{\partial A_{fr,slabs}}{\partial W_{slab}} U_{W_{slab}} \right)^2} \qquad \text{A.51}$$

$$U_{A_{fr,slabs}} = \pm \sqrt{\left(W_{slab} \times U_{t_{slab}} \right)^2 + \left(t_{slab} \times U_{W_{slab}} \right)^2} \qquad \text{A.52}$$

$$U_{t_{slab}} = \pm\sqrt{\left(B_{caliper}\right)^2 + \left(P_{t_{slab}}\right)^2} = \pm 1.0 \times 10^{-5} \qquad \text{A.53}$$

$$U_{W_{slab}} = \pm\sqrt{\left(B_{caliper}\right)^2 + \left(P_{W_{slab}}\right)^2} = \pm 2.0 \times 10^{-4} \qquad \text{A.54}$$

$$U_{A_{fr,slabs}} = 3.074 \times 10^{-6} \qquad \text{A.55}$$

$$U_{A_{fr,slabs}} = \frac{3.074 \times 10^{-6}}{3.048 \times 10^{-3}} \times 100 = \pm 0.1\% \qquad \text{A.56}$$

A.7.2.3 Uncertainty of the min free air area of the airside is attained below

$$A_{min,a} = A_{fr,a} - A_{blocked,a} = 0.026 \ \text{m}^2 \qquad \text{A.57}$$

$$U_{A_{min,a}} = \pm\sqrt{\left(\frac{\partial A_{min,a}}{\partial A_{fr,a}} U_{A_{fr,a}}\right)^2 + \left(\frac{\partial A_{min,a}}{\partial blocked,a} U_{blocked,a}\right)^2} \qquad \text{A.58}$$

$$U_{A_{min,a}} = \pm 1.6 \times 10^{-4} \ m \qquad \text{A.59}$$

$$U_{A_{min,a}} = \frac{1.6 \times 10^{-4}}{25.76 \times 10^{-3}} \times 100 = \pm 0.62\% \qquad \text{A.60}$$

A.7.2.4 uncertainty for the slabs heat transfer area is calculated as following,

$$
\begin{aligned}
A_{HT,slabs,a} = N_{slab} & \\
& \times \left(\left(\left(2 \times (t_{slab} \times W_{slab}) + 2 \times (W_{slab} \times L_{slab})\right)\right)\right. \qquad \text{A.61} \\
& \left. - \left(2 \times N_{fin,slab} \times L_{fin} \times t_{fin}\right)\right)
\end{aligned}
$$

$$A_{HT,slabs,a} = 3.054 \times 10^{-1} \ \text{m}^2 \qquad \text{A.62}$$

$$U_{A_{HT,slabs,a}}$$

$$= \pm\sqrt{\left(\frac{\partial A_{HT,slabs,a}}{\partial t_{slab}}U_{t_{slab}}\right)^2 + \left(\frac{\partial A_{HT,slabs,a}}{\partial W_{slab}}U_{W_{slab}}\right)^2 + \left(\frac{\partial A_{HT,slabs,a}}{\partial L_{slab}}U_{L_{sl}}\right.}$$

A.63

$$U_{A_{HT,slabs,a}}$$

$$= \pm\sqrt{\left(2N_{slab}\,W_{slab}U_{t_{slab}}\right)^2 + \left((2N_{slab}t_{slab} + 2L_{slab})U_{W_{slab}}\right)^2 + \left(2\right.}$$

A.64

$$U_{A_{HT,slabs,a}} = 1.32 \times 10^{-4}\ \text{m}^2$$

A.65

A.7.2.5 Uncertainty of the Airside Hydraulic Diameter

The Absolute airside hydraulic diameter is found from the theoretical formula from Kays and London [2]

$$D_{h,a} = f\left(L_a, A_{fr,a}, A_a\right) = 4 \times L_a \times \frac{A_{min,a}}{A_{a,HT}} = 0.004\ \text{m}$$

A.66

$$U_{D_{h,a}} = \pm\sqrt{\left(\frac{\partial D_{h,a}}{\partial L_a}U_{L_a}\right)^2 + \left(\frac{\partial D_{h,a}}{\partial A_{min,a}}U_{A_{min,a}}\right)^2 + \left(\frac{\partial D_{h,a}}{\partial A_{a,HT}}U_{A_{a,HT}}\right)^2}$$

A.67

$$U_{D_{h,a}}$$

$$= \pm\sqrt{\left(\frac{A_{min,a}}{A_{a,HT}}U_{L_a}\right)^2 + \left(\frac{L_a}{A_{a,HT}}U_{A_{min,a}}\right)^2 + \left(-\frac{L_aA_{min,a}}{A_{a,HT}^2}U_{A_{a,HT}}\right)^2}$$

A.68

The absolute and relative uncertainty of the airside hydraulic diameter is presented as follows,

$$U_{D_{h,a}} = \pm 2.0\ X10^{-5}\ m$$

A.69

$$U_{D_{h,a}} = \pm\frac{U_{D_{h,a}}}{D_{h,a}}X100 = \pm 0.5\%$$

A.70

A.8 Uncertainty of Key Dimensional Parameters

The uncertainty for the key dimensional parameters are presented in Table A.1

Table A.1 Uncertainty of key parameters of the MICHX

Description	Mean Value	Unit	Uncertainty (%)
Height of the heat exchanger, H_{HX}	1.016×10^{-1}	m	±0.22
Width of heat exchanger, W_{HX}	3.048×10^{-1}	m	±0.15
Length of the heat exchanger, L_{HX}	1.000×10^{-1}	m	±0.22
Water-side heat transfer area, A_w	7.854×10^{-7}	m^2	±6.96
Water-side heat transfer area, A_w	0.3256	m^2	±3.48
Air-side heat transfer length, L_a	1.000×10^{-1}	m	±0.22
Air-side total frontal area, $A_{fr,a}$	3.0907×10^{-2}	m^2	±0.52
Airside frontal blocked area, $A_{blocked,a}$	5.148×10^{-3}	m^2	±0.12
Air-side minimum free flow area, $A_{min,a}$	2.575×10^{-2}	m^2	±0.62
Air-side heat transfer area, $A_{a,HT}$	2.585	m^2	±0.44
Airside hydraulic diameter, $D_{h,a}$	4.00×10^{-3}	m	±1.62
MICHX hydraulic diameter, $D_{h,w}$	0.001	m	±3.48

A.9 Uncertainty for one Operating Condition

$$V_a = 6 \text{ m/s}, T_{a,i} = 13 \text{ °C}, T_{w,i} = 22 \text{ °C}, \dot{m}_w = 0.060 \frac{kg}{s}$$

$$Re_a = \frac{\rho_a V_a D_{h,a}}{\mu_a} = \frac{1.237 \times 6 \times 4.00 \times 10 - 3}{1.812 \times 10^{-5}} = 1638$$

Table A.2 Different parameters at Tb for one operating condition

Parameter	Mean Value	Unit	Uncertainty%
De-water inlet temperature, $T_{w,i}$	22	°C	±0.75
De-water outlet temperature, $T_{w,o}$	18.5	°C	±0.87
DI-Water mass flow rate, $\dot{m}_w$	0.060	Kg/s	±0.00006
Waterside velocity, V_w	1.128	m/s	±0.14
Waterside Density, ρ_w	997.8	Kg/m^3	±0.02
Waterside specific heat, $C_{p,w}$	4.076	j/kg.°C	±0.06
Waterside Viscosity, μ_w	9.77×10^{-4}	Kg/m.s	±43.7
Waterside Reynolds number, Re_w	1150	-	35
Waterside Heat transfer rate, $\dot{Q}_w$	0.952	kW	
Air-side Heat transfer rate, $\dot{Q}_a$	0.980	kW	
Overall Heat transfer rate, $\dot{Q}_{Overall}$	0.966	kW	
Air inlet temperature, $T_{a,i}$	13	°C	
Air outlet temperature, $T_{a,o}$	17.5	°C	
Air mass flow rate, $\dot{m}_a$	0.222	Kg/s	
Airside Reynolds number, Re_a	1638	-	

A.10 Uncertainties of the di-water properties

A.10.1 Uncertainty of water viscosity

The uncertainty of water viscosity is considered from following formula:

$$U_{\mu_w} = \frac{1}{2}\left|\mu_w@T_{b,w,max} - \mu_w@T_{b,w,min}\right| \qquad \text{A.71}$$

$$T_{b,w} = \frac{\overline{T_{w,i}} + \overline{T_{w,out}}}{2} \qquad \text{A.72}$$

$$\mu_{b,w} = \frac{\mu_{T_{w,max}} + \mu_{T_{w,min}}}{2} \qquad \text{A.73}$$

A.10.2 Uncertainty of water density

The uncertainty of water density is calculated from succeeding method:,

$$U_{\rho_w} = \frac{1}{2}\left|\rho_w @T_{b,w,max} - \rho_w @T_{b,w,min}\right| \qquad \text{A.74}$$

A.10.3 Uncertainty of water specific heat

The uncertainty of water specific heat is calculated from the below equation,

$$U_{Cp_w} = \frac{1}{2}\left|Cp_w @T_{b,w,max} - Cp_w @T_{b,w,min}\right| \qquad \text{A.75}$$

A.10.4 Uncertainty of water thermal conductivity

The uncertainty of water thermal conductivity is found from succeeding equation:,

$$U_{K_w} = \frac{1}{2}\left|K_w @T_{b,w,max} - K_w @T_{b,w,min}\right| \qquad \text{A.76}$$

A.11 Uncertainty of the heat transfer rate

A.11.1 Uncertainty of the waterside heat transfer rate

The liquid side heat transfer rate is given in Equation 3.10 from which by partial derivatives the uncertainty is calculated as follows;

$$U_{Q_L} = \pm\sqrt{\left(\frac{\partial Q_L}{\partial \dot{m}_L}U_{\dot{m}_L}\right)^2 + \left(\frac{\partial Q_L}{\partial Cp_L}U_{Cp_L}\right)^2 + \left(\frac{\partial Q_L}{\partial \Delta T_L}U_{\Delta T_L}\right)^2} \qquad \text{A.77}$$

$$U_{Q_L} = \pm \sqrt{ \begin{array}{l} \left(Cp_L(\Delta T_{L,i} - \Delta T_{L,o})U_{\dot{m}_L}\right)^2 + \\ \left(\dot{m}_L(\Delta T_{L,i} - \Delta T_{L,o})U_{Cp_L}\right)^2 + \left(\dot{m}_L Cp_L U_{\Delta T_L}\right)^2 \end{array} }$$

A.78

A.11.2 Uncertainty of the airside heat transfer area is found as,

$$U_{A_{HT,a}} = 1 \times U_{A_{HT,fins,a}} + 1 \times U_{A_{HT,slab,a}}$$

A.79

$$U_{A_{HT,a}} = 1.32 \times 10^{-4} + 0.038 = 0.038 \ \text{m}^2$$

A.80

Uncertainty of the airside heat transfer area is found as,

$$A_{HT,w} = N_{slab} \times N_{channel} \times (\pi \, D_{h,w} W_{slab})$$

A.81

$$A_{HT,w} = 0.3256 \ \text{m}^2$$

A.82

$$U_{A_{HT,w}} = \pm \sqrt{ \left(\pi N_{slab} N_{fins} W_{slab} U_{D_{h,w}}\right)^2 + \left((\pi N_{slab} N_{fins} D_{h,w} U_{W_{slab}} \right)^2 }$$

A.83

$$U_{A_{HT,w}} = 0.2735 \ \text{m}^2$$

A.84

A.12. Uncertainty of heat transfer rate

A.12.1 Uncertainty of the airside heat transfer rate

The air-side heat transfer rate is defined by Equation 3.11. Similar to liquid side, the uncertainty in air-side heat transfer rate is calculated as follows;

$$q_{L=\dot{m}_a Cp_a \Delta T_a}$$

A.85

From partial derivation

$$\frac{\partial q,a}{\partial \dot{m},a} = Cp_a \Delta T_a \qquad \frac{\partial q,a}{\partial Cp_a} = \dot{m}_a \Delta T_a \qquad \frac{\partial q,a}{\partial \Delta T_a} = \dot{m}_a Cp_a \qquad \text{A.86}$$

Absolute Uncertainty is considered as

$$U_{q_a} = \sqrt{(Cp.\Delta T.U\dot{m})_a^2 + (\dot{m}.\Delta T.UCp)_a^2 + (\dot{m}.Cp.U\Delta T)_a^2} \qquad \text{A.87}$$

And Relative Uncertainty as,

$$\frac{U_{q_a}}{q_a} * 100 = \sqrt{(\frac{U\dot{m}}{\dot{m}})_a^2 + (\frac{UCp}{Cp})_a^2 + (\frac{U\Delta T}{\Delta T})_a^2} \qquad \text{A.88}$$

Where Ucp, $U\dot{m}$, and $U\Delta T$ are obtained previously

A.12.2 Uncertainty of the Di-water Reynolds number

Reynold number is calculated base on the formula for the minichannel heat exchanger as below

$$Re_{w,ch} = \frac{\dot{m}_w}{17\pi\mu_w D_{h,w}} \qquad \text{A.89}$$

$$U_{Re_w} = \pm\sqrt{\left(\frac{\partial Re_{w,ch}}{\partial \dot{m}_w}U_{\dot{m}_w}\right)^2 + \left(\frac{\partial Re_{w,ch}}{\partial \mu_w}U_{\mu_w}\right)^2 + \left(\frac{\partial Re_{w,ch}}{\partial D_{h,w}}U_{D_{h,w}}\right)^2} \qquad \text{A.90}$$

U_{Re_w}

$$= \pm\sqrt{\left(\frac{1}{17\pi\mu_w D_{h,w}}U_{\dot{m}_w}\right)^2 + \left(\frac{\dot{m}_w}{17\pi D_{h,w}\mu_w^2}U_{\mu_w}\right)^2 + \left(\frac{\dot{m}_w}{17\pi\mu_w D_{h,w}^2}U_{D_{h,w}}\right)^2} \qquad \text{A.91}$$

A.13. Overall Uncertainties for All Operating Conditions

The uncertainties are estimated for all operating conditions as shown in Table A.3.

Table A.3 Overall experimental uncertainty

Key parameters	Relative uncertainties of the mean value
Re_a	±3.03%
$\dot{Q}_a$	±7.82%
$\dot{m}_w$	±2.41 %
Re_w	±4.57%
$\dot{Q}_w$	±8.5%
$\dot{Q}_{Overall,a}$	±5.79%

References

[1]   R.S., Figliola, and D.E., Beasley "Theory and Design for Mechanical Measurements" 5th edition, John Wiley and Sons, Inc., New York, USA, 2011.

[2]   W.M. Kays, and A.L. London "Compact Heat Exchangers" 3rd ed., McGraw-Hill: New York, USA, 1984.

APPENDIX B

GOVERNING EQUATIONS OF AN ANALYTICAL MODEL

The transient study of heat exchangers is based on some assumptions which are listed in the following,

- Both fluids have a constant inlet temperature while mass flow rate changes on the inlet of the hot fluid

- No thermal energy sources inside the wall and the fluids

- The temperatures of the single-phase fluid and the wall are only functions of time t and position x;

- The thermal properties of the fluid, wall and convective heat transfer coefficient on both fluids are constant

- Negligible longitudinal heat conduction inside the wall compared to convection

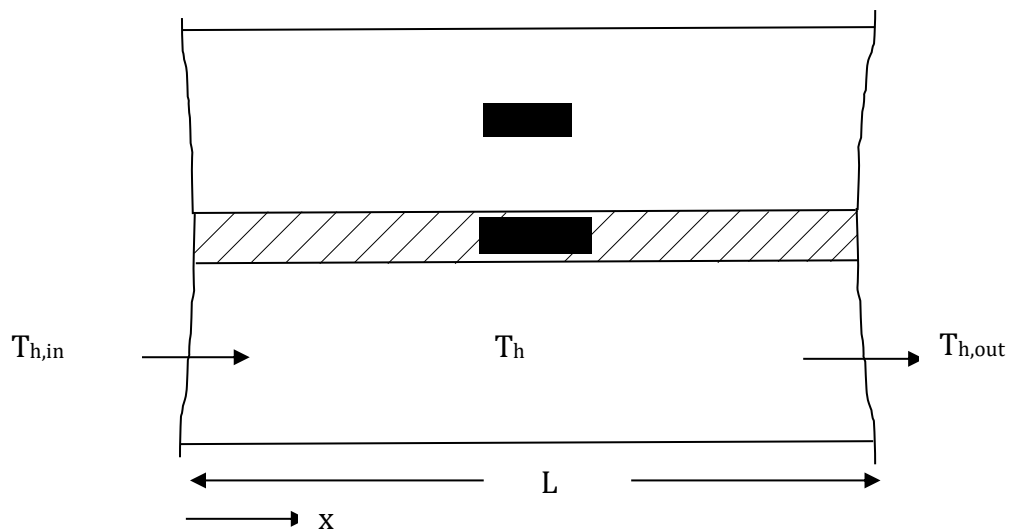- Convective heat convection on the both fluids are constant

Figure B.1. Thermal energy balance on an element in the liquid side of the heat exchanger

Based on the above assumptions, an Energy balance on an element of this heat exchanger shown in figure B.1 leads to the following set of equations, describing the transient heat exchanger process [1].

$$m_h\, c_{p,h}\frac{\partial T_h}{\partial t} + \dot{m}_h\, c_{p,h}\, L\frac{\partial T_h}{\partial x} = h_h A_h (T_h - T_w) \qquad\qquad B.1$$

$$m_w\, c_{p,w}\frac{\partial T_w}{\partial t} + h_c A_c (T_w - T_c) = h_h A_h (T_h - T_w) \qquad\qquad B.2$$

Define the following dimensionless variables and parameters

$$t^* = \frac{t}{t_{res}} \qquad\qquad\qquad x^* = \frac{x}{L} \qquad\qquad B.3$$

$$T^* = \frac{T - T_{h,i}}{T_{c,\infty} - T_{h,i}} \qquad\qquad B.4$$

$$T_h^{*,0} = \frac{T_h^0 - T_{h,i}}{T_{c,\infty} - T_{h,i}} \qquad\qquad T_w^{*,0} = \frac{T_w^0 - T_{h,i}}{T_{c,\infty} - T_{h,i}} \qquad\qquad B.5$$

$$m_c\, c_{p,c}\frac{\partial T_c}{\partial t} + \dot{m}_c\, c_{p,c}\, L\frac{\partial T_c}{\partial x} = h_c A_c (T_w - T_c) \qquad\qquad B.6$$

$$m_w\, c_{p,w}\frac{\partial T_w}{\partial t} + h_c A_c (T_w - T_c) = h_h A_h (T_h - T_c) \qquad\qquad B.7$$

$$N_1 = \frac{m_w C_{p,w}}{m_h C_{p,h}} \qquad\qquad B.8$$

$$N_2(x) = \frac{h_a(x) A_a}{m_h C_{p,h}} \qquad\qquad B.9$$

$$N_3(x) = \frac{h_h(x) A_h}{m_h C_{p,h}} \qquad\qquad B.10$$

$$\frac{1}{NTU} = (mc)_{min}\left[\frac{1}{(hA)_c} + \frac{1}{(hA)_h}\right] = (mc)_{min}\left[\frac{h_h A_h + h_c A_c}{h_c A_c h_h A_h}\right] \qquad B.11$$

$$\frac{1}{NTU} = (mc)_{min}\left[\frac{1}{(hA)_c} + \frac{1}{(hA)_h}\right] = (mc)_{min}\left[\frac{h_h A_h + h_c A_c}{h_c A_c h_h A_h}\right] \qquad B.12$$

$$TU = \frac{\frac{h_c A_c \, h_h A_h}{(mc)_c}}{(h_h A_h + h_c A_c)} = \frac{\frac{h_c A_c \, h_h A_h}{(mc)_c (mc)_h}}{\frac{(h_h A_h + h_c A_c)}{(mc)_h}} \qquad\qquad B.13$$

$$NTU = \frac{N_2 N_3}{N_2 + N_3} \qquad\qquad B.14$$

$$T^* = \frac{T - T_{h,i}}{T_{c,\infty} - T_{h,i}} \qquad\qquad B.15$$

The dimensionless form of the energy equations become,

$$\frac{\partial T_h^*}{\partial t} + \frac{\partial T_h^*}{\partial x} = N_3 (T_w^* - T_h^*) \qquad\qquad B.16$$

$$\frac{\partial T_c^*}{\partial t} + \frac{\partial T_c^*}{\partial x} = N_3 (T_w^* - T_c^*) \qquad\qquad B.17$$

$$N_1 \frac{\partial T_w^*}{\partial t^*} + N_2 (T_w^* - 1) + N_3 (T_w^* - T_h^*) = 0 \qquad\qquad B.18$$

Integrating the governing partial differential equations over the length of the heat exchanger,

$$\frac{\partial}{\partial t} \left(\int_0^1 T_h^* dx^* \right) + [T_{h,\,x^*=1}^* - T_{h,\,x^*=0}^*]$$
$$= N_3 \frac{\partial}{\partial x} \left(\int_0^1 T_w^* dx^* - \int_0^1 T_h^* dx^* \right) \qquad\qquad B.19$$

$$\frac{\partial}{\partial t} \left(\int_0^1 T_c^* dx^* \right) + [T_{c,\,x^*=1}^* - T_{c,\,x^*=0}^*]$$
$$= N_3 \frac{\partial}{\partial x} \left(\int_0^1 T_w^* dx^* - \int_0^1 T_c^* dx^* \right) \qquad\qquad B.20$$

$$N_1 \frac{\partial}{\partial t^*}\left(\int_0^1 T_w^* dx^*\right) + N_2\left(\int_0^1 T_w^* dx^* - 1\right) + N_3\left(\int_0^1 T_w^* dx^*\right.$$

$$\left. - \int_0^1 T_h^* dx^*\right) = 0 \qquad\qquad B.21$$

Two fluid temperature distributions are assumed to be approximated by the following form

$$T_h^* = T_h^{*,0} + \left(T_h^{*,\infty} - T_h^{*,0}\right) f(t^*) \qquad\qquad B.22$$

$$T_w^* = T_w^{*,0} + \left(T_w^{*,\infty} - T_w^{*,0}\right) g(t^*) \qquad\qquad B.23$$

Deriving the dimensionless energy equations B.13, B.14, and B15 for the steady state condition

$$\frac{\partial T_h^*}{\partial x} = N_3(T_w^* - T_h^*) \qquad\qquad B.24$$

$$N_2(T_w^* - 1) + N_3(T_w^* - T_h^*) = 0 \qquad\qquad B.25$$

Solving the two above equations

$$T_w^* - T_h^* = \frac{N_2}{N_2 + N_3} + \left(\frac{N_3}{N_2 + N_3} - 1\right)T_h^* \qquad\qquad B.26$$

then from equ. B.19

$$T_w^*(N_2 + N_3) = N_2 + N_3 T_h^* \qquad\qquad B.27$$

$$\frac{\partial T_h^*}{\partial x} = N_3\left(\frac{N_2}{N_2 + N_3} + \left(\frac{N_3}{N_2 + N_3} - 1\right)T_h^*\right) \qquad\qquad B.28$$

$$\frac{\partial T_c^*}{\partial x} = N_3\left(\frac{N_2}{N_2 + N_3} + \left(\frac{N_3}{N_2 + N_3} - 1\right)T_c^*\right) \qquad\qquad B.29$$

$$\frac{\partial T_h^*}{\partial x} - \frac{N_2 N_3}{N_2 + N_3} T_h^* = \frac{N_2 N_3}{N_2 + N_3} \qquad\qquad B.30$$

$$\frac{\partial T_h^*}{\partial x} - NTU \ T_h^* = NTU \qquad\qquad B.31$$

Using integral factor method multiplying the equation by

$$e^{\int NTU dx^*} = e^{NTU.x^*} e^{NTU.x^*} \frac{\partial}{\partial x} T_h^* - NTU \ e^{NTU.x^*} \ T_h^* \qquad\qquad B.32$$

$$= NTU \ e^{NTU.x^*}$$

$$\frac{\partial}{\partial x} \left[T_h^* \ e^{NTU.x^*} \right] = NTU \ e^{NTU.x^*} \qquad\qquad B.33$$

Integrate the above equation

$$T_h^* \ e^{NTU.x^*} = NTU \frac{1}{NTU} e^{NTU.x^*} + K = e^{NTU.x^*} + K \qquad\qquad B.34$$

$$T_h^* = 1 + K e^{-NTU.x^*} \qquad\qquad B.35$$

Fluid temperature for the initial steady state condition $T_h^{*,0} \rightarrow 0$ k = -1

Then fluid temperature for steady state condition,

$$T_h^{*,0} = 1 - e^{-NTU^0.x^*} \qquad\qquad B.36$$

Hot fluid temperature for the exit position become

$$T_h^{*,0} = 1 - e^{-NTU^0} \qquad\qquad B.37$$

Subset this equation into eq. 19

$$T_w^* = \frac{N_2 + N_3 T_h^*}{(N_2 + N_3)} = \frac{N_2}{(N_2 + N_3)} + \frac{N_3}{(N_2 + N_3)}[1 - e^{-NTU.x^*}] \qquad B.38$$

Wall temperature for steady state condition,

$$T_w^{*,0} = 1 - \frac{NTU^0}{N_2^{\,0}} e^{-NTU^0.x^*} \qquad\qquad B.39$$

Wall temperature at the liquid exit position become,

$$T_w^{*,0} = 1 - \frac{NTU^0}{N_2^{\,0}} e^{-NTU^0} \qquad\qquad B.40$$

Then the temperature distribution for the exit position become

$$T_h^{*,\infty} = 1 - e^{-NTU^\infty} \qquad\qquad B.41$$

$$T_w^{*,\infty} = 1 - \frac{NTU^\infty}{N_2^{\,\infty}} e^{-NTU^\infty} \qquad\qquad B.42$$

By substituting the eq. B.30, B.32, B.33, and B.34 into the eq. B.19 and B.20 dimensionless temperature is found,

$$T_h^* = (1 - e^{-NTU^0}) + (e^{-NTU^0} - e^{-NTU^\infty})f(t^*) \qquad B.43$$

$$T_w^* = (1 - \frac{NTU^0}{N_2^{\ 0}} e^{-NTU^0})$$

$$+ \left(\frac{NTU^0}{N_2^{\ 0}} e^{-NTU^0} - \frac{NTU^\infty}{N_2^{\ \infty}} e^{-NTU^\infty} \right) g(t^*)$$

B.44

Substituting the assumed initial liquid and wall temperature, eq. B.35 and B.36, into

equation, B.16 and B.18, and integrating, the following equations are found

$$\frac{df(t^*)}{dt^*} = C1f(t^*) + C2g(t^*) + C3$$

B.45

$$\frac{dg(t^*)}{dt^*} = D1f(t^*) + D2g(t^*) + D3$$

B.46

where

$$C_1 = \frac{\dfrac{N_3^\infty \varepsilon^\infty}{N_2^\infty} - (\dfrac{N_3^\infty}{NTU^0} - 1)\varepsilon^0}{\dfrac{\varepsilon^0}{NTU^0} - \dfrac{\varepsilon^\infty}{NTU^\infty}}$$

B.47

$$C_2 = \frac{\dfrac{N_3^\infty \varepsilon^0}{N_2} - (\dfrac{N_3 \varepsilon^\infty}{N_2^\infty} - 1)\varepsilon^0}{\dfrac{\varepsilon^0}{NTU^0} - \dfrac{\varepsilon^\infty}{NTU^\infty}}$$

B.48

$$C_3 = \frac{\varepsilon^0(\dfrac{N_3^\infty}{N_3^0} - 1)}{(\dfrac{\varepsilon^0}{NTU^0} - \dfrac{\varepsilon^\infty}{NTU^\infty})}$$

B.49

$$D_1 = \frac{N_3^\infty(\dfrac{\varepsilon^0}{NTU^0} - \dfrac{\varepsilon^\infty}{NTU^\infty})}{N_1(\dfrac{\varepsilon^0}{N_2^0} - \dfrac{\varepsilon^\infty}{N_2^\infty})}$$

B.50

$$D_2 = -\frac{(N_2^\infty + N_3^\infty)}{N_1}$$

B.51

$$D_1 = \frac{N_3^\infty \varepsilon^0 (\frac{1}{NTU^0} - \frac{N_2^\infty \varepsilon^\infty}{N_2^0 NTU^\infty})}{N_1 (\frac{\varepsilon^0}{N_2^0} - \frac{\varepsilon^\infty}{N_2^\infty})} \qquad B.52$$

Second derivation of B.37 is found

$$f''(t^*) = C1\acute{f}(t^*) + C2\acute{g}(t^*) \qquad B.53$$

Solving this equation for f (t) by using equation B.38

$$f''(t^*) = C1\acute{f}(t^*) + C2\,(D1f(t^*) + D2g(t^*) + D3) \qquad B.54$$

$$f''(t^*) = C1\acute{f}(t^*) + C2D1f(t^*) + D2(\acute{f}(t^*) - C1f(t^*) - C3) \qquad B.55$$
$$+ \, C2D3$$

$$f''(t^*) - (C1 + D2)\,\acute{f}(t^*) + (C1D2 + C2D1)f(t^*) \qquad B.56$$
$$= -C3D2 + C2D3$$

This equation is solved using the following model

$$y''+a_1y'+a_0y=b_0 \qquad B.57$$

and the auxiliary equation,

$$\lambda^2 + a_1\,\lambda + a_0 = 0 \qquad B.58$$

It is found,

$$\lambda_{1,2} = \frac{(C1 + D2) \pm \sqrt{(C1 + D2)^2 + 4(C2D1 - C1D2)}}{2} \qquad B.59$$

The $\lambda 1$ and $\lambda 2$ are real numbers

202

Define ε^0 and ε^∞ as follows

$$\varepsilon^0 = 1 - e^{-NTU^0} \qquad\qquad \varepsilon^\infty = 1 - e^{-NTU^\infty} \qquad\qquad B.60$$

Then the f(t) is found as,

$$f(t) = 1 - \frac{(\lambda_2 + C_3)e^{\lambda_1 t^*} - (\lambda_1 + C_3)e^{\lambda_2 t^*}}{(\lambda_2 - \lambda_1)} \qquad\qquad B.61$$

$$g(t) = 1 - \frac{(\lambda_2 + C_3)(\lambda_1 + C_1)e^{\lambda_1 t^*} - (\lambda_1 + C_3)(\lambda_2 + C_1)e^{\lambda_2 t^*}}{C_2(\lambda_2 - \lambda_1)} \qquad B.62$$

Where λ1 and λ2 is same as Eq. B.60, and C1, C2, C3 are defined as Eq. B48, B49, and B50. The outlet temperatures of fluids and wall are achieved by substituting Eqs. B.62 and B.63 into Eqs. B.44 and B.45.

Reference

[1]   J., Yin, M.K., Jersen "Analytical model for transient heat exchanger response" International Journal of heat and mass transfer, vol. 46, 3255-3264, 2003. https://doi.org/10.1016/S0017-9310(03)00118-2

APPENDIX C

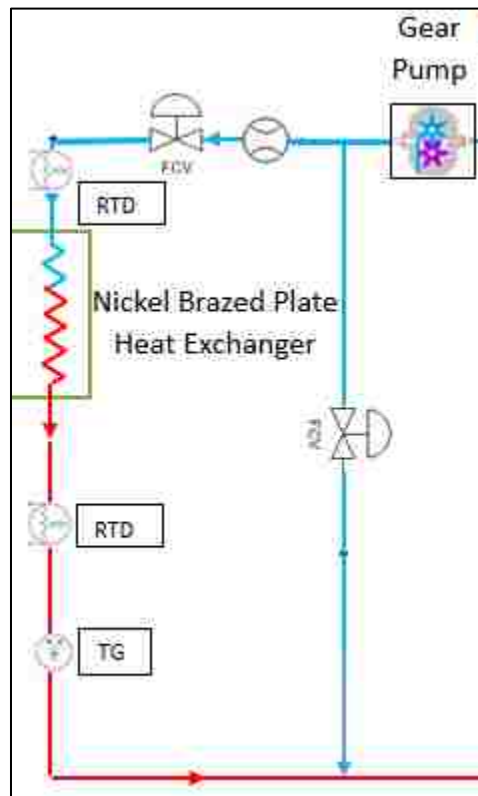Protocols for the temperature and mass flow rate step changes

Figure C.1. Schematic diagram of the experimental set up

- The liquid side is consisting of two circuits

    a. Primary circuit
    b. Secondary circuit

- The secondary circuit produces a desired flow and temperature using secondary

  flow pump and heater using a microprocessor

- This flow provide heat to the primary fluid using a brazed plate heat exchanger

  (BPHX)

- The flow of the primary fluid divided into two adjustable portions

a. One portion goes through a needle control valve (direct fluid line) without heating

b. The other portion goes through another needle control valve (bypass fluid line), then goes through the BPHX to get heat from secondary flow before mixing with cold fluid to produce desired temperature fluid at the inlet of the main heat exchanger.

- The predetermined condition of the control flow valves is recorded before running the transient test.

The directional control flow valve provides precision flow control (fine adjustments). using different colors for every turns of the adjusting knob and every turn has gradient of 10 equal degrees. A flow control valve conveys a constant flow regardless of the pressure drop through the valve.

The protocol for creating a step change in mass flow rate:

In order to create any mass flow rate step variation from its initial condition, the step by step procedure is appended below;

1- The secondary circuit of plate heat exchangers initializes by

a. Starting the secondary circuit gear pump at a particular speed

b. Starting the inline 20kw immersion heater to maintain the temperature of the plate heat exchanger using a microprocessor. This temperature is higher than the primary fluid operating temperature.

The intention is to heat up the water of secondary circuit until its temperature reaches to pre-set value with an offset of 0.1°C.

2- Once the temperature of the heater outlet of the secondary circuit reaches steady state of the predetermined pre-set value, the main circuit gear pump is turned on letting primary fluid, water, passes through the system.

3- Initially, the primary fluid mass flow rate of 20g/s is maintained by controlling the pump frequency. Then, simultaneously adjusting both direct and bypass fluid valves at predetermined positions to keep the inlet fluid temperature of 70°C.

4- When the outlet temperature of the primary fluid becomes steady state, then we go for step change and follow the steps below;

    a. Promptly changes the frequency of the pump to get the next mass flow rate of primary fluid.

    b. Simultaneously adjusting both direct and bypass fluid valves at predetermined positions to keep the inlet fluid temperature of 70°C.

The protocol for creating a step change in temperature step change:

In order to achieve any temperature step change from its initial condition, the step by step procedure is appended below;

1. The steps 1 and 2 from the mass flow rate step variation protocol are repeated.

2. Initially, the primary fluid mass flow rate of 60g/s is maintained by controlling the pump frequency. Then, simultaneously adjusting both direct and bypass fluid valves at predetermined positions to keep the inlet fluid temperature of 22°C.

3. When the outlet temperature of the primary fluid becomes steady state, then we go for step change and follow the steps below;

    a. Simultaneously adjusting both direct and bypass fluid valves at predetermined positions to get the next temperature step of the primary fluid.

b. If the mass flow rate needs adjustment due to the change if density of the primary fluid promptly adjusts the frequency of the pump to get the exactly 60g/s mass flow rate of primary fluid.

VITA AUCTORIS

NAME   Shahram Fotowat

PLACE OF BIRTH   Shiraz, Fars, Iran

YEAR OF BIRTH   1960

EDUCATION

High school diploma, Shiraz University high school, 1977.

Bachelor of Applied Science (B. A. Sc.) in Mechanical Engineering from Isfahan University of Technology, Isfahan, Iran, 1985.

Master of Applied Science candidate in Mechanical Engineering, University of Windsor, Windsor, Ontario, Canada, 2012.

EXPERIENCE

Since 1991, he established and has managed the Zarnegar Engineering & Construction Company in the field of Petrochemical, Oil and Gas, Shiraz, Iran.

MAJOR PROJECTS

Project manager responsible for installing insulation of pipes and equipments in the 7th refinery contract with TPL (Italy), Arak, Iran.

Senior manager of Aromatic Petrochemical plant piping project, Bandar Imam Petrochemical Complex, Iran.

Senior manager of the Parazylene Petrochemical plant piping project, Bandar Imam Petrochemical complex, Iran.

Project manager of the water distribution Project of Estahban city, Fars, Iran.

Senior project manager of the water distribution project of Bam city, Kerman, Iran.

Senior project manager of a large scale gas distribution in Sadra, Shairaz, Iran.

As well as many other projects that could not be included, however, the most recent one is the Dehdasht pipeline project, Kohgiluyeh and Boyer-Ahmad, Iran.